

Aberystwyth University

Stratigraphy, age and correlation of Lepu  Tephra

Alloway, Brent V.; Moreno, Patricio I.; Pearce, Nicholas; De Pol-Holz, Ricardo; Henriquez, William I.; Pesce, Oscar H.; Sagredo, Esteban; Villarosa, Gustavo; Outes, Valeria

Published in:

Journal of Quaternary Science

DOI:

[10.1002/jqs.2976](https://doi.org/10.1002/jqs.2976)

Publication date:

2017

Citation for published version (APA):

Alloway, B. V., Moreno, P. I., Pearce, N., De Pol-Holz, R., Henriquez, W. I., Pesce, O. H., Sagredo, E., Villarosa, G., & Outes, V. (2017). Stratigraphy, age and correlation of Lepu  Tephra: A widespread c. 11 000 cal a BP marker horizon sourced from the Chait n Sector of southern Chile. *Journal of Quaternary Science*, 32(6), 795-829. <https://doi.org/10.1002/jqs.2976>

General rights

Copyright and moral rights for the publications made accessible in the Aberystwyth Research Portal (the Institutional Repository) are retained by the authors and/or other copyright owners and it is a condition of accessing publications that users recognise and abide by the legal requirements associated with these rights.

- Users may download and print one copy of any publication from the Aberystwyth Research Portal for the purpose of private study or research.
- You may not further distribute the material or use it for any profit-making activity or commercial gain
- You may freely distribute the URL identifying the publication in the Aberystwyth Research Portal

Take down policy

If you believe that this document breaches copyright please contact us providing details, and we will remove access to the work immediately and investigate your claim.

tel: +44 1970 62 2400
email: is@aber.ac.uk

Stratigraphy, age and correlation of Lepué Tephra: a widespread c. 11,000 cal. a BP marker horizon sourced from the Chaitén Sector of southern Chile

Journal:	<i>Journal of Quaternary Science</i>
Manuscript ID	JQS-16-0147.R1
Wiley - Manuscript type:	Special Issue: SHAPE
Date Submitted by the Author:	23-May-2017
Complete List of Authors:	<p>Alloway, Brent; School of Environment, The University of Auckland, Private Bag 92019, Auckland, New Zealand, Moreno, Patricio; Universidad de Chile, Ecological Sciences and Institute of Ecology and Biodiversity and Department of Ecological Sciences Pearce, Nick; Aberystwyth University, DGES De Pol-Holz, Ricardo; GAIA Universidad de Magallanes Henríquez, William; Victoria University of Wellington, School of Geography, Environment and Earth Sciences Pesce, Oscar; Universidad de Chile, Departamento de Ciencias Ecológicas Sagredo, Esteban; Pontificia Universidad Católica de Chile, Instituto de Geografía Villarosa, Gustavo; Universidad Nacional del Comahue Centro Regional Universitario Bariloche, IPATEC, CONICET Outes, Valeria; Universidad Nacional del Comahue Centro Regional Universitario Bariloche, IPATEC, CONICET</p>
Keywords:	northwest Patagonia, tephrostratigraphy, Volcán Chaitén, Volcán Michimahuida, Lepué Tephra

SCHOLARONE™
Manuscripts

Stratigraphy, age and correlation of Lepué Tephra: a widespread c. 11,000 cal. a BP marker horizon sourced from the Chaitén Sector of southern Chile

Brent V. Alloway^{1,2*}, Patricio I. Moreno³, Nick J.G. Pearce⁴, Ricardo De Pol-Holz⁵, William I. Henríquez⁶, Oscar H. Pesce³, Esteban Sagredo⁷, Gustavo Villarosa⁸ and Valeria Outes⁸

¹ *School of Environment, The University of Auckland, Private Bag 92019, Auckland, New Zealand*

² *Centre for Archaeological Science (CAS), School of Earth and Environmental Sciences, University of Wollongong, Wollongong, NSW 2522, Australia*

³ *Instituto de Ecología y Biodiversidad, Departamento de Ciencias Ecológicas, Universidad de Chile, Casilla 653, Santiago, Chile*

⁴ *Department of Geography & Earth Sciences, Aberystwyth University, SY23 3DB Wales, United Kingdom*

⁵ *GAIA-Antártica, Universidad de Magallanes, Avda. Bulnes 01855, Punta Arenas, Chile*

⁶ *School of Geography, Environment and Earth Sciences, Victoria University of Wellington, PO Box 600, Wellington, New Zealand*

⁷ *Instituto de Geografía, Pontificia Universidad Católica de Chile, Av. Vicuña Mackenna 4860, Santiago, Chile*

⁸ *IPATEC, CONICET-Universidad Nacional del Comahue, Bariloche, Argentina*

Corresponding author: *Brent V. Alloway*

*E-mail: brent.alloway@gmail.com

ABSTRACT

We describe the stratigraphy, age and correlation of a prominent tephra marker, named Lepué Tephra, extensively distributed in northwestern Patagonia. Lepué Tephra is well-dated at c.11,000 cal. a BP from numerous lake and soil cover-bed sequences and its recognition is useful for assessing the rate and timing of deglaciation as well as associated environmental changes in this region during the last glacial termination and early Holocene. Lepué Tephra has attributes typical of a complex and compositionally zoned phreatomagmatic eruptive. While the initial rhyolitic phase can be readily distinguished from multiple eruptive products sourced

Alloway *et al.* - May 12th, 2017
JQS-16-0147-R1: SHAPE Special Volume

1
2
3 37 from the adjacent Volcán Chaitén, the main erupted end member is of basaltic-
4 38 andesite bulk composition - similar to younger tephra sourced from Holocene
5 39 monogenetic cones adjacent to the Volcán Michimahuida massif (tMim).

6
7
8 40 Lepué Tephra can be correlated to an equivalent-aged pyroclastic flow deposit
9 41 (Amarillo Ignimbrite) prominently distributed in the southeastern sector of tMim. The
10 42 source vent for these co-eruptive events is obscured by an extensive ice field and is
11 43 currently unknown. The widespread radially symmetrical distribution of Lepué
12 44 Tephra centred on tMim cannot be attributed solely to volcanological considerations.
13 45 Reduced Southern Hemisphere westerly wind influence interpreted from climate
14 46 proxies at the time of eruption are also implicated.

15
16
17
18
19
20 47 **[Words: 200]**

21 48
22
23 49 **Key Words:** northwest Patagonia, tephrostratigraphy, Lepué Tephra, Volcán
24 50 Michimahuida, Volcán Chaitén

25
26 51

27 28 52 **INTRODUCTION**

29 53 The ability to recognise, correlate and characterise tephra of mafic to
30 54 intermediate-silicic compositions that have been subjected to intense post-depositional
31 55 weathering and disturbance in temperate- to tropical-climate environments is a
32 56 significant obstacle to tephra studies in many proximal to distal volcanic settings. For
33 57 not only does the intense post-depositional pedogenic weathering effectively mask
34 58 fine-grained and/or thin tephra inter-beds within soil-dominated cover-beds, it
35 59 potentially compromises the morphological expression of the tephra as well as its
36 60 constituent geochemistry and grain-size characteristics - all attributes of which are
37 61 fundamental in tephra correlation. The characterisation of such tephra already
38 62 susceptible to post-depositional alteration can be further complicated by
39 63 compositional heterogeneity – that is, upward changes in tephra composition as an
40 64 eruption progresses. Such changes may reflect sequential surface discharge of either a
41 65 compositionally segregated magma body in the sub-volcanic system or a sudden
42 66 magmatic recharge event into an already fractionating body.

43
44
45
46
47
48
49
50
51
52
53 67 The principal objective of this study is to describe the stratigraphy, distribution,
54 68 age and geochemistry of a prominent tephra marker (here formally named Lepué
55 69 Tephra) located in the hyper-humid and high-weathering andic environment of
56 70 northwestern Patagonia (Fig. 1). The stratigraphy, age and chemistry of associated

1
2
3 71 rhyolitic tephra sourced from Volcán Chaitén will be presented in a companion paper
4 72 (see *Alloway et al., submitted*). Lepué Tephra is regionally important for three
5 73 reasons: First, it is one of the most widespread tephra marker beds to occur in this
6 74 sector and is therefore ideal for assessing the timing and rate of deglaciation and
7 75 associated environmental changes in this region during the Pleistocene-Holocene
8 76 transition. Second, Lepué Tephra can be recognised in high resolution lacustrine and
9 77 marine records and is therefore an important isochron potentially useful in assessing
10 78 proxy record synchronicity between equivalent-aged offshore and onshore sequences.
11 79 Third, Lepué Tephra is difficult to chemically characterise on account of the
12 80 ubiquitous occurrence of microphenocrysts and compositional heterogeneity of glassy
13 81 constituents. Hence, the application of a combination of grain discrete and bulk major
14 82 and trace elemental techniques may be a useful template by which other similarly
15 83 difficult tephra might be characterised, Finally, Lepué Tephra provides a unique
16 84 insight into a compositionally zoned and complex phreatomagmatic eruption
17 85 associated with a permanent Andean ice cap.

86

87 **Setting**

88 Northwestern Patagonia encompasses the Chilean Lake District and Chilotan
89 Archipelago (40° to 44°S), and is bounded in the east by the Andes Cordillera and a
90 lower lying coastal range in the west adjacent the Pacific Ocean (*Fig. 1*). This region
91 frequently experiences intermittent eruptions of varying magnitude from
92 compositionally diverse volcanoes situated within the Andean Southern Volcanic
93 Zone (SVZ). At least 60 active or potentially active volcanoes in Chile and Argentina,
94 as well as three caldera systems and numerous minor eruptive centres (*Stern, 2004;*
95 *Stern et al. 2007*) occur within this zone. Volcanism results from the subduction of the
96 Nazca Plate beneath the westward moving South American Plate (*Stern, 2004*), along
97 a narrow volcanic arc that follows the Liquiñe-Ofqui fault system in Chile between
98 33° and 46°S. Several volcanoes within this zone have recently erupted - the most
99 notable being Volcán Chaitén (VCha) in 2008, Puyehue-Cordon Caulle in 2011 and
100 Calbuco in 2015.

101 Over the last two decades, there has been a number of studies detailing the late
102 last glacial to Holocene tephrostratigraphy of northwestern Patagonia in order to
103 develop an inventory of eruptive events, determine source as well as characterize size,
104 composition and timing (i.e. *Naranjo and Stern, 2004*). While some eruptive histories

Alloway *et al.* - May 12th, 2017
JQS-16-0147-R1: SHAPE Special Volume

1
2
3 105 of individual volcanic centres within the central portions of the SVZ have been
4 106 described in detail (Lara *et al.* 2006; Singer *et al.* 2008), the eruptive histories of
5 107 many centers particularly within the southern SVZ (SSVZ) are insufficiently known
6 108 owing to their remote locations and inaccessibility (Watt *et al.* 2011). Tephra layers
7 109 have been routinely recorded in lakes (i.e. Haberle and Lumley, 1998; Daga *et al.*
8 110 2010; Moreno *et al.* 2014) but in many studies the occurrence of tephra has been a
9 111 subordinate focus in dominantly paleoecologically and paleoclimatically directed
10 112 investigations (i.e. Abarzúa *et al.* 2004; Bertrand *et al.* 2008; Iglesias *et al.* 2012;
11 113 Moreno and Videla, 2016). The need to better utilize tephra within sedimentary
12 114 archives as an effective means to synchronize records was recently highlighted by
13 115 Fontijn *et al.* (2016). Recent research efforts has also tended to focus on examining
14 116 composite eruptive records in order to better assess region-wide hazards based on
15 117 magnitude/frequency of historic and prehistoric eruptive events across large swaths of
16 118 Patagonia (i.e. Watt *et al.* 2011; Fontijn *et al.* 2014; Rawson *et al.* 2015; Naranjo *et al.*
17 119 2017). Recent eruptions (i.e. Hudson, 1991; Chaitén, 2008; Puyehue Cordón-Caulle,
18 120 2011; Calbuco, 2015) have also served as a driver for renewed field-investigations so
19 121 that eruptive histories and potential hazards posed to adjacent and downwind
20 122 communities can be better clarified (i.e. Wilson *et al.* 2010, 2011; Amigo *et al.* 2013;
21 123 Lara *et al.* 2013; Watt *et al.* 2013; Alloway *et al.* 2015, submitted).

22
23
24
25
26
27
28
29
30
31
32
33
34 124 Another dominant landscape feature is ubiquitous glacial landforms and ice-
35 125 carved lake basins formed from Andean piedmont glaciers during episodes of cold
36 126 (glacial) and/or temperate climate through the Quaternary. The configuration of these
37 127 Andean piedmont ice lobes in northwestern Patagonia is well known largely based
38 128 from the glacial morphologic mapping of moraines and outwash plains adjacent to
39 129 lakes and ocean alongside the western margin of the Andes (Anderson *et al.* 1999;
40 130 Denton *et al.* 1999). These seminal maps not only demarcated moraines and outwash
41 131 plains deposited during the maximum phases of the last glaciation (locally referred to
42 132 as Llanquihue glaciation) but also displayed older Casma and Colegual moraines and
43 133 outwash plains first described by Mercer (1976). Radiocarbon dating of Llanquihue
44 134 landforms show that the Andean ice lobes advanced into the moraine belt depicted in
45 135 red in Fig. 1C numerous times during glacial and/or cool inter-stadial phases of
46 136 Marine Isotope Stage (MIS) 4, 3 and 2, rather than simply being formed during the
47 137 Last Glacial Maximum (LGM) in MIS 2. The chronology of the youngest advance is
48 138 constrained by an extensive array of radiocarbon dates from sites tied to the former
49
50
51
52
53
54
55
56
57
58
59
60

1
2
3 139 Llanquihue, Reloncaví, Ancud and Golfo de Corcovado ice lobes (Denton *et al.* 1999;
4 140 Moreno *et al.* 2015). Overall this chronology shows a culmination of the glacial
5
6 141 readvance at 17,800 cal. a BP The advance of the two northern lobes (Llanquihue and
7
8 142 Reloncaví) reached the inner margin of the LGM moraine belt whereas the two
9
10 143 southern lobes (Ancud and Golfo de Corcovado) was either the most extensive, or
11
12 144 close to the most extensive, of MIS 2.

13
14 145 Of particular relevance to this study are sites located in areas formerly occupied
15
16 146 by ice lobes that overlie glacial deposits and contain the Lepué Tephra, as they can
17
18 147 assist in constraining the recessional chronology of ice lobes as climate warmed
19
20 148 abruptly during the Last Glacial Termination (LGT) (Moreno *et al.* 2015).

21 149

22 150 STRATIGRAPHY

23 151 In sections directly adjacent to the Volcán Michimahuida massif (tMim), Lepué
24
25 152 Tephra is typically characterised by compact, dark grey to brownish-grey, poorly
26
27 153 sorted, massive to weakly stratified, scoriaceous lapilli to lapilli-‘tuff’ (consolidated
28
29 154 ash, Fisher and Schmincke, 1984) beds often containing accretionary lapilli. These
30
31 155 textural and sorting characteristics, together with highly variable depositional
32
33 156 architecture between adjacent sections, suggest ‘molten fuel-coolant interactions’
34
35 157 (MFCI; Zimanowski, 1998) resulting in a complex succession of magmatic and
36
37 158 phreatomagmatic eruptive products (e.g. Cas and Wright, 1987; Ort and Carrasco-
38
39 159 Núñez, 2009; Ngwa *et al.*, 2010; van Otterloo and Cas, 2016).

40 160

41 161 *Proximal*

42 162 Within sections in the vicinity of Chaitén and Santa Barbara and those sections
43
44 163 further north towards Caleta Gonzalo (Fig. 2), a prominent decimetre(dm)-thick
45
46 164 reddish-brown crudely stratified medium to coarse scoriaceous fall unit is directly
47
48 165 overlain by a compact, dm-thick brownish-grey, crudely stratified, very poorly sorted
49
50 166 ash with conspicuous dispersed accretionary and scoriaceous lapilli layers. At Section
51
52 167 9B (Fig. 3-F) the upper phreatomagmatic unit, clearly over-thickened at the base of a
53
54 168 steeply inclined hillslope, infills an eroded lower scoriaceous fall unit suggesting a
55
56 169 brief hiatus between these two syn-eruptive events. At all other sections in this sector
57
58 170 both units appear conformable without any indication of an intervening break or soil
59
60 171 development. At Section 9D (Fig. 3-E) the basal scoriaceous lapilli bed is itself
172
underlain by a centimetre (cm)-thick surge deposit comprising compact, brownish-

Alloway *et al.* - May 12th, 2017
JQS-16-0147-R1: SHAPE Special Volume

1
2
3 173 grey, low-angle cross-bedded fine to medium ash with few medium-scoriaceous
4 174 lapilli dispersed randomly throughout. This surge deposit appears localised and most
5
6 175 likely relates to its passage down an isolated stream tributary.
7

8 176 Further north, at Section 4 on the southern side of a formerly glaciated mountain
9
10 177 pass (~264-m a.s.l) separating Lago Blanco (south) with Lago Negro (north) the
11 178 stratigraphy of Lepué Tephra is well exposed (Fig. 4). Here, the stratigraphy reveals a
12
13 179 prominent (metre-thick) rhyolitic pumiceous lapilli fall unit (Cha-1 *sensu stricto*
14 180 [Naranjo and Stern, 2004](#); dated at *c.* 8700 ¹⁴C a BP, [Watt *et al.* 2011](#)) sourced from an
15
16 181 ancestral VCha, separated from a lower scoriaceous surge and fall couplet below by ~
17
18 182 0.4 m of medial-ashy andic material (paleosol). This lower couplet is characterised by
19
20 183 a basal fall sub-unit characterised by multiple, normal graded centimetre-thick beds of
21
22 184 well-sorted coarse to very-fine sand textured scoriaceous ash, grading upwards to a
23
24 185 more prominent fall sub-unit comprising weakly stratified, poorly sorted, scoriaceous
25
26 186 coarse lapilli. This fall unit is unconformably overlain by a surge unit containing
27
28 187 conspicuous, moderately sorted, inclined planar to low-angle cross-bedded,
29
30 188 scoriaceous ash and lapilli beds. Charcoal fragments retrieved from within this upper
31
32 189 surge unit were dated at 11483 ± 1034 cal. a BP (9960 ± 330 ¹⁴C a BP; UCIAMS-
33
34 190 145938) and are distinguishable from those radiocarbon ages acquired for Lepué
35
36 191 Tephra correlatives elsewhere (see Age Section). At Section-4, Lepué Tephra
37
38 192 (represented as a fall-flow couplet) is closely underlain by widespread and distinctive
39
40 193 layers of banded rhyolite breccia and rhyolitic ashy material unconformably overlying
41
42 194 basement bedrock. This layer of rhyolitic breccia underlying Lepué Tephra can be
43
44 195 correlated to Section 6 (Lago Blanco) and Section 7 (within Chaitén township) (see
45
46 196 [Fig. 2](#)) and likely represents explosive fragmental debris originating from a pre-Cha-1
47
48 197 lava dome (ancestral VCha). Such pre-Cha-1 rhyolitic sequences are rarely observed
49
50 198 proximal to inferred source due to deep burial and/or pervasive Andean glaciation
51
52 199 ([Alloway *et al.* submitted](#)).

53
54 200 Northwards along the continental coastline (see [Fig. 5](#)), Lepué Tephra can be
55
56 201 reliably traced from Section 5 at Puente Águila to sections in the vicinity of Seno
57
58 202 Reloncaví. In most sections, Lepué Tephra is subtly expressed within the andic soil
59
60 203 material as laterally discontinuous cemented aggregates of olive-brown to reddish-
204
205 204 brown fine to medium ash. Often Lepué Tephra is stratigraphically associated with
206
207 205 Cha-1 tephra above ([Fig. 5](#)). At Puente Pichileufú on the Hualaihue Peninsula, Lepué
208
209 206 Tephra is unconformably overlain by a scoriaceous coarse ash bed of presumed

1
2
3 207 Apagado-source (Ap-1? of [Watt *et al.* 2011](#)) whereas further north-eastwards (i.e.
4 208 Chapo-S1) towards Ralún, Lepué Tephra is enveloped by a steadily increasing
5 209 number of discontinuous weathered lapilli of presumed Calbuco-source dispersed in
6 210 andic medial material.

211

212 *Relationship with pyroclastic flow and surge deposits*

213 In sections along road W-887 located directly adjacent to Río Michimahuida (i.e.
214 Pumalín Section 1), a massive > 40 m-thick unconsolidated lithic-rich pyroclastic
215 density current (PDC) deposit can be observed with metre-sized oriented lithic intra-
216 clasts and rare, dispersed centimetre-sized charred wood fragments ([Fig. 6A, B](#)). At
217 other sections along road W-887 (i.e. Pumalín-4), syn-eruptive fall deposits that
218 overlie this PDC deposit can occasionally be observed. At these sections, the
219 uppermost co-eruptive scoriaceous fall deposits are separated from Cha-1 above (i.e.
220 Pum 4-T8) by a pervasive wedge of colluvial debris of mixed lithologies indicating
221 widespread landscape instability in the devastating aftermath of this eruption.
222 Northward from the W-887 road-end an extensive elevated sloping remnant valley-fill
223 surface can be clearly observed within the confines of the glacially dissected Río
224 Michimahuida valley and extending down to the Río Mallines–Michimahuida
225 confluence ([Fig. 6C](#)). This same PDC-deposit and surface was recognised by [Amigo
226 *et al.* \(2013\)](#) and named Amarillo Ignimbrite. Two radiocarbon samples acquired from
227 within and just above the Amarillo Ignimbrite were dated at 9260 ± 50 and 9510 ± 50
228 ^{14}C a BP respectively and are broadly in accord with an age of 9785 ± 30 ^{14}C a BP
229 (LLNL-122960) from our sample retrieved from Pumalín-1. These ages are also
230 indistinguishable from a radiocarbon age associated with the prominent surge deposit
231 occurring at Section 4 in the northwestern sector of Michimahuida (see [Fig. 4](#)). While
232 the voluminous scoriaceous-rich PDC-deposit can be clearly identified in both the
233 south-eastern and northwestern sectors of tMim, the precise location of the eruptive
234 source vent is obscured by ice fields and is currently unknown.

235

236 *Southern Sectors*

237 At sections 1, 13 and 14 located on Ruta 7 between Amarillo and Puerto
238 Cárdenas (see [Figs. 7 and 8](#)), Lepué Tephra (previously referred to as *Cor-1* by
239 [Naranjo and Stern, 2004](#)) is enveloped by a sequence of at least six cm- to dm-thick,
240 basaltic-andesite to andesitic ash and lapilli inter-beds within dominantly reddish-

Alloway *et al.* - May 12th, 2017
JQS-16-0147-R1: SHAPE Special Volume

1
2
3 241 brown andic soil material that typically overlies glacial diamict (till) draping bedrock.
4 242 While some of these enveloping tephra (i.e. Unk-2) can be reliably traced northwards
5 243 towards Michimahuida, the eruptive origins of the majority (i.e. Yan-1, Cor-2 and
6 244 Cor-3 named by [Naranjo and Stern, 2004](#)) have yet to be determined. In this sector,
7
8 245 Lepu  Tephra is typically characterised by a dm-thick weakly stratified, brownish-
9 246 grey, very poorly sorted cemented ash with indistinct centimetre-sized accretionary
10 247 lapilli and scoriaceous lapilli-rich ashy intrabeds. Cemented fine ash frequently
11 248 contains open interstitial pore spaces, which are typically indicative of syn-
12 249 depositional rain flushing ([Fig. 8](#)). Beneath this cemented grey ash are common,
13 250 highly weathered reddish-brown scoriaceous fine to very fine lapilli dispersed within
14 251 underlying medial andic material. Lepu  Tephra can be traced south to the vicinity of
15 252 Santa Luc a where it occurs as a laterally discontinuous, variably thick (8 to 13-cm)
16 253 grey cemented fine ash intervening between Yan-1 and Cor-2 correlatives above
17 254 clast-supported breccia (talus deposit).
18
19
20
21
22
23
24
25
26
27

256 *Eastern Sectors*

28
29 257 Lepu  Tephra can be reliably correlated eastwards to distal sections in Chile
30 258 (Lago Espejo, Futaleuf ) and Argentina (Alerce-6 and La Zeta) ([Fig. 9](#)). Correlation
31 259 is based on a combination of morphological expression, chronostratigraphic
32 260 association and correspondence of glass shard major element compositions. The
33 261 Lepu  Tephra correlative at Lago Espejo, Alerce-6 and La Zeta is overlain by two
34 262 prominent rhyolitic coarse ash beds that are be correlated with Cha-2 and Cha-1
35 263 tephtras dated at *c.* 4950 and 9750 cal. a BP respectively ([Watt *et al.* 2013](#)). At La
36 264 Zeta, a ~11-cm thick tephra is prominently expressed within a ~ 5-metre-thick lake
37 265 sequence that contains numerous other mm- to cm-thick tephra inter-beds of basaltic
38 266 through to rhyolitic compositions. A radiocarbon age ($14,840 \pm 70$ ^{14}C a BP;
39 267 UCIAMS-145920) from basal lake sediments directly overlying glacial diamict (till)
40 268 establishes a maximum age of ~17,800 cal. a BP for the lake sequence. While the
41 269 Lepu  Tephra correlative at La Zeta is not directly dated, it is loosely constrained by
42 270 radiocarbon dates obtained from enveloping tephra inter-beds within the lake
43 271 sequence. Certainty of correlation is achieved by glass shard major element chemistry
44 272 (see below).
45
46
47
48
49
50
51
52
53
54
55

56 273 At La Zeta, the Lepu  Tephra correlative consists of three distinct fall units. The
57 274 lowermost unit consists of dark gray well-sorted coarse ash (< 1-cm thick, layer a in

1
2
3 275 [Fig. 9](#) photo inset). This unit is overlain by a compact, subtly bedded, pale gray,
4 276 moderately sorted fine to very fine ash (~2-cm thick, layer b in photo inset) which in
5 277 turn is overlain by a ~8-cm thick uppermost unit (layer c in photo inset) comprising
6 278 loose, well-sorted, very coarse to fine, grey scoriaceous ash. The internal architecture
7 279 of Lepué Tephra at this locality affirms the complex phreatomagmatic to magmatic
8 280 origin of this deposit.
9
10
11
12

13 281

14 282 *Western Sectors*

15
16 283 Through most of Isla Grande de Chiloé and its adjacent islands, Lepué Tephra is
17 284 the only macroscopic tephra that can be systematically observed within the late last
18 285 glacial to post-glacial andic cover-beds. Stratigraphic columns show the correlation of
19 286 Lepué Tephra along a western transect from south-central Isla Grande de Chiloé
20 287 northwards towards Puerto Montt in southernmost continental Chile ([Fig. 10](#)).
21 288 Typically in this sector, Lepué Tephra forms highly irregular, discontinuous pods of
22 289 crudely bedded, cemented fine- to medium-ash enveloped by reddish-brown andic
23 290 soil material and closely overlying late last glacial to Last Glacial Maximum (LGM)-
24 291 aged colluvium, bedded fluvio-glacial gravels and sands, and glacial diamicts (till).
25 292 The morphological expression of Lepué Tephra within andic cover-bed sections of
26 293 Isla Grande de Chiloé can be highly variable depending on the thickness of
27 294 encapsulating andic material and the permeability of the underlying substrate. Where
28 295 Lepué Tephra occurs within thin andic soil material closely overlying impermeable
29 296 glacial diamicts (which seasonally perches the local water table), tephra colour is
30 297 strongly altered to strong brown chromas (i.e. Queilen and Chonchi sections, [Fig. 11](#)),
31 298 whereas Lepué Tephra overlain by a thicker interval of free-draining andic soil
32 299 material typically have grey to pale brown chromas (i.e. Lago Natri, Castro, Puente
33 300 Punta and Chacao sections, [Fig. 11](#)). In northern sections (i.e. Huelmo and along
34 301 Ruta 5 connecting Pargua with Puerto Montt; [Figs. 10 and 12](#)) Lepué Tephra is
35 302 closely underlain by intensely weathered andesitic ash and lapilli ‘ghosts’ that are
36 303 most likely sourced from either Volcán Calbuco or Volcán Yate located eastwards
37 304 along the Andean mountain divide. These highly weathered tephra have yet to be
38 305 geochemically characterized.
39
40
41
42
43
44
45
46
47
48
49
50
51
52
53
54
55

56 306

57 307 *Lake Records*

58 308 A large number of cores over many years have been retrieved from bogs ([Heusser](#)
59
60

Alloway *et al.* - May 12th, 2017
JQS-16-0147-R1: SHAPE Special Volume

1
2
3 309 *et al.* 2003) and shallow lakes throughout northwestern Patagonia in order to elucidate
4 310 vegetation-climate change, fire regime shifts and volcanic disturbance (i.e. Moreno
5 311 and León, 2003; Pesce and Moreno, 2014; Henríquez *et al.* 2015). A key priority for
6 312 these ongoing investigations has been to disentangle the role of paleofires and
7 313 explosive volcanism from climate drivers of past vegetation change. Until recently,
8 314 the occurrence of Lepué Tephra has been a subordinate focus in dominantly
9 315 paleoecologically directed investigations. However, there is growing appreciation of
10 316 the utility this tephra is able to play in terms of vegetation-climate synchronization
11 317 within equivalent-aged lake records of diverse latitude and elevation.

12
13
14
15
16
17
18 318 Lepué Tephra can be readily identified in most sediment cores as a macroscopic
19 319 layer (centimetre-thick) showing primary fall deposition with minimal post-
20 320 depositional reworking. However, in some lakes (i.e. Lago Lepué; Pesce and
21 321 Moreno, 2014) Lepué Tephra shows evidence of reworking and is substantially
22 322 overthickened compared with adjacent lake sequences. In all cases, Lepué Tephra can
23 323 be readily identified as a very prominent down-core inorganic density (gr/cc) peak
24 324 (Fig. 13). For cores throughout Isla Grande de Chiloé (i.e. Lago (L.) Quilque, L.
25 325 Tarumán, L. Lepué, L. Melli and L. Tahui) this peak occurs at ~750-cm depth with a
26 326 subordinate inorganic peak at ~650-cm likely representing a VCha-sourced tephra,
27 327 which is not typically expressed macroscopically in adjacent andic soil cover-beds
28 328 (Alloway *et al.* submitted). For continental cores south of Puerto Montt (i.e. L.
29 329 Condorito, Huelmo mire, L. El Salto), Lepué Tephra occurs at ~650-cm depth
30 330 whereas at L. Proschle and Puelche Section Lepué Tephra occurs at ~350-cm depth,
31 331 and is associated with minor inorganic spikes likely representing tephra additions
32 332 from Volcán (V.) Chaitén, V. Apagado and V. Calbuco. In all lake cores throughout
33 333 the region, the ages of Lepué Tephra are well-constrained by numerous radiocarbon
34 334 dates (see Age Section below).

35
36
37
38
39
40
41
42
43
44
45
46 335 So far the northern-most occurrence of Lepué Tephra within lake sediments is
47 336 found at Lago Pichilaguna, located immediately west of Llanquihue township and
48 337 ~178-km north-west of V. Michimahuida. Here, Lepué Tephra occurs at 382 to 390-
49 338 cm depth within core 1402AT3 as a ~8-cm-thick dark olive-grey, normal graded
50 339 coarse to very fine ash (see photo inset Fig. 10) and is chronologically constrained by
51 340 bracketing radiocarbon dates of 8905 ± 35 ^{14}C a BP (CAMS-158137; 9989 ± 113 cal.
52 341 a BP) above and $10,100 \pm 25$ ^{14}C a BP (UCIAMS-177595; $11,576 \pm 109$ cal. a BP)
53 342 below. In this same vicinity, Lepué Tephra is not macroscopically preserved within
54
55
56
57
58
59
60

1
2
3 343 the andic soil-forming environment.

4 344 In lakes close to its presumed Michimahuida source, only sediments and tephra
5 345 post-dating Lepu  Tephra have been retrieved since it forms a prominent hardpan and
6 346 a significant obstacle for further core penetration. For example, at Lago Teo located
7 347 near Chait n (Moreno *et al.* 2014), no core penetration beyond 3.02 m depth was
8 348 achieved. Lepu  Tephra was not encountered despite being prominently expressed in
9 349 all adjacent road sections. An age of 8925 ± 30 ¹⁴C a BP of organic sediments from
10 350 the base of the Lago Teo core provides a minimum age of 10,021 cal. a BP for Lepu 
11 351 Tephra in this sector.

12 352

13 353 *Offshore Record*

14 354 Site 1233 was drilled during ODP Leg 202 off southern continental Chile
15 355 (41 0.01'S, 74 26.99'W; 40-km offshore; 838-m water depth) in a small basin on the
16 356 upper continental slope away from the pathway of major turbidity currents. This
17 357 offshore site is located at the northern margin of the Antarctic Circumpolar Current
18 358 (ACC) and at the origin of the Per -Chile Current (PCC), the most latitudinally
19 359 extensive Eastern Boundary Current system in the world, driven by along-shore
20 360 parallel winds along the Pacific coast of South America. This offshore core yielded
21 361 high-resolution alkenone-based sea surface temperature (SST) and vegetation records
22 362 extending over the last 50-70,000 years (Kaiser *et al.* 2005; 2008; Heusser *et al.* 2006;
23 363 Lamy *et al.* 2007). A prominent macroscopic tephra layer was registered in core
24 364 1233D within clay and silty clays between 14.52-14.83 mcd and was accompanied by
25 365 a prominent spike in magnetic susceptibility (916.8 m.mol^{-1} (SI)) (Fig. 14).
26 366 Unfortunately, no radiocarbon dates were obtained directly associated with the upper
27 367 and lower contacts of this tephra but bracketing radiocarbon samples from 12.94 and
28 368 17.01 mcd yielded calibrated ages of 10,040 and 12,260 cal. a BP, respectively.

29 369

30 370 **AGE**

31 371 A weighted mean age determination of 9588 ± 20 ¹⁴C a BP (95% probability:
32 372 10,080 to 10,714 cal. a BP) was modeled for Lepu  Tephra based on four R-combine-
33 373 statistically grouped samples (UCIAMS-145938, LLNL-158290, LLNL-123032 and
34 374 LLNL-12329) from Sections 4, 12A, Pichileuf  and Puelche, respectively (Fig. 15;
35 375 Table 1). Three sample outliers from Sections 9, 12A and Pumal n -1, (LLNL-
36 376 158125, LLNL-158291 and LLNL-122960) were rejected. This modeled age of Lepu 

Alloway *et al.* - May 12th, 2017
JQS-16-0147-R1: SHAPE Special Volume

1
2
3 377 Tephra compares closely with a similarly modeled age of 9725 ± 23 ^{14}C a BP based
4 378 on samples retrieved from Huelmo (Moreno and Leon, 2003), Lago (L.) Condorito
5 379 (Moreno, 2004), L. Tahui (Abarzúa *et al.* 2004), L. Melli (Abarzúa and Moreno,
6 380 2008) and L. Lepué (Pesce and Moreno, 2014) (Fig. 16; Table 1). The associated
7
8 381 mean calendar age of $10,994 \pm 124$ cal. a BP collated from previous research is
9 382 indistinguishable from a mean calendar age of $10,909 \pm 228$ cal. a BP determined for
10 383 Lepué Tephra in this study from Chaitén (S-4, S-12A), Puelche and Pichileufú (see
11
12 384 Fig. 5).
13
14
15
16
17

18 386 ISOPACH

19
20 387 Lepué Tephra is extensively distributed from the Chaitén Section of southern
21 388 Chile in a wide arc from Isla Grande de Chiloé in the west to Esquel, Argentina across
22 389 the Andes in the east (Fig. 17). Lepué Tephra can also be traced northwards to the
23 390 vicinity of Seno Reloncaví and immediately south of Puerto Montt. In routinely
24 391 measuring the thickness of Lepué Tephra two problems are encountered. Thicknesses
25 392 recorded in the soil-forming (andic) environment bear little resemblance to those
26 393 determined from lake/peat records. We consider that the most accurate thicknesses are
27 394 likely to be derived from lakes and organic-rich lens, though bedding characteristics
28 395 need to be carefully scrutinised to distinguish between primary and secondary
29 396 depositional features. For example in L. Lepué (Pesce and Moreno, 2014) – Lepué
30 397 Tephra is recorded as being ~ 44-cm thick with this thickness being significantly at
31 398 odds with those from adjacent cored lakes (i.e. L. Melli, 11-cm; L. Tahui, 16-cm),
32 399 with no mention of bedding characteristics that might distinguish primary airfall
33 400 products from secondary redeposition and reworking.

41
42
43 401 Within the andic soil environment Lepué Tephra typically forms a highly
44 402 irregular and laterally intermittent layer of well-cemented ashy material. This lateral
45 403 distribution is presumably coincident with the density and distribution of vegetation
46 404 that likely existed at the time of deposition with continued biological disturbance
47 405 since (i.e. interference by roots, tree-throw). At any one particular section within the
48 406 Chaitén sector, thickness values for Lepué Tephra are highly variable and are for the
49 407 most part, interpreted as being over-thickened within the valleys and lower slopes
50 408 adjacent the Andean range-front (along which most roads follow). This pervasive
51 409 over-thickening certainly restricts the production of a reliable isopach map and by
52 410 proxy - any accurate estimate of eruptive volume. However, these thickness

1
2
3 411 measurement obstacles certainly do not diminish the utility of this tephra as one of the
4 412 most important early Holocene stratigraphic markers in this sector.

5
6 413

7
8 414 **GEOCHEMISTRY**

9
10 415 We report major- and trace-element chemistry of pumice and matrix glass from
11 416 Lepu  Tephra utilising grain-discrete EMPA and LA-ICP-MS techniques (see [Tables](#)
12 417 [2, 3 and SI Methods](#)) as well as bulk solution nebulisation inductively coupled plasma
13 418 mass spectrometry (SN-ICP-MS) analyses (see [Table 4 and SI Methods](#)). The key
14 419 objective for this paper is to demonstrate its utility in supporting field correlations and
15 420 is not intended to detail the genesis of the melt body (or melt bodies) involved. Thus,
16 421 while a (micro)phenocryst assemblage dominated by plagioclase, with subordinate
17 422 pyroxene and Fe-Ti oxide phases was noted, their routine analysis was not undertaken
18 423 as mineral compositions, and their implications for petrogenesis of the deposit, were
19 424 not considered central to this particular study. The grain specific major- and trace-
20 425 element characterisation of the pure glass phase of the Lepu  Tephra has proven to be
21 426 difficult because of the progressive increase in the concentration of microphenocrysts
22 427 (dominantly plagioclase) occurring within the tephra glass shards as the eruption
23 428 proceeded.

24
25
26 429

27 430 Back-scatter electron (BSE) images of selected glass shards from Lepu  Tephra
28 431 correlatives indicate low microlite concentrations are observed within glassy grains at
29 432 the base of the tephra sequence referred to as “microlite-poor glass” which are
30 433 broadly rhyolitic in composition (onset of the Lepu  eruption; [Fig. 18-A to -C](#)).
31 434 Higher up in the tephra sequence, the microlite concentration within the glassy grains
32 435 significantly increases ([Fig. 18-D to -F](#)) giving “intensely microlitic glass” which
33 436 typically have a basaltic andesite composition. Analysing the intensely microlitic
34 437 glass either by EMPA and/or LA-ICP-MS is highly problematic in that microlites are
35 438 inevitably included in the material analysed (i.e. [Fig. 18-G, -H](#)), even when using a 10
36 439 µm diameter EMPA, or LA-ICP-MS, spot. However, with sufficient analyses, glass
37 440 chemistry can be determined as an end-member to a trend of analyses contaminated
38 441 by (dominantly) plagioclase phenocrysts, and in some cases “microlite-free” analyses
39 442 can be produced, particularly so from the microlite-poor glass shards. Coinciding with
40 443 the increase in microlite concentration, the proportion of well-formed oriented

Alloway *et al.* - May 12th, 2017
JQS-16-0147-R1: SHAPE Special Volume

1
2
3 444 vesicles also decreases with a corresponding increase in irregular shaped (collapsed)
4 445 and coalesced voids (Fig. 18-D, -F).

5 446 Selected major element compositions (weight percent SiO₂ vs Na₂O + K₂O and
6
7 447 FeO vs K₂O and CaO) of glass shards from Lepu  Tephra correlatives are presented in
8 448 Fig. 19A to C. Two glass shard types can be clearly distinguished by differences in
9 449 the major element analyses, viz. (i) the rhyolitic composition of glass from the
10 450 microlite-poor shards and (ii) the broadly basaltic-andesite composition of the
11 451 intensely microlitic shards, which represent analyses of mixed glass and phenocrysts,
12 452 approximating to a “bulk” (modal) analyses of the glass shard, and not the glass phase
13 453 only (*cf.* Platz *et al.* 2007). The insets on Fig. 19 show the tight compositional
14 454 clustering of rhyolitic glass shards erupted at the onset of the Lepu  eruption and
15 455 these likely represent the initial magma withdrawal from the top of a melt body
16 456 dominated by fractionated magma (~71 wt % SiO₂). Note that the rhyolitic end-
17 457 member composition of Lepu  Tephra can be clearly differentiated from all post
18 458 18,000 cal. a BP rhyolitic tephra sourced from V. Chait n-sourced tephra (indicated in
19 459 greyscale).

20
21 460 Selected trace element (Nd vs Th and Sr vs Y, Ho, Nd, Zr) compositions of glass
22 461 shards from Lepu  Tephra correlatives as determined by grain discrete LA-ICP-MS
23 462 analyses are presented in Fig. 20. Data for glass shards from proximal sites at La Zeta,
24 463 Puente  guila (S5) and Paso Lago Blanco (S4) sites are broadly coincident, showing
25 464 strong linear relationships between the data in all plots. Samples from the more distal
26 465 locations of Lago Lepu  (020DT8-1804-cm) and ODP-1233D (14.68-m) plot slightly
27 466 away from the trend displayed in the other Lepu  samples, but the low Sr end-point of
28 467 this compositional array is coincident, and the differences result from issues
29 468 associated with the volume of material sampled during LA-ICP-MS microanalysis of
30 469 microcryst-bearing glass shards.

31 470 All data display a range of compositions ranging from pure rhyolitic glass with a
32 471 composition of ~ 72 to 113-ppm Sr (i.e. microlite-free analyses from microlite-poor
33 472 glass shards) to high Sr compositions (~1000-ppm Sr) where the glasses become
34 473 increasingly microlite-rich, with the highest Sr compositions coming from analyses
35 474 which will have ablated almost entirely feldspar, with very little glass in the intensely
36 475 microlitic shards. With increasing Sr, incompatible element concentrations decrease,
37 476 associated with low incompatible element concentrations in feldspar. All analyses
38 477 were calculated using the glass SiO₂ composition from the shards (determined by
39
40
41
42
43
44
45
46
47
48
49
50
51
52
53
54
55
56
57
58
59
60

1
2
3 478 EPMA) as the internal standard (I.S.). This will give accurate analyses for the pure
4 479 glass component (i.e. low Sr analyses), but the change in glass composition by
5 480 inclusion of feldspar in the analyses will mean that, as more feldspar is ablated, the
6 481 true SiO₂ content of the ablated mixture (the I.S. composition) moves further from the
7
8 482 pure glass composition and the analyses will become progressively less accurate (see
9
10 483 [Pearce, 2014](#)). Incorporation of plagioclase in rhyolitic glass causes the SiO₂ content
11
12 484 in the ablated mixture to drop, and thus, using the glass SiO₂ composition as I.S.,
13
14 485 analysed elements will be marginally overestimated. It is not possible to correct the
15
16 486 internal standard concentration for this effect unless the amount of feldspar ablated
17
18 487 with glass and the SiO₂ composition of feldspar and glass are both accurately known.
19
20 488 The effect of ablation of feldspar increases the reported Sr (compatible in feldspar)
21
22 489 considerably and decreases incompatible element concentrations (by dilution, as
23
24 490 feldspar has very low incompatible element contents), and this dilution effect
25
26 491 competes with the increase in concentration from the change in I.S. composition, with
27
28 492 the overall effect depending strongly on exactly how much phenocryst has been
29
30 493 ablated (see [Pearce, 2014](#)), however without knowing its composition, the amount
31
32 494 cannot be calculated. The offset of the Sr-rich analyses of microcryst-bearing glasses
33
34 495 from the distal sites at Lago Lépúe and ODP-1233D when compared with data from
35
36 496 the more proximal sites may relate to differences in glass composition and phenocryst
37
38 497 assemblage/content associated with deposition at different stages of the eruption, and the
39
40 498 effects these variables may introduce into the LA-ICP-MS analyses described above.
41
42 499 What is apparent though is that the microcryst-poor and microcryst-free glass
43
44 500 analyses (i.e. where Sr \sim 150-ppm) from the more distal localities have the same
45
46 501 glass composition as the microcryst-free glass analyses from the proximal localities,
47
48 502 which establishes the correlation between these deposits ([see Table 3](#)) consistent with
49
50 503 the well constrained chronologies at these sites. This microcryst-free glass
51
52 504 composition (Sr 73 to 113-ppm) defines the composition (and compositional range) of
53
54 505 the rhyolitic component of the Michimahuida magma at the onset of the eruption.

51
52 507 Solution-nebulisation-ICP-MS analyses were also conducted on bulk ash material
53
54 508 and individual accretionary lapilli from a number of proximal- to distal-sites. Plots of
55
56 509 the highly immobile elements (i.e. Th vs Zr) from Lépúe Tephra correlatives from six
57
58 510 proximal sites and sixteen distal sites located on Isla Grande de Chiloé and the coastal
59
60 511 Chilean mainland are presented in [Fig. 21A](#). These results are compared with

Alloway *et al.* - May 12th, 2017
JQS-16-0147-R1: SHAPE Special Volume

1
2
3 512 individually analysed accretionary lapilli from seven proximal Lepué Tephra
4 513 localities (Fig. 21B). While bulk ash analyses exhibit a wide elemental range (even
5 514 between duplicate samples) and predominantly along a tightly clustered linear
6 515 fractional crystallization pathway, accretionary lapilli samples exhibit a narrower
7 516 elemental range positioned on the same linear pathway as the bulk ash samples. Lepué
8 517 analyses were compared with similar analyses from Holocene-aged tephra beds (13)
9 518 of tMim and its adjacent monogenetic satellite cones (here named Michimahuida
10 519 Volcanic Complex, MimVC) (Fig. 21C). The elemental spread and orientation of
11 520 tephra points are coincident along the Lepué Tephra linear evolutionary trend. These
12 521 results indicate the limited utility of bulk analyses in the absence of associated
13 522 chrono-stratigraphic contexts to be able to adequately differentiate MimVC-sourced
14 523 eruptives. Results also indicate that all MimVC-sourced tephra irrespective of age, are
15 524 fractionating under broadly similar phase equilibria constraints.

16 525

17 526 *Confirming Michimahuida as the eruptive source*

18 527 Glass shard major-element chemistry indicates that the initial eruptive phase of
19 528 Lepué Tephra is rhyolitic in composition but distinguishable from all post-18,000 cal.
20 529 a BP Chaitén-sourced tephra. As the Lepué eruption progresses the composition
21 530 steadily becomes more basic and terminates in a compositional field that broadly
22 531 straddles the Trachyte-andesite, Andesite, Basaltic-trachyte-andesite and Basaltic-
23 532 andesite fields (see Fig. 19). This trend suggests a zoned magma body with a volatile-
24 533 rich aphyric cap above a more mafic and phenocryst-rich magma. This more mafic
25 534 end member of Lepué Tephra is similar to the composition (Basaltic-andesite) of
26 535 proximal MimVC deposits exposed at Campo Grande, Pumalín-2 and Pumalín-4 (see
27 536 Fig. 22). At these localities, dm-thick lapilli beds (CG-T3, Pum 2-T4, and Pum 4-T5)
28 537 can be directly associated with adjacent MimVC monogenetic scoria cone complexes
29 538 and lava flows. Two coarse-grained pumiceous lapilli and ash beds (Pum 2-T5 and
30 539 Pum 4-T7) have distinct compositions that straddle the Trachyte and Dacite fields and
31 540 on the same compositional trend as MimVC-sourced tephra (see Fig. 23). While these
32 541 two tephra cannot be associated with an identifiable MimVC source vent - coarse
33 542 grain-size and thickening characteristics would tend to indicate a putative MimVC-
34 543 source. The three compositional groups identified from proximal MimVC-sites are
35 544 similar to those identified from L. Teo (Moreno *et al.* 2014) and indicate a diverse
36 545 range of discrete small-volumed silicic to mafic melt bodies resident at different

1
2
3 546 levels within the MimVC sub-volcanic system and may reflect contributions from
4 547 different upper mantle components (i.e. [Hickey *et al.* 1986](#); [Hickey-Vargas *et al.*](#)
5 548 [2002](#)), differences in rates of crustal stagnation and differentiation as well as
6 549 structural controls (i.e. [Lopez-Escobar *et al.* 1995](#)).
7
8
9

550

551 **DISCUSSION**

552 **Relationship of Lepué Tephra to deglaciation**

553 Lepué Tephra is one of the most widespread tephra marker beds to occur in this
554 sector in the last 11,000 years and its early Holocene age is ideal for assessing the
555 timing and rate of deglaciation and associated environmental changes as the climate
556 ameliorated at the transition between the LGM and early Holocene.

557 Radiocarbon dates of organic material retrieved from the base of cores and
558 sections through lacustrine and organic-rich sediments that overlie glacial deposits
559 situated in areas formerly covered by ice lobes have been pivotal in terms of assessing
560 the temporal-spatial extent of glaciers in this region and of relevance to this study, the
561 timing of rapid ice lobe recession that followed the LGT advance into the LGM
562 moraine belt. For example, a basal radiocarbon date from a low-elevation
563 stratigraphic section containing Lepué Tephra at Puelche ([see Fig. 5](#)) indicates a
564 minimum-limiting age of $14,070 \pm 35$ ^{14}C a BP ($17,107 \pm 99$ cal. a BP) for recession
565 of the Seno Reloncaví ice lobe. Similarly a radiocarbon date from a coastal roadside
566 outcrop just north of Chaitén (section 12A, [Fig. 2](#)) (also containing Lepué Tephra)
567 indicates a minimum-limiting age of $13,830 \pm 50$ ^{14}C a BP ($16,737 \pm 125$ cal. a BP)
568 for recession of the Golfo de Corcovado ice lobe. The persistence of ice lobes within
569 low-elevation Cordilleran valley sites is indicated from minimum ages of *c.* 12,500
570 ^{14}C a BP ($14,600$ cal. a BP) from basal organic mud sequences overlying glacial till
571 (i.e. Sta. Lucía, [Fig. 7](#)). Certainly, the spatial range of dates presented in this study
572 support the findings of [Moreno *et al.* \(2015\)](#) that wholesale glacial recession in this
573 region following the final advance of Andean ice lobes during a cold and wet LGT
574 episode ($17,700$ - $18,100$ cal. a BP) was very abrupt with diminished lobes recessed
575 within the confines of continental Andean valleys in less than 1000 years.

576

577 **Synchronisation of late last glacial to early post-glacial vegetation and climate** 578 **records**

579 Pollen percentage curves of selected key taxa from six sites (arranged south to
59
60

Alloway *et al.* - May 12th, 2017
JQS-16-0147-R1: SHAPE Special Volume

1
2
3 580 north; L. Melli, L. Tahui, L. Lepué, L. El Salto, Huelmo mire and L. Condorito)
4 581 between 8000 and 15,000 cal. a BP are shown in Fig. 24. While sediment cores from
5 582 these sites have been individually described in the literature, the recognition of the
6 583 widespread Lepué Tephra within these cores enable us to effectively time-slice and
7 584 synchronise vegetation/climate records across a broad latitudinal swath of
8 585 northwestern Patagonia and west of the Cordillera de los Andes. An intra-regional
9 586 summary of these synchronised records is presented here.

10 587 Palynological studies of organic sediments from numerous lake cores and cover-
11 588 bed sections that overlie glacial deposits or bedrock situated in areas formerly covered
12 589 by ice lobes indicate that the interval preceding Lepué Tephra (11,700-15,000 cal. a
13 590 BP) features dominance of closed-canopy temperate rainforests. Palynological records
14 591 from lowlands sites indicate a prominent increase in the cold-resistant conifer
15 592 *Podocarpus nubigena* starting at ~14,500 cal. a BP, concomitant with a decline in
16 593 thermophilous rainforest trees (*Myrtaceae*) and vines (*Hydrangea*) (Moreno 1997,
17 594 2004; Moreno *et al.* 1997, 2004; Moreno *et al.* 1999, Moreno *et al.* 2001; Moreno and
18 595 Leon, 2003). The species *P. nubigena* attained its maximum abundance between
19 596 12,700-13,000 cal. a BP, declined between 11,000-12,700 cal. a BP and then reached
20 597 minimum abundance until 8000 cal. a BP These changes suggest a cooling trend and
21 598 increase in precipitation between ~12,700-14,500 cal. a BP, followed by a decline in
22 599 precipitation and/or enhanced precipitation seasonality with intense fire activity
23 600 between ~11,000 -12,700 cal. a BP. Mainland sites show that fire disturbance
24 601 promoted forest gaps and colonization of the opportunistic, shade-intolerant tree
25 602 *Weinmannia trichosperma* over a cold and highly variable interval between ~11,000-
26 603 12,700 cal. a BP. Over the same interval, sites in Isla Grande de Chiloé (Abarzúa and
27 604 Moreno 2008; Abarzúa *et al.* 2004; Pesce and Moreno, 2014) show diversification of
28 605 the forest canopy, lake-level lowering and encroachment of species of the myrtle
29 606 family along the lake periphery. Deposition of the Lepué Tephra at ~11,000 cal. a BP
30 607 occurred when *P. nubigena* had already reached low abundance in mainland
31 608 palynological sites (L. Condorito, Huelmo mire), and at the culmination of a rapid
32 609 decline of this conifer in Chilotan sites (L. Lepué, L. Melli, L. Tahui). Chilotan sites
33 610 show abrupt increases in *W. trichosperma* following deposition of the Lepué Tephra;
34 611 likewise, mainland sites exhibit a secondary expansion of this species. These changes
35 612 have been interpreted as changes in temperature and precipitation, the latter associated
36 613 with variation in intensity in the southern westerly winds (SWW) attributable to

1
2
3 614 latitudinal shifts or intensity variations. Recent studies (Moreno *et al.* 2015; Moreno
4 615 *et al.* 2010; Moreno *et al.* 2012) have proposed that the SWW intensified during the
5
6 616 Antarctic Cold Reversal (~12,700-14,500 cal. a BP), shifted pole-ward during
7
8 617 Younger Dryas time (~11,500-12,700 cal. a BP) and then weakened during the early
9
10 618 Holocene (~7800-11,500 cal. a BP). These changes covaried with temperature and
11
12 619 paleofires, with warm/dry conditions featuring enhanced fire activity and cold/wet
13
14 620 climates inhibiting paleofires. Deposition of the Lepu  Tephra occurred at the
15
16 621 beginning of the warmest/driest interval of the last glacial-interglacial cycle, when the
17
18 622 SWW attained their weakest condition and when SST's from core ODP-1233 reach a
19
20 623 maximum of 15.6 C in the early Holocene (11,000 to 9000 cal. a BP) (Kaiser *et al.*
21
22 624 2005, 2008; Heusser *et al.* 2006).

23
24 625 Prevailing warm/dry climate conditions coupled with weak SWW flow might
25
26 626 account for the broad distribution of Lepu  Tephra west of Volc n Michimahuida at a
27
28 627 time when zonal atmospheric flow did not impede its northwestward distribution
29
30 628 toward the SE Pacific. However, the distribution of Lepu  Tephra may have also been
31
32 629 influenced by volcanological factors - in particular - a hybrid dry/wet plume that
33
34 630 expands outward as a powerfully spreading umbrella cloud (see section below).
35

36
37 631

38 632 ***Eruption style and hazard implications***

39
40 633 A schematic representation of the Lepu  eruptive sequence centred at tMim is
41
42 634 represented in Fig. 25. Dark grey, poorly-sorted, fine-grained sub-units of Lepu 
43
44 635 Tephra with accretionary lapilli and rain-flushed pore spaces within the ashy matrix
45
46 636 clearly indicate the involvement of external water within the erupted mixture. The
47
48 637 eruption comprising Lepu  Tephra and its co-eruptive PDC (Amarillo Ignimbrite) is
49
50 638 an excellent example of an early Holocene dominantly phreatomagmatic eruption
51
52 639 derived from a volcanic massif presently mantled by an extensive area of permanent
53
54 640 ice. Such eruptions are less usual compared with the more typical background of
55
56 641 Strombolian to Plinian volcanism frequently experienced in this region during the
57
58 642 Holocene. Thus, in the absence of proximal exposures on Volc n Michimahuida, it's
59
60 643 not known if Lepu  eruption was point-sourced and derived from a single magma
644
645 644 reservoir, or alternatively, derived from a network of coalescing and/or discrete
646
647 645 multiple co-genetic melt bodies (i.e. similar to the 2011 Puyehue-Cord n Caulle
648
649 646 eruption, see Alloway *et al.*, 2015).

Alloway *et al.* - May 12th, 2017
JQS-16-0147-R1: SHAPE Special Volume

1
2
3 647 Within most sections adjacent to tMim, metre-thick accretionary lapilli bearing
4 648 ash deposits with weak stratification between coarser and finer components can be
5 649 observed and indicate fluctuating multilevel deposition – that is – coarse ash and
6 650 lapilli transported farther during stable phases of the eruption (less water content with
7 651 higher vertical velocities), yet deposited closer to source during periods of unstable
8 652 water-rich plumes where moist convection simultaneously occurs both vertically and
9 653 laterally away from the vent. If moist convection was a dominant feature of the Lepué
10 654 plume, then a substantial portion of the initially erupted mass was likely ejected and
11 655 maintained in the troposphere where temperature inversions inhibit the rise of the
12 656 weaker, less stable portions of the eruption column. Under such circumstances, the
13 657 ash plume would have had the tendency to spread outward as a broad, umbrella-
14 658 shaped cloud. The combination of fluctuating multilevel transport/deposition and
15 659 upwind/cross wind expansion at the troposphere would have likely favored the
16 660 formation of a radially symmetrical ash cloud (see Houghton *et al.* 2015). Indeed,
17 661 recorded thicknesses of Lepué Tephra over such an extensive area in all directions
18 662 from source appear to support this scenario (see Fig. 17). While eruptive conditions
19 663 were likely conducive to the broad radial distribution noted for Lepué Tephra, this
20 664 distribution could also be attributed to the reduced SWW intensity interpreted from
21 665 equivalent-aged environmental records.

22
23
24
25
26
27
28
29
30
31
32
33
34
35 666 In the advent of a future sustained eruption of similar magnitude to the Lepué
36 667 eruption centred upon the ice-capped tMim, a centimetre-thick wet ash fall could be
37 668 reasonably expected up to ~ 200-km from volcanic source and potentially affecting
38 669 communities and critical infrastructure westward in Isla Grande de Chiloé,
39 670 northwards towards the city of Puerto Montt and east and south-eastwards towards the
40 671 communities of Futaleufú on the Chilean frontier and Esquel and Trevelin located in
41 672 Argentina. Eruption-induced sub-glacial and surface melting of ice and snow on tMim
42 673 is also likely to occur and lead to significant melt-water formation, jökulhlaups, and
43 674 lahars extending down adjacent tributaries. Such events have already been shown to
44 675 be a significant hazard in areas of Iceland (i.e. Katla, 1918; Eyjafjallajökull 2010),
45 676 Alaska (i.e. Redoubt, 2009), Cascades (i.e. Mt. Rainier), Antarctica (i.e. Deception
46 677 Island, 1969) and in parts of the Andes (i.e. Nevado del Ruiz, 1985). Although the
47 678 area surrounding Volcán Michimahuida is sparsely populated with little critical
48 679 infrastructure, melt-water floods and/or water-supported mass-flows would inundate
49 680 picturesque and increasingly popular low-lying river-side tourist campgrounds within
50
51
52
53
54
55
56
57
58
59
60

1
2
3 681 Parque Pumalín and scattered farm dwellings farther down-stream. The community of
4 682 Amarillo would likely be affected, though inundation is likely to be minimized by
5 683 recent engineering works that have elevated and armored adjacent river-banks.
6
7
8 684

9
10 685 In summary, while Lepué Tephra is temporally associated with rhyolitic products
11 686 from nearby Volcan Chaitén, its physical and geochemical attributes are typical of
12 687 a complex (zoned) phreatomagmatic eruption sourced from tMim. We propose that
13 688 the eruption commenced with initial magma withdrawal from the top of a melt body
14 689 dominated by fractionated Si-rich magma (~71 wt % SiO₂), which propagated
15 690 downwards into the hosting crystalline-rich magma and ultimately resulted in the Si-
16 691 rich magma being rapidly and almost entirely replaced by microphenocrysts with very
17 692 minor interstitial melt (~55 wt % bulk SiO₂). Despite compositional heterogeneity, we
18 693 were still able to characterise both the aphyric and microlitic glass of the Lepué
19 694 Tephra by grain discrete and bulk analytical techniques to define a broad
20 695 compositional array enabling us to distinguish and widely correlate this tephra marker
21 696 in both terrestrial and marine realms of northwestern Patagonia. While discrete and
22 697 bulk glass shard trace element analyses maybe of significant use in petrogenetic
23 698 studies, this study also illustrates its utility in substantiating correlation beyond that
24 699 already established from major element (EMP) analyses.
25
26
27
28
29
30
31
32
33

34 700 Lepué Tephra with its phreatomagmatic style and its compositional heterogeneity
35 701 is exceptional in the context of other documented eruptions known from this Andean
36 702 sector. We consider that our integrative approach of intensive mapping supported by
37 703 multi-technique geochemical analysis is a useful template for the characterisation and
38 704 correlation of such complex and compositionally variable tephra deposits elsewhere.
39 705 Ultimately, our approach applied to weathered tephra in wet, hyper-humid
40 706 environments, like that of northwestern Patagonia, will be of great assistance in the
41 707 synchronisation of different equivalent-aged sedimentary archives.
42
43
44
45
46
47
48

49 709 [Words 7418]
50
51
52

53 711 **ACKNOWLEDGEMENTS**

54 712 This study was funded by Iniciativa Científica Milenio grants P02-51 and NC120066,
55 713 Fondecyt 1151469 (to PIM), part funded by a Victoria University of Wellington
56 714 Science Faculty Research Grant (to BVA), Aberystwyth University Research Fund (to
57
58
59
60

Alloway *et al.* - May 12th, 2017
JQS-16-0147-R1: SHAPE Special Volume

1
2
3 715 NJGP), Fondecyt 1160488 (to ES) and PIP CONICET 2011 0311 (to GV). Andy
4 716 Brown (IGES, Aberystwyth University, UK) is thanked for conducting solution-ICP-
5 717 MS acid digestions and Craig Wickham for conducting acid digestions and solution-
6 718 ICP-MS analyses on Lepué Tephra accretionary lapilli (under supervision by NJGP).
7
8 719 Ignacio Jara, Rodrigo Ras and Craig Wickham are thanked for their assistance in the
9 720 field and Matt Ryan for his statistical analysis of radiocarbon dates. We are grateful to
10 721 Frank Lamy and Thomas Ronge (Alfred Wegener Institute, Bremerhaven, Germany)
11 722 for tephra samples and data from ODP Site 1233. We extend our appreciation to
12 723 Horacio Griffiero and Gabriela Piezug of Posada Kahuel (km-4 Camino Chaitén-Santa
13 724 Bárbara; www.posadakahuel.cl) for their continuing hospitality and friendship while
14 725 engaging in field-work. Our sincere thanks to the residents of Chaitén township for
15 726 their hospitality, as well as unwavering curiosity and support of this research. P.A.
16 727 Shane and an anonymous reviewer are thanked for their comments. The authors also
17 728 wish to thank Andrew Lorrey for his editorial inputs.
18
19
20
21
22
23
24
25
26
27

729

730 REFERENCES

- 28
29
30 731 Abarzúa AM, Moreno PI. 2008. Changing fire regimes in the temperate rainforest
31 732 region of southern Chile over the last 16,000 yr. *Quaternary Research* **69**: 62-71.
32
33 733 Abarzúa AM, Villagran C, Moreno PI. 2004. Deglacial and postglacial climate history
34 734 in east-central Isla Grande de Chiloé, southern Chile (43 degrees S). *Quaternary*
35 735 *Research* **62**: 49-59.
36
37 736 Alloway BV, Pearce NJ, Villarosa G, Outes V, and Moreno, PI. 2015. Multiple melt
38 737 bodies fed the AD 2011 eruption of Puyehue-Cordón Caulle, Chile. *Nature SR* **5**,
39 738 17589; doi: 10.1038/srep17589
40
41
42 739 Alloway BV, Pearce NJG, Moreno PI, Villarosa G, Jara I, De Pol-Holz R, and Outes
43 740 V. An 18,000 year-long eruptive record from Volcán Chaitén, northwestern
44 741 Patagonia: paleoenvironmental and hazard-assessment implications. *Quaternary*
45 742 *Science Reviews* (submitted)
46
47 743 Amigo A, Lara LE, Smith VC. 2013. Holocene record of large explosive eruptions
48 744 from Chaitén and Michimahuida Volcanoes, Chile. *Andean Geology* **40**: 227-
49 745 248.
50
51 746 Andersen BG, Denton GH, Lowell TV. 1999. Glacial geomorphologic maps of the
52 747 Llanquihue drift in the area of the Southern Lake District, Chile. *Geografiska*
53 748 *Annaler Series A Physical Geography* **81A**: 155-166.
54
55
56
57
58
59
60

- 1
2
3 749 Bertrand S, Charlet F, Charlier B, Renson V, Fagel N. 2008. Climate variability of
4 750 southern Chile since the Last Glacial maximum: a continuous sedimentological
5 751 record from Lago Puyehue (40 S). *Journal of Paleolimnology* **39**: 179-195.
6
7
8 752 Cas RAF, Wright JV. 1987. Volcanic Successions, Modern and Ancient. Chapman
9 753 and Hall, London. 528 pp.
10
11 754 Daga R, Ribeiro Guevara S, Sanchez ML, Arribere M. 2010. Tephrochronology of
12 755 recent events in the Andean Range (northern Patagonia): spatial distribution and
13 756 provenance of lacustrine ash layers in the Nahuel Huapi National Park. *Journal of*
14 757 *Quaternary Science* **25**: 1113–1123.
15
16
17
18 758 Denton GH, Lowell TV, Heusser CJ, Schlüchter C, Anderson BG, Heusser LE,
19 759 Moreno PI, Marchant DR. 1999. Geomorphology, stratigraphy and radiocarbon
20 760 chronology of Llanquihue drift in the area of the Southern Lake District, Seno
21 761 Relongcaví and Isla Grande de Chiloé, Chile. *Geografiska Annaler Series A*
22 762 *Physical Geography* **81B**: 167-229.
23
24
25
26 763 Fisher RV, Schmincke H.-U. 1984. Pyroclastic Rocks. Springer-Verlag Berlin
27 764 Heidelberg 472 pp.
28
29
30 765 Fontijn K, Lachowycz SM, Rawson H, Pyle DM, Mather TA, Naranjo JA, Moreno-
31 766 Roa H. 2014. Late Quaternary tephrostratigraphy of southern Chile and
32 767 Argentina. *Quaternary Science Reviews* **89**: 70-84.
33
34
35 768 Fontijn K, Rawson H, Van Daele M, Moernaut J, Abarzúa AM, Heirman K, Bertrand
36 769 S, Pyle DM, Mather TA, De Batist M, Naranjo J-A, Moreno H. 2016.
37 770 Synchronisation of sedimentary records using tephra: A postglacial
38 771 tephrochronological model for the Chilean Lake District. *Quaternary Science*
39 772 *Reviews* **137**: 234-254.
40
41
42
43 773 Haberle SG, Lumley SH. 1998. Age and origin of tephtras recorded in postglacial lake
44 774 sediments to the west of the southern Andes, 44°S to 47°S. *Journal of*
45 775 *Volcanology and Geothermal Research* **84**: 239-256.
46
47
48 776 Henríquez WI, Moreno PI, Alloway BV, Villarosa G. 2015. Vegetation and climate
49 777 change, fire-regime shifts and volcanic disturbance in Chiloé Continental (43°S)
50 778 during the last 10,000 years *Quaternary Science Reviews* **123**: 158-167.
51
52
53 779 Heusser L, Heusser C, Pisias N. 2006. Vegetation and climate dynamics of southern
54 780 Chile during the past 50,000: results of ODP 1233 pollen analysis. *Quaternary*
55 781 *Science Reviews* **25**: 474-485.
56
57
58 782 Hickey RL, Frey FA, Gerlach DC, Lopez-Escobar L. 1986. Multiple sources for
59
60

Alloway *et al.* - May 12th, 2017
JQS-16-0147-R1: SHAPE Special Volume

- 1
2
3 783 basaltic arc rocks from the southern volcanic zone of the Andes (34°–41°S):
4 784 Trace element and isotopic evidence for contributions from subducted oceanic
5 785 crust, mantle, and continental crust. *Journal Geophysical Research* **91**: 5963-
6 786 5983.
7
8
9
10 787 Hickey-Vargas R, Sun M, Lopez-Escobar L, Moreno-Roa H, Reagan MK, Morris JD,
11 788 Ryan JG. 2002. Multiple subduction components in the mantle wedge: Evidence
12 789 from eruptive centres in the Central southern volcanic zone, Chile. *Geology* **30**:
13 790 199-202.
14
15
16 791 Houghton B, White JDL, Van Eaton AR. 2015. Phreatomagmatic and related eruption
17 792 styles. In *The Encyclopedia of Volcanoes*, Sigurdsson H (ed.) Academic Press:
18 793 San Diego; 537-552.
19
20
21 794 Iglesias V, Whitlock C, Bianchi MM, Villarosa G, Outes V. 2012. Holocene climate
22 795 variability and environmental history at the Patagonian forest/steppe ecotone:
23 796 Lago Mosquito (42°29'37.89"S, 71°24'14.57"W) and Laguna del Cóndor
24 797 (42°20'47.22"S, 71°17'07.62"W). *The Holocene* **22**: 1297-1307.
25
26
27
28 798 Kaiser J, Lamy F, Hebbeln D. 2005. A 70-kyr sea surface temperature record off
29 799 southern Chile (Ocean Drilling Program Site 1233). *Paleoceanography* **20**:
30 800 PA4009, doi:10.1029/2005PA001146.
31
32
33 801 Kaiser J, Schefuß E, Lamy F, Mohtadi M, Hebbeln D. 2008. Glacial to Holocene
34 802 changes in sea surface temperature and coastal vegetation in north central Chile:
35 803 high versus low latitude forcing. *Quaternary Science Reviews* **27**: 2064–2075
36
37
38 804 Lamy F, Kaiser J, Arz HW, Hebbeln D, Ninnemann US, Timm O, Timmermann A,
39 805 Toggweiler RJ. 2007. Modulation of the bipolar seesaw in the Southeast Pacific
40 806 during Termination 1. *Earth and Planetary Science Letters* **259**: 400-413.
41
42
43 807 Lara LE, Moreno H, Naranjo JA, Matthews S, Pérez de Arce C. 2006. Magmatic
44 808 evolution of the Puyehue-Cordón Caulle Volcanic Complex (40°S), Southern
45 809 Andean Volcanic Zone: From shield to unusual rhyodacitic fissure volcanism.
46 810 *Journal of Volcanology and Geothermal Research* **157**: 343-366.
47
48
49 811 Lara LE. 2009. The 2008 eruption of the Chaitén Volcano, Chile: A preliminary
50 812 report. *Andean Geology*, **36**: 125–129.
51
52
53 813 Lara LE, Moreno R, Amigo A, Hoblitt RP, Pierson TC. 2013. Late Holocene history
54 814 of Chaitén Volcano: New evidence for a 17th century eruption: *Andean Geology*
55 815 **40**: 249-261.
56
57
58 816 López-Escobar L, Kempton PD, Moreno H, Parada MA, Hickey-Vargas R, Frey FA.
59
60

- 1
2
3 817 1995. Calbuco volcano and minor eruptive centers distributed along the Liquine-
4 818 Ofqui fault zone, Chile (41°-42°S): contrasting origin of andesitic and basaltic
5 819 magma in the Southern Volcanic Zone of the Andes. *Contributions to Mineralogy*
6 820 *and Petrology* **119**: 345-361.
- 7
8
9 821 Mercer JH. 1976. Glacial history of southern-most South America. *Quaternary*
10 822 *Research* **6**: 125-166.
- 11
12 823 Moreno PI. 1997. Vegetation and climate near Lago Llanquihue in the Chilean Lake
13 824 District between 20200 and 9500 C-14 yr BP. *Journal of Quaternary Science* **12**:
14 825 485-500.
- 15
16
17 826 Moreno PI. 2004. Millennial-scale climate variability in northwest Patagonia over the
18 827 last 15000 yr. *Journal of Quaternary Science* **19**: 35-47.
- 19
20
21 828 Moreno, PI, Denton GH, Moreno H, Lowell TV, Putnam AE, Kaplan MR. 2015.
22 829 Radiocarbon chronology of the last glacial maximum and its termination in
23 830 northwestern Patagonia. *Quaternary Science Reviews* **122**: 233-249.
- 24
25
26 831 Moreno PI, Francois JP, Villa-Martínez R, Moy CM. 2010. Covariability of the
27 832 Southern Westerlies and atmospheric CO₂ during the Holocene. *Geology* **39**: 727-
28 833 730.
- 29
30
31 834 Moreno PI, Jacobson GL, Andersen BG, Lowell TV, Denton GH. 1999. Abrupt
32 835 vegetation and climate changes during the last glacial maximum and the last
33 836 Termination in the Chilean Lake District: A case study from Canal de la Puntilla
34 837 (41°S). *Geografiska Annaler Series A-Physical Geography* **81 A**: 285-311.
- 35
36
37 838 Moreno PI, Jacobson GL, Lowell TV, Denton GH. 2001. Interhemispheric climate
38 839 links revealed by a late-glacial cooling episode in southern Chile. *Nature* **409**:
39 840 804-808.
- 40
41
42 841 Moreno PI, Leon AL. 2003. Abrupt vegetation changes during the last glacial to
43 842 Holocene transition in mid-latitude South America. *Journal of Quaternary*
44 843 *Science* **18**: 787-800.
- 45
46
47 844 Moreno PI, Videla J. 2016. Centennial and millennia-scale hydroclimate changes in
48 845 Northwestern Patagonia since 16,000 yr BP. *Quaternary Science Reviews* **149**:
49 846 326-337.
- 50
51
52 847 Moreno PI, Villa-Martinez R, Cardenas ML, Sagredo EA. 2012. Deglacial changes of
53 848 the southern margin of the southern westerly winds revealed by terrestrial records
54 849 from SW Patagonia (52°S). *Quaternary Science Reviews* **41**: 1-21.
- 55
56
57 850 Moreno PI, Alloway BV, Villarosa G, Outes V, Henriquez WI, De Pol-Holz R,
58
59
60

Alloway *et al.* - May 12th, 2017
JQS-16-0147-R1: SHAPE Special Volume

- 1
2
3 851 Pearce NJG. 2014. A past-millennium maximum in post-glacial activity from
4 852 Volcán Chaitén, southern Chile. *Geology* doi:10.1130/G36248.1
5
6 853 Naranjo JA, Stern CR. 2004. Holocene tephrochronology of the southernmost part
7
8 854 (42°30' - 45°S) of the Andean Southern Volcanic Zone. *Revista Geológica de*
9
10 855 *Chile* **31**: 225-240.
11 856 Naranjo JA, Singer, BS, Jicha BR, Moreno H, and Lara LE. 2017. Holocene tephra
12
13 857 succession of Puyehue-Cordón Caulle and Antillanca/Casablanca volcanic
14
15 858 complexes, southern Andes (40-41°S). *Journal of Volcanology and Geothermal*
16
17 859 *Research*, doi:[10.1016/j.jvolgeores.2016.11.017](https://doi.org/10.1016/j.jvolgeores.2016.11.017)
18 860 Ngwa CN, Suh CE, Devey CW. 2010. Phreatomagmatic deposits and stratigraphic
19
20 861 reconstruction at Debunsha Maar (Mt Cameroon volcano). *Journal of*
21
22 862 *Volcanology and Geothermal Research*, **192**: 201-211.
23 863 Ort MH, Carrasco-Núñez G. 2009. Lateral vent migration during phreatomagmatic
24
25 864 and magmatic eruptions at Tecuitlapa Maar, east-central Mexico. *Journal of*
26
27 865 *Volcanology and Geothermal Research*, **181**: 67-77.
28 866 Otterloo van J, Cas RAF. 2016. Low-temperature emplacement of phreatomagmatic
29
30 867 pyroclastic flow deposits at the monogenetic Mt Gambier Volcanic Complex,
31
32 868 South Australia, and their relevance for understanding some deposits in
33
34 869 diatremes. *Journal of the Geological Society*, **173**: 701-710.
35 870 Pearce NJG. 2014. Towards a protocol for the analysis of rhyolitic glass shards in
36
37 871 tephra deposits by laser ablation ICP-MS. *Journal of Quaternary Science*, **29**:
38
39 872 627–640, ISSN 0267-8179. doi: 10.1002/jqs.2727
40 873 Pesce OH, Moreno PI. 2014. Vegetation, fire and climate change in central-east Isla
41
42 874 Grande de Chiloé (43°S) since the Last Glacial Maximum, northwestern
43
44 875 Patagonia. *Quaternary Science Reviews* **90**: 143-157.
45 876 Platz T, Cronin SJ, Smith IEM, et al. 2007. Improving the reliability of microprobe-
46
47 877 based analyses of andesitic glasses for tephra correlation. *The Holocene* **17**: 573–
48
49 878 583.
50 879 Rawson H, Naranjo J-A, Smith V, Fontijn K, Pyle DM, Mather TA, and Moreno H.
51
52 880 2015. The frequency and magnitude of post-glacial explosive eruptions at Volcán
53
54 881 Mocho-Choshuenco, southern Chile. *Journal of Volcanology and Geothermal*
55
56 882 *Research* **299**: 103-129.
57 883 Singer BS, Jicha BR, Harper MA, Naranjo JA, Lara LE, Moreno-Roa H. 2008.
58
59 884 Eruptive history, geochronology, and magmatic evolution of the Puyehue-Cordón
60

- 1
2
3 885 Caulle volcanic complex, Chile. *Geological Society of America Bulletin* **120**:
4 886 599-618.
5
6 887 Stern C. 2004. Active Andean volcanism: its geologic and tectonic setting. *Revista*
7 888 *Geologica de Chile* **31**:161-206.
8
9 889 Stern CR. 2008. Holocene tephrochronology record of large explosive eruption in the
10 890 southernmost Patagonian Andes. *Bulletin of Volcanology* **70**: 435-454.
11
12 891 Stern CR, Moreno H, Lopez-Escobar L, Clavero JE, Lara LE, Naranjo J-A, Parada
13 892 MA, Skewes MA. 2007. *Chilean Volcanoes*. In *The Geology of Chile*. Moreno T,
14 893 Gibbons W. (eds.) The Geological Society, London; 147-178.
15
16 894 Watt SFL, Pyle DM, Naranjo J-A, Rosqvist G, Mella M, Mather TA, Moreno H.
17 895 2011. Holocene tephrochronology of the Hualaihue region (Andean southern
18 896 volcanic zone, ~42°S), southern Chile. *Quaternary International* **246**: 324-343.
19
20 897 Watt SFL, Pyle DM, Mather, TA. 2013. Evidence of mid- to late-Holocene explosive
21 898 rhyolitic eruptions from Chaitén Volcano, Chile. *Andean Geology* **40**: p. 216–
22 899 226, doi: 10.5027 /andgeoV40n2-a02.
23
24 900 Wilson TM, Cole JW, Stewart C, Cronin SJ, Johnston DM, 2010. Ash storm: impacts
25 901 of wind remobilised volcanic ash on rural communities and agriculture following
26 902 the 1991 Hudson eruption, southern Patagonia, Chile. *Bulletin of Volcanology*
27 903 doi:10.1007/s00445-010-0396-1
28
29 904 Wilson TM, Cole JW, Cronin SJ, Stewart C, Johnston DM. 2011. Impacts on
30 905 agriculture following the 1991 eruption of Volcán Hudson, Patagonia: lessons for
31 906 recovery. *Natural Hazards* **57**: 185-212.
32
33 907 Zimanowski B. 1998. Phreatomagmatic explosions. In: Freundt, A., Rosi, M. (Eds.),
34 908 From Magma to Tephra: Developments in Volcanology 4. Elsevier, Amsterdam,
35 909 pp. 25–54.
36
37
38
39
40
41
42
43
44
45

911 FIGURES

912 **Fig. 1. A, B.** The location of the study area in Llanquihue-Puerto Montt, Hornopirén,
913 Chaitén, Isla Grande de Chiloé and Esquel Sectors of northwestern Patagonia.
914 Coloured insets within Fig. 1B indicate the location of key transects presented in this
915 paper that detail the stratigraphy of Lepué Tephra. **C.** Extent of ice lobes within the
916 study area during the Last Glacial Maximum (LGM) (modified from Plates 1-4 in
917 **Denton *et al.* 1999**). Moraine ridges or hills are indicated in red and areas of present-
918 day permanent ice are indicated in black. The location of core ODP Site 1233

Alloway *et al.* - May 12th, 2017
JQS-16-0147-R1: SHAPE Special Volume

1
2
3 919 offshore of southern continental Chile is also indicated.

4
5 920

6
7 **Fig. 2.** Stratigraphic columns showing the correlation of Lepu  Tephra and
8 enveloping tephra beds from Section 7 located within Chait n township northward to
9 Section 5 at Puente  guila on Ruta 7 ~ 8.2-km south of Caleta Gonzalo.
10 923

11
12 924

13 **Fig. 3.** Lepu  Tephra at Sections 7 (A), 8 (B, C), 9 (D), 9D (E), 9B (F, G) and 5 (H)
14 that illustrate the complex internal architecture of magmatic (LT-m) and
15 phreatomagmatic (LT-phr-m) fall and flow (LT-sur) co-eruptive phases (see Fig. 2).
16 927

17
18 928

19 **Fig. 4.** The stratigraphy of Section 4 located on Ruta 7 on the southern side of the
20 pass connecting Lago Blanco (south) with Lago Negro (north). The stratigraphy at
21 this section reveals a prominent rhyolitic pumiceous lapilli (Cha-1 *sensu stricto*) dated
22 at *c.* 8700 ¹⁴C a BP and sourced from an ancestral Chait n Volcano. Cha-1 tephra
23 (now formally renamed Chana Tephra; Alloway *et al.* submitted) closely overlies a
24 lower fall and surge co-eruptive couplet (Lepu  Tephra) of presumed Michimahuida-
25 source. The surge deposit is directly dated at 11,483 ± 1034 cal. a BP (9960 ± 330 ¹⁴C
26 a BP; UCIAMS-145938). The spade is 1-m length; (B) Low-angle cross-bedding and
27 cross-cutting relationship of the surge across its co-eruptive fall deposit; (C) The
28 entire sequence is underlain by a widespread and distinctive layer of banded rhyolite
29 breccia (indicated by arrows) that likely represent an explosion of a pre-Cha-1/Chana
30 Tephra lava dome (ancestral VCha).
31 936
32 937
33 938
34 939
35 940
36 941

37
38 942

39 **Fig. 5.** Stratigraphic columns showing the correlation of Lepu  Tephra and
40 enveloping tephra beds from Section 5 at Puente  guila northwards to sections
41 located in the vicinity of Seno Reloncav  and Ral n. Note the closely overlying
42 occurrence of Cha-1 (now formally named Chana Tephra, see Alloway *et al.*
43 submitted) sourced from VCha.
44 946
45 947

46
47 948

48 **Fig. 6. A.** Massive > 40-m thick pyroclastic density current (PDC) deposit exposed at
49 Pumal n-1 (Pum-1) section along road W-887 located directly adjacent to R o
50 Michimahuida. This PDC-deposit correlates with Amarillo Ignimbrite of Amigo *et al.*
51 (2013) and is considered contemporaneous with Lepu  Tephra on the basis of its
52 equivalent stratigraphic position and age. Arrow indicates oriented, metre-sized, lithic
53 949
54 950
55 951
56 952
57
58
59
60

1
2
3 953 clast transported within this PDC; **B.** Typical PDC-internal architecture with
4 954 dispersed poorly sorted, angular, lithic clasts and rare charcoal fragments that are
5 955 dated at $11,190 \pm 88$ cal. a BP (9785 ± 30 ^{14}C a BP; LLNL-122960); **C.** Remnant
6 956 Amarillo Ignimbrite valley-infill surface viewed northwest from W-887 roadside
7 957 lookout ($42^\circ 55'18.33''$ S; $72^\circ 23' 46.99''$ W); ~ 436 -m asl). Note that this surface is
8 958 clearly inclined towards the Michimahuida massif (tMim).
9
10
11
12

13 959

14 960 **Fig. 7.** Stratigraphic columns showing the correlation of Lepu  Tephra and
15 961 enveloping tephra beds from Section Pumal n-3 southward to Santa Luc a-3 ~ 2.4 -km
16 962 north of the Sta. Luc a-Futaleuf  junction. Note the occurrence of a diamict (1.82 to
17 963 2.68-m below surface) within Sta. Luc a-1 containing fragmental rock clasts, wood
18 964 and organic rip-up clasts (dated at *c.* 9400 ^{14}C a BP; *c.* 10,600 cal. a BP). The internal
19 965 architecture strongly suggests deposition from a debris avalanche event. Although the
20 966 erosional base of this debris avalanche deposit is associated with a prominent tephra,
21 967 the two events do not appear to be chronologically related. On this basis it seems
22 968 more likely that this catastrophic avalanche event was probably triggered by tectonic
23 969 seismicity.
24
25
26
27
28
29
30

31 970

32
33 971 **Fig. 8.** Lepu  Tephra at Sections 1 (A), 13 (B) and 14 (C, D, E) of the southern
34 972 transect (see Fig. 7). Here, Lepu  Tephra is dominated by compact grey, poorly-sorted
35 973 and crudely stratified ‘lapilli-tuff’ deposits (phreatomagmatic phase) containing
36 974 dispersed centimetre-sized accretionary lapilli (D) and obvious open interstitial pore
37 975 spaces (E) indicative of rain flushing. No co-eruptive magmatic phase was identified.
38
39
40

41 976

42
43 977 **Fig. 9.** Stratigraphic columns showing the correlation of Lepu  Tephra and
44 978 enveloping tephra beds from Section Pumal n-2 eastwards to La Zeta 3-km west of
45 979 Esquel in Argentina. A lake record from Lago Espejo, Futaleuf , Chile is also
46 980 included to show correlation of Lepu  Tephra as well as rhyolitic tephra sourced from
47 981 an ancestral Volcan Chait n. The inset photo shows Lepu  Tephra as preserved
48 982 enveloped by paleolake sediments at La Zeta. Note the well-defined shower bedding
49 983 with a thin, well-sorted coarse ash base (initial magmatic phase) overlain by compact,
50 984 grey-coloured poorly-sorted massive structured very fine ash (phreatomagmatic
51 985 phase) followed by proportionally thicker normal-graded moderately well sorted very
52 986 coarse to fine ash (magmatic phase). This eruptive architecture is in accord with
53
54
55
56
57
58
59
60

Alloway *et al.* - May 12th, 2017
JQS-16-0147-R1: SHAPE Special Volume

1
2
3 987 features from more proximal localities that similarly indicate a complex
4 988 phreatomagmatic-magmatic eruption style for Lepué Tephra.

5
6 989

7
8 990 **Fig. 10.** Stratigraphic columns showing the correlation of Lepué Tephra along the
9 991 western transect from south-central Isla Grande de Chiloé northward towards Puerto
10 992 Montt in southernmost continental Chile. In northern sections (i.e. Huelmo and along
11 993 Ruta 5 connecting Pargua with Puerto Montt) Lepué Tephra is closely underlain by
12 994 intensely weathered andesitic ash and lapilli ‘ghosts’ that are most likely derived from
13 995 either Volcanes Calbuco or Yate located to the eastward along the Andean mountain
14 996 divide. These weathered tephra have yet to be geochemically characterized. At the La
15 997 Paloma site located between Puerto Montt and Alerce, Lepué Tephra forms a
16 998 continuous layer ~12-cm thick within peat and is closely overlain (~20-cm) by
17 999 discontinuous and irregularly thick (< 1-cm) of Cha-1 (Chana Tephra). The other
18 1000 photo inset shows the Lepué Tephra at its northernmost occurrence within Lago
19 1001 Pichilaguna, immediately west of Llanquihue township and 180-km northwest of
20 1002 Volcán Michimahuida. Here, Lepué Tephra occurs within core 1402AT3 at 382 to
21 1003 390-cm depth as a ~8-cm thick dark olive-grey, normal graded coarse to very fine ash.
22 1004 In this same vicinity, Lepué Tephra is not recognized macroscopically within the
23 1005 andic soil-forming environment.

24
25 1006

26 1007 **Fig. 11.** The variable morphological expression of Lepué Tephra within cover-bed
27 1008 sections (Queilen, Lago Natri, Chonchi, Castro, Puente Puntra and Chacao) in Isla
28 1009 Grande de Chiloé (see Fig. 10). The position of Lepué Tephra is indicated by yellow
29 1010 arrows. At all sections in this sector Lepué Tephra is the only macroscopic tephra
30 1011 observable within the cover-bed sequence and forms highly irregular, discontinuous
31 1012 pods of cemented fine ash. Typically in this sector, Lepué Tephra is enveloped by
32 1013 andic soil material and closely overlies colluvium, bedded fluvio-glacial gravels and
33 1014 sands and glacial diamictons (till). In cases where Lepué Tephra closely overlies
34 1015 impermeable glacial diamictons which seasonally perch the local water table, tephra
35 1016 colour is strongly altered to strong brown chromas, whereas Lepué Tephra enveloped
36 1017 by thicker successions of free-draining andic soil material typically have grey to pale
37 1018 brown chromas.

38
39 1019

40 1020 **Fig. 12.** Lepué Tephra occurring within cover-bed sections in southernmost

1
2
3 1021 continental Chile (San Augustin, Huelmo and Ruta 5 connecting Pargua with Puerto
4 1022 Montt). Sections (Caleta La Arena, 13-S7, 13-S8, Chapo S1) in the vicinity of Seno
5 1023 Reloncaví are also shown (see Figs. 5 and 10). Note that Cha-1 is now formally
6 1024 renamed Chana Tephra (Alloway *et al.*, submitted).
7
8
9

1025

10 1026 **Fig. 13.** Down-core inorganic densities (gr/cc) of lake sediments retrieved from Isla
11 1027 Grande de Chiloé (i.e. Quilque, Tarumán, Lepué, Melli and Tahui), coastal
12 1028 continental lakes and mires east of Golfo de Ancud (Lago Proschle and Puelche),
13 1029 south (i.e. Condorito, Huelmo, El Salto) and north (i.e. Pichilaguna) of Puerto Montt.
14 1030 The occurrence of Lepué Tephra is strongly indicated in all records and is closely
15 1031 overlain by a subordinate peak. This lesser peak (i.e. Isla Grande de Chiloé sites)
16 1032 likely coincides with a c. 8 cal. ka Chaitén-sourced rhyolitic cryptotephra (Puma
17 1033 Verde Tephra, see Alloway *et al.*, submitted), which unlike Lepué Tephra is not
18 1034 typically expressed macroscopically in adjacent andic soil cover-beds.
19
20
21
22
23
24
25

1035

26 1036 **Fig. 14.** Magnetic susceptibility (SI units; indicated in green) and alkenone-based Sea
27 1037 Surface Temperature estimates (°C) of ODP-202 Site-1233 (indicated in red). The
28 1038 position of calibrated radiocarbon ages are indicated on the right. The inset shows a
29 1039 prominent macroscopic tephra encapsulated within clay and silty clays between 14.52
30 1040 and 14.83-mcd and is accompanied by a prominent spike in magnetic susceptibility
31 1041 (916.8-m.mol^{-1} (SI)). Unfortunately, no radiocarbon dates were obtained directly
32 1042 associated with the upper and lower contacts of this tephra but bracketing radiocarbon
33 1043 samples from 12.94 and 17.01-mcd yielded calibrated ages of 10,040 and 12,260 cal.
34 1044 a BP, respectively.
35
36
37
38
39
40
41
42

1045

43 1046 **Fig. 15.** Weighted mean modeled age determination (9588 ± 20 ^{14}C a BP) for Lepué
44 1047 Tephra based on four R-combine-statistically grouped samples (UCIAMS-145938,
45 1048 LLNL-158290, LLNL-123032 and LLNL-12329) from Sections 4, 12A, Pichileufú
46 1049 and Puelche, respectively. Three ^{14}C sample outliers from Sections 9, 12A and
47 1050 Pumalín -1, (LLNL-158125, LLNL-158291 and LLNL-122960) were rejected. The
48 1051 Southern Hemisphere terrestrial calibration curve (SHCal13) and OxCal Program
49 1052 (v.4.2.4) were used for all samples radiocarbon dated in this study.
50
51
52
53
54
55

1053

56 1054 **Fig. 16.** Modeled ages determinations of Lepué Tephra from Huelmo mire (Moreno
57
58
59
60

1
2
3 1055 and Leon, 2003), L. Condorito (Moreno, 2004), L. Tahui (Abarzúa *et al.*, 2004), L.
4 1056 Melli (Abarzúa and Moreno, 2008) and L. Lepué (Pesce and Moreno, 2014).
5
6 1057 Modelled ages are arranged according to intervals (cm) sampled with respect to the
7
8 1058 basal contact of Lepué Tephra. Error bars represent $\pm 2 \sigma$. A weighted mean modeled
9
10 1059 age determination of 9725 ± 23 ^{14}C a BP for Lepué Tephra is based on eight R-
11 1060 combine-statistically grouped samples from Huelmo mire (ETH-20386), L. Condorito
12 1061 (A8069), L. Tahui (NSRL-12473 and GX28215), L. Melli (ETH-25249) and L. Lepué
13 1062 (CAMS-125915 and ETH-25451). The associated mean age of $10,994 \pm 124$ cal. a BP
14 1063 is indistinguishable from a mean age of $10,909 \pm 228$ cal. a BP determined for Lepué
15 1064 Tephra from Chaitén (S-4, S-12A), Puelche and Pichileufú (this study; Fig. 5).
16
17
18
19
20

21 1065
22 1066 **Fig. 17.** Map of the study area indicating the maximum-recorded thicknesses (in
23 1067 centimetres) of Lepué Tephra occurring within andic soil cover-bed sections. At any
24 1068 one site, it is usually very difficult to derive a representative thickness for the
25 1069 pocketed, highly irregular and variably thick Lepué Tephra. Thickness values from
26 1070 lake cores are also shown and indicate considerable thickness differences between
27 1071 adjacent soil and lacustrine depositional environments. Large thickness variations
28 1072 were also noted between closely situated closed basin lakes suggesting that either
29 1073 tephra thickness measurements made from previous studies may not have
30 1074 distinguished between primary and secondarily tephric inputs or perhaps, the
31 1075 existence of more complex sedimentary inputs to these lake systems.
32
33
34
35
36
37
38

39 1076
40 1077 **Fig. 18.** Selected back-scatter electron (BSE) images of glass shards from Lepué
41 1078 Tephra correlatives showing the varying concentration of dominantly plagioclase
42 1079 microlites within their glassy matrix (A, B – lowermost Lepué, Section 4; C –
43 1080 lowermost Lepué, Section 5; D – uppermost Lepué, Section 5; E - 1819-1821 cm, L.
44 1081 Lepué; F - 1831-1838 cm, L. Lepué; G – Lepué Tephra, Puente Puntra, Isla Grande
45 1082 de Chiloé; H – 14.68 m, ODP-1233D). Low microlite concentrations were observed
46 1083 within glassy grains at base of the tephra (onset of the Lepué eruption; A, B, C),
47 1084 however, the microlite concentration within the matrix of glassy grains significantly
48 1085 increases (D, E, F) progressively upwards within the tephra deposit. In distal
49 1086 localities, the overwhelming dominance of glass grains containing profuse microlites
50 1087 made it very difficult and in many cases, impossible for 10-20 μm diameter electron
51
52
53
54
55
56
57
58
59
60

1
2
3 1088 and laser beams to be positioned on glass and without any obvious microlite
4 1089 contamination (i.e. **G, H**). Note that as the microlite concentration increases, the
5 1090 proportion of well-formed oriented vesicles decrease with a corresponding increase in
6 1091 irregular shaped (collapsed) and coalesced voids (**D, F**).
7
8
9

10 1092

11 1093 **Fig. 19.** Selected major element compositions (weight percent SiO_2 vs $\text{Na}_2\text{O} + \text{K}_2\text{O}$
12 1094 and FeO vs K_2O and CaO) of glass shards from Lepu  Tephra correlatives. Two glass
13 1095 end members, microlite-poor and microlitic, are plotted to show compositional and
14 1096 elemental concentration differences occurring between these two end members. All
15 1097 post-18,000 cal. a BP Chait n-sourced tephra are plotted for comparison.
16
17
18
19

20 1098

21 1099 **Fig. 20.** Nd vs Th and Sr vs Y, Ho, Nd, Zr compositions of glass shards from Lepu 
22 1100 Tephra correlatives determined by grain discrete LA-ICP-MS analysis. Microlite-poor
23 1101 and microlitic glass data are plotted and show significant concentration differences
24 1102 between these two glass types associated with the ablation of (dominantly)
25 1103 plagioclase with glass. The microlite-poor glass compositions occur between 73 -113
26 1104 ppm Sr, and these analyses are indicated on the plot of Nd vs Th. See text for
27 1105 explanation.
28
29
30
31
32

33 1106

34 1107 **Fig. 21.** Th vs Zr (ppm) plots as determined by bulk sample solution-ICP-MS analysis
35 1108 showing Lepu  Tephra correlatives from proximal and distal (continental Chile and
36 1109 Isla Grande de Chilo ). These results are compared with individually analysed
37 1110 accretionary lapilli from seven proximal Lepu  Tephra localities. Tephra beds of
38 1111 presumed MimVC-source stratigraphically associated with Lepu  Tephra are plotted
39 1112 for comparison.
40
41
42
43
44

45 1113

46 1114 **Fig. 22.** Sections containing analysed proximal tephra beds sourced from satellite
47 1115 MimVC monogenetic scoria cones. Inset map shows the location of associated
48 1116 satellite MimVC monogenetic scoria cone complexes and lava flows, sections
49 1117 containing analysed Lepu  Tephra and Amarillo Ignimbrite and its remnant valley-fill
50 1118 surface.
51
52
53
54

55 1119

56 1120 **Fig. 23.** SiO_2 vs $\text{Na}_2\text{O} + \text{K}_2\text{O}$ (wt. %) compositions of glass shards from **A.** proximal-
57 1121 distal Lepu  Tephra compared with proximal tephra beds sourced from satellite
58
59
60

Alloway *et al.* - May 12th, 2017
JQS-16-0147-R1: SHAPE Special Volume

1
2
3 1122 MimVC monogenetic scoria cones, and **B.** post-11,000 cal. a BP tephra beds from L.
4 1123 Teo (Moreno *et al.*, 2014). All tephra beds (except Pum 4-T7) as well as Group 2 and
5 1124 3 tephra inter-beds from L. Teo occur on the same fractional crystallisation pathway
6 1125 as analysed Lepué Tephra. The compositions of all post-18,000 cal. a BP. Chaitén-
7 1126 sourced tephra are indicated for comparison.
8
9
10

1127

1128 **Fig. 24.** Pollen percentage curves of key taxa from 6 sites (arranged south to north; L.
1129 Melli, L. Tahui, L. Lepué, L. El Salto, Huelmo mire and L. Condorito; see Fig. 17)
1130 between 8000 and 15,000 cal. a BP Background blue represents an interval of
1131 interpreted cold/wet climate, green - an interval of cold and seasonally dry climate,
1132 and pink – an interval of warm and dry climate. Lepué Tephra occurs at all sites and
1133 its position within each record is indicated (LT).
1134

1134

1135 **Fig. 25.** A schematic model for Lepué Tephra and its co-eruptive PDC (Amarillo
1136 Ignimbrite). **A.** A zoned magma body within the MimVC sub-volcanic system
1137 comprising a volatile-rich cap of dominantly fractionated glass occurring on top of a
1138 more mafic phenocryst-rich magma; **B.** Explosive phreatomagmatic eruption
1139 involving snow and ice from tMim and dominantly upward thrust of volatile-rich
1140 fractionated magma forming a stable column with associated fall dominated by
1141 aphyric glass; Episodic moist convection generates flanking PDC deposits; **C.** As the
1142 eruption continues, magma withdrawal steadily propagates downwards into the
1143 underlying crystal-rich magma and results in a fall increasingly dominated by
1144 microphenocrysts with very minor interstitial melt; Intensified water vaporisation
1145 results in heightened convection and plume instability; **D.** Continued oscillations
1146 between buoyant (dry) and wet eruptive phases leads to the development of a
1147 multilevel plume; Continued sustained moist convection and climactic plume collapse
1148 generates the Amarillo Ignimbrite.
1149

1149

1150 **Table Captions**

1151 **Table 1.** Radiocarbon dates and ages associated with Lepué Tephra and its distal
1152 correlatives. The Southern Hemisphere terrestrial calibration curve (SHCal13) and
1153 OxCal Program (v.4.2.4) were used for all radiocarbon samples dated in this study.
1154

1154

1
2
3 1155 **Table 2.** Summary of individual glass shard major-element compositions (normalised
4 1156 to an anhydrous basis) of proximal to distal Lepué Tephra in the Chaitén, Isla Grande
5 1157 de Chiloé and Esquel Sectors of NW Patagonia.
6
7
8 1158

9
10 1159 **Table 3.** Summary of individual glass shard trace-element compositions of proximal
11 1160 to distal Lepué Tephra in the Chaitén, Isla Grande de Chiloé and Esquel Sectors of
12 1161 NW Patagonia obtained by LA-ICP-MS at Aberystwyth. All concentrations in ppm
13 1162 unless otherwise stated.
14
15 1163

16
17 1164 **Table 4.** All trace-element concentrations from bulk Lepué Tephra correlative samples
18 1165 obtained by Solution-nebulisation-ICP-MS at Aberystwyth University, Wales. All
19 1166 concentrations in ppm unless otherwise stated.
20
21 1167

22 1168 **SUPPLEMENTARY INFORMATION**

23 1169

24 1170 **METHODS**

25 1171 **Electron Microprobe (EMP) technique**

26 1172 Major-element determinations were made on a JEOL Superprobe (JXA-8230)
27 1173 housed at Victoria University of Wellington, using the ZAF correction method.
28 1174 Analyses were performed with 15 kV accelerating voltage, 8 nA beam current, and an
29 1175 electron beam defocused to between 20 to 10 μm . Standardization was achieved by
30 1176 means of mineral and glass standards. A rhyolitic glass standard (ATHO-G) was
31 1177 routinely used to monitor calibration in all analytical runs, and used to evaluate any
32 1178 day-to-day differences in the calibration. The large number of samples precluded
33 1179 conducting all analyses in a single batch. All analyses are normalized to 100 wt. %
34 1180 anhydrous, with H₂O by difference being given, and total Fe is reported as FeO. Glass
35 1181 shard major-element analyses are presented in [Table 2](#). All analyses are available
36 1182 upon request to the corresponding author.
37
38 1183

39 1184 **Laser ablation inductively coupled plasma-mass spectrometry (LA-ICP-MS)** 40 1185 **technique**

41 1186 Trace-element analyses on individual glass shards were performed by laser
42 1187 ablation (LA) ICP-MS in the Department of Geography and Earth Sciences,
43
44
45
46
47
48
49
50
51
52
53
54
55
56
57
58
59
60

Alloway *et al.* - May 12th, 2017
JQS-16-0147-R1: SHAPE Special Volume

1
2
3 1188 Aberystwyth University, using a Coherent GeoLas ArF 193 nm Excimer LA system
4 1189 coupled to a Thermo Finnegan Element 2 sector field ICP-MS. Trace element data
5 1190 were collected for individual shards with the majority of analyses performed using 20
6
7 1191 μm ablation craters. Laser fluence was 10 Jcm^{-2} at a repetition rate of 5 Hz for a 24
8 1192 second acquisition. The minor ^{29}Si isotope was used as the internal standard, with
9 1193 SiO_2 (determined by EMPA) used to calibrate each analysis, after normalization to an
10 1194 anhydrous basis. The NIST 612 reference glass was used for calibration, taking
11 1195 concentrations from [Pearce *et al.* \(1997\)](#). A fractionation factor was applied to the
12 1196 data to account for analytical bias related to the different matrices of the reference
13 1197 standard and the sample. For this factor as well as ICP-MS and laser operating
14 1198 conditions see [Pearce *et al.* \(2011\)](#), and references therein. The MPI-DING reference
15 1199 glass ATHO-G ([Jochum *et al.* 2006](#)) was analysed as an unknown under the same
16 1200 operating conditions at the same time. Analytical precision is typically between ± 5 -
17 1201 10%, and accuracy is typically around $\pm 5\%$, when compared with the published
18 1202 GeoReM concentrations for ATHO-G. Glass shard trace-element analyses are
19 1203 presented in [Table 3](#).
20
21
22
23
24
25
26
27
28
29
30

1204

1205 **Solution nebulisation inductively coupled plasma mass spectrometry (ICP-MS)** 1206 **technique**

1207

1208 Dried bulk samples were crushed and homogenised using an agate mortar and
1209 pestle to a fine powder and bagged. To ensure no sample cross-contamination
1210 occurred, all crushing equipment was washed with $18.2 \text{ M}\Omega$ deionised H_2O
1211 (MilliQ®), 5% HCl (hydrochloric acid) and 5% HNO_3 (nitric acid) between the each
1212 sample. Subsequently, 0.25 g of each homogenised sample was weighed into
1213 polytetrafluoroethylene (PTFE) beakers ready for standard HF/ HClO_4 acid digestion
1214 (performed by Andy Brown in the Geochemistry Laboratory, DGES). Initially
1215 samples were treated with 5 mL concentrated HCl and evaporated to dryness,
1216 followed by an open HF/ HClO_4 digestion (15 mL/4 mL) which was left cold
1217 overnight before evaporation to dryness at about 170°C . A second HF/ HClO_4
1218 digestion was used if needed. Once dry, 4 mL of HClO_4 was added to each sample
1219 and evaporated to dryness to remove any residual HF, and the samples were then
1220 taken up to a final volume of 250 ml in 2.5% HCl and stored in Nalgene™ sample
1221 bottles ready for analysis by solution nebulisation Inductively Coupled Plasma – Mass
1222 spectrometry (SN-ICP-MS) to determine their trace-element content in the

1
2
3 1223 Department of Geography and Earth Sciences, Aberystwyth University. All acids
4 1224 were AnalaR grade or better, and blanks were prepared with all batches of samples.
5
6 1225 Analyses were performed on and Agilent 7700 ICP-MS, which determined a range of
7
8 1226 trace elements, with low masses (<52) determined using He as a collision gas to
9
10 1227 reduce polyatomic interferences (He-mode). Calibration was achieved against multi-
11 1228 element synthetic standards produced from stock single element standard solutions,
12 1229 and Te was used as the internal standard for analyses. Some samples were prepared in
13
14 1230 triplicate and dispersed through the analytical run, and indicate analytical precision is
15
16 1231 better than 4% on average (although this varies with within element concentration
17 1232 etc., see [Pearce *et al.* 2004](#)). Two reference materials (USGS QLO-1 Quartz Latite
18 1233 and GSJ JA-3 Andesite) were routinely analysed to check accuracy. Analyses are
19 1234 presented in [Table 4](#).

1235

24 1236 Pearce NJG, Westgate JA, Perkins WT and Preece SJ. 2004. The application of ICP-
25 1237 MS methods to tephrochronological problems. *Applied Geochemistry* **19**: 289-
26 1238 322.

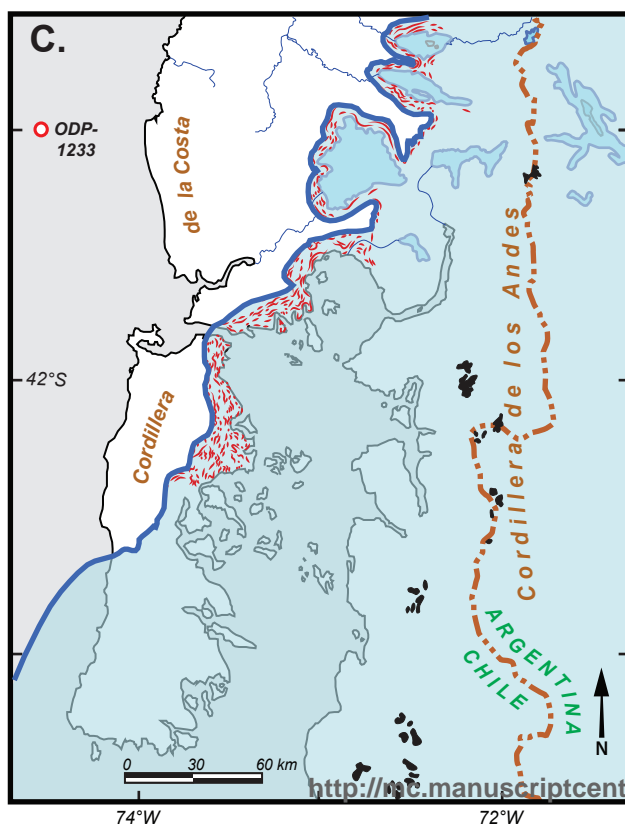
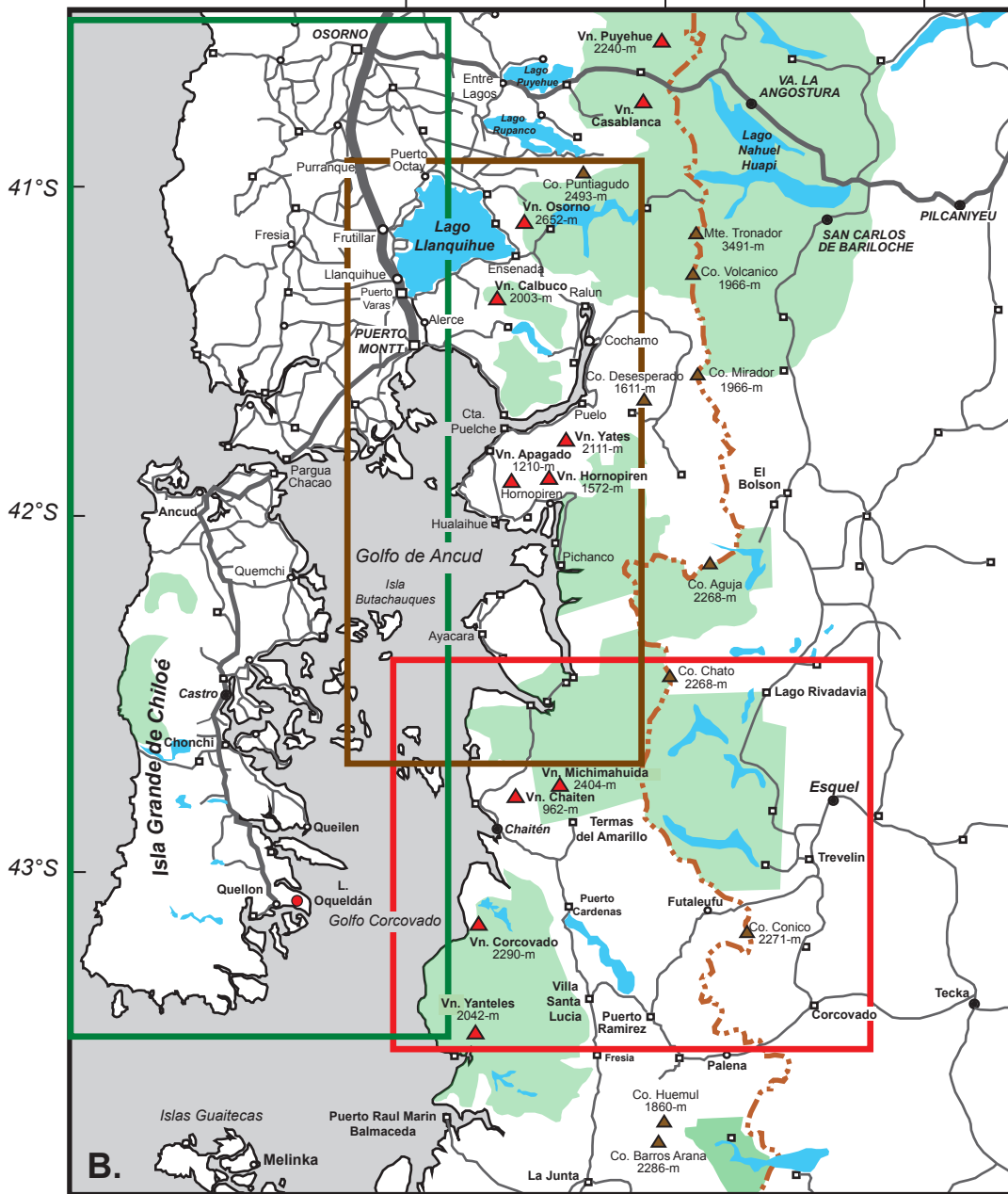
29 1239 Pearce NJG. *et al.* 1997. A compilation of new and published major and trace element
30 1240 data for NIST SRM 610 and NIST SRM 612 glass reference materials.
31 1241 *Geostandards Newsletter* **21**: 115-144.

34 1242 Pearce, NJG. *et al.* 2011. Trace-element analysis by LA- ICP-MS: the quest for
35 1243 comprehensive chemical characterisation of single sub-10um volcanic glass
36 1244 shards. *Quaternary International* **246**: 57-81.

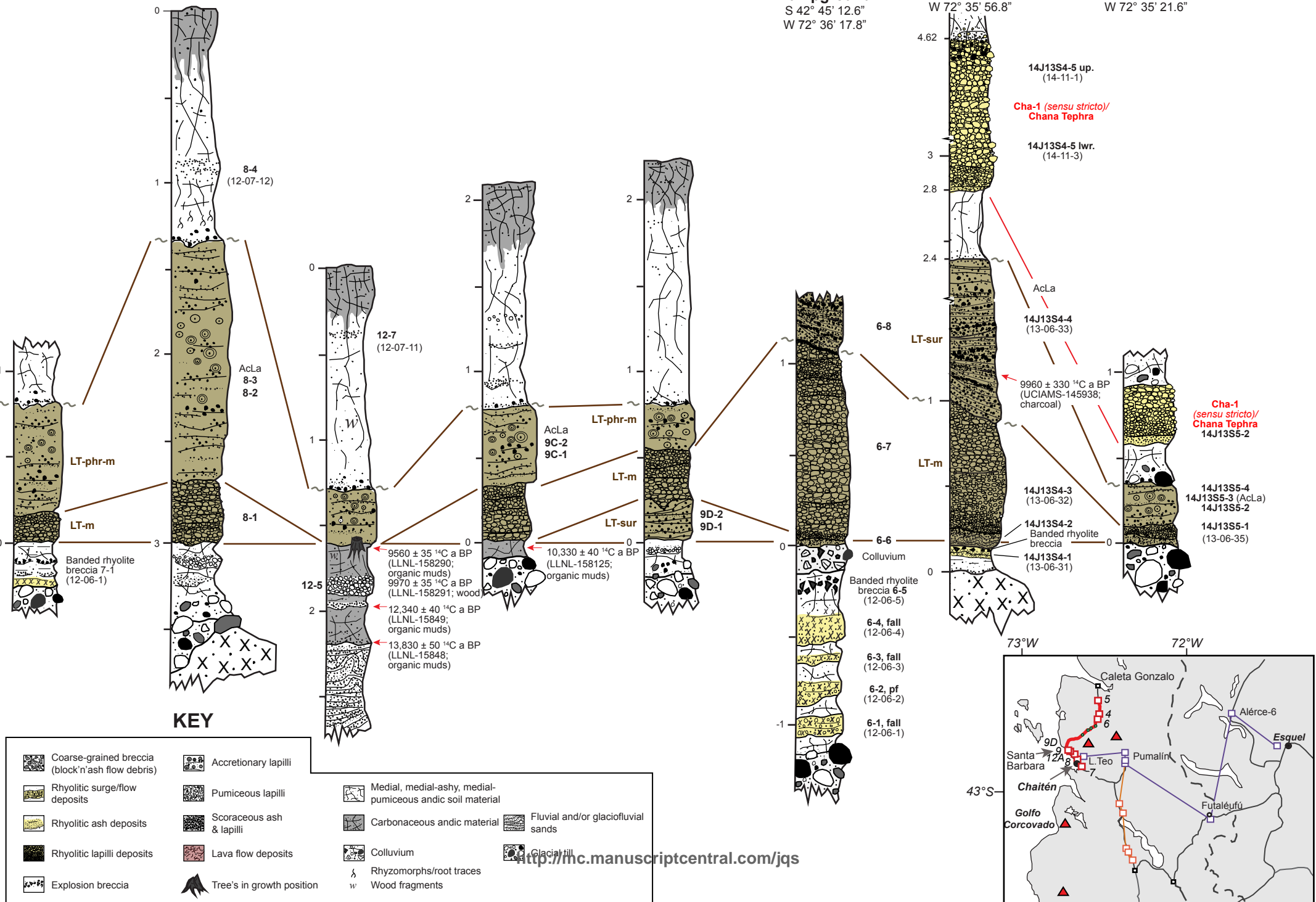
39 1245 Jochum, KP, Stoll B, Herwig K. *et al.* 2006. MPI-DING reference glasses for in situ
40 1246 microanalysis: new reference values for element concentrations and isotope
41 1247 ratios. *Geochemistry, Geophysics, Geosystems* **7**: Q02008,
42 1248 doi:02010.01029/02005GC001060.

1249

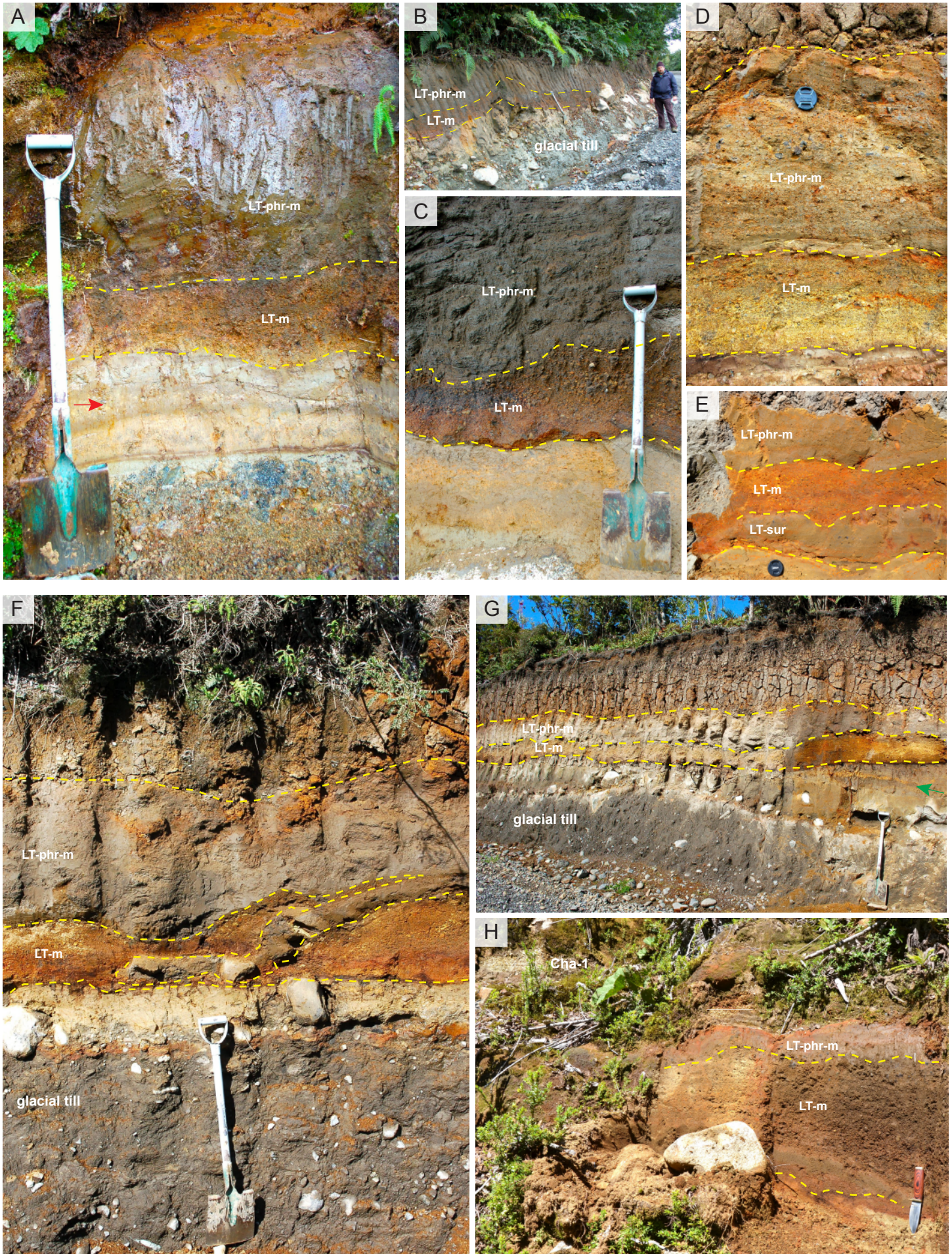
1
2
3
4
5
6
7
8
9
10
11
12
13
14
15
16
17
18
19
20
21
22
23
24
25
26
27
28
29
30
31
32
33
34
35
36
37
38
39
40
41
42
43
44
45
46
47
48
49
50
51
52
53
54
55
56
57
58
59
60



1
2
3
4
5
6
7
8
9
10
11
12
13
14
15
16
17
18
19
20
21
22
23
24
25
26
27
28
29
30
31
32
33
34
35
36
37
38
39
40
41
42
43
44
45
46
47



1
2
3
4
5
6
7
8
9
10
11
12
13
14
15
16
17
18
19
20
21
22
23
24
25
26
27
28
29
30
31
32
33
34
35
36
37
38
39
40
41
42
43
44
45
46
47
48
49
50
51
52
53
54
55
56
57
58
59
60

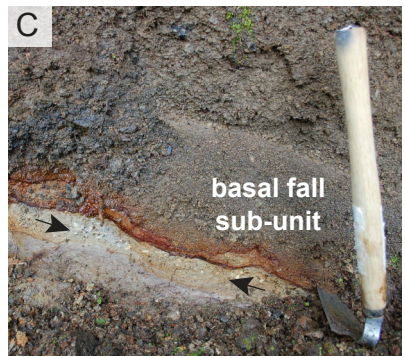
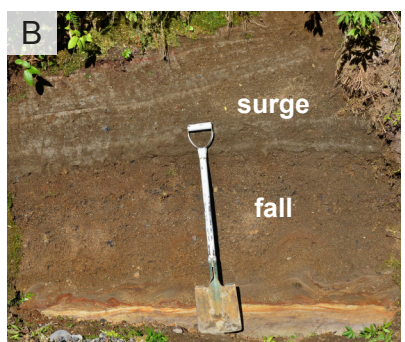
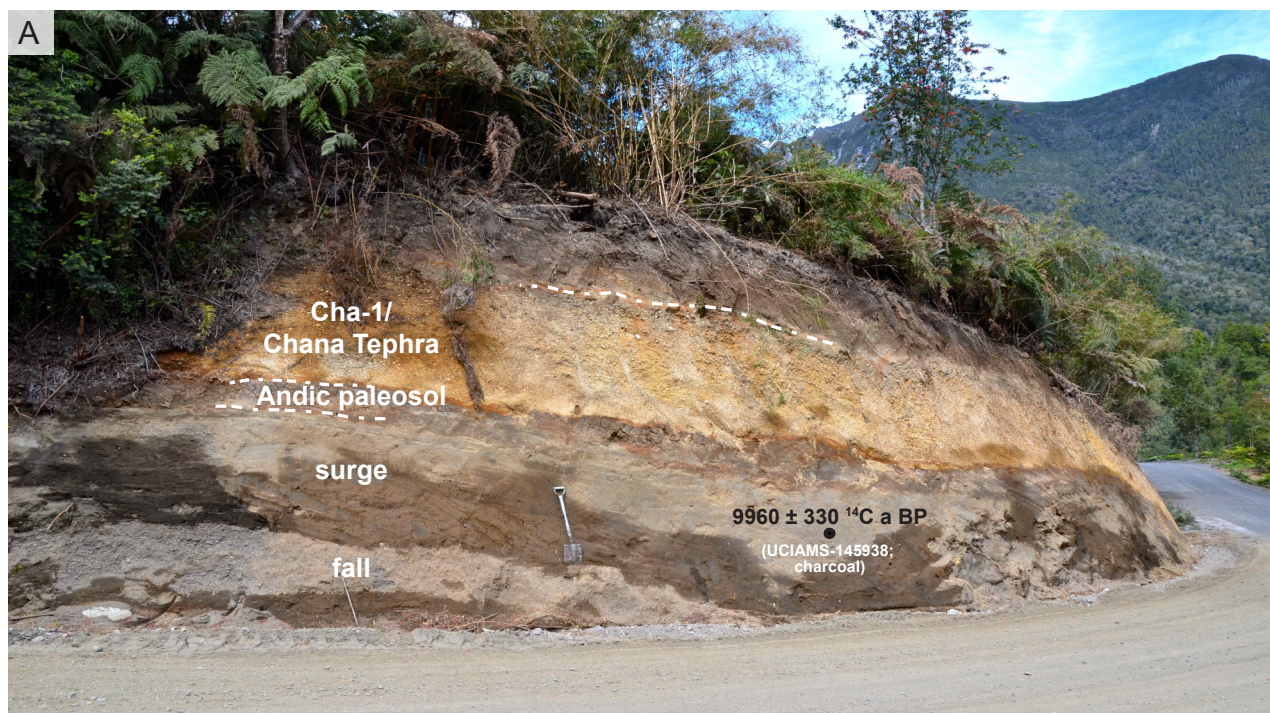
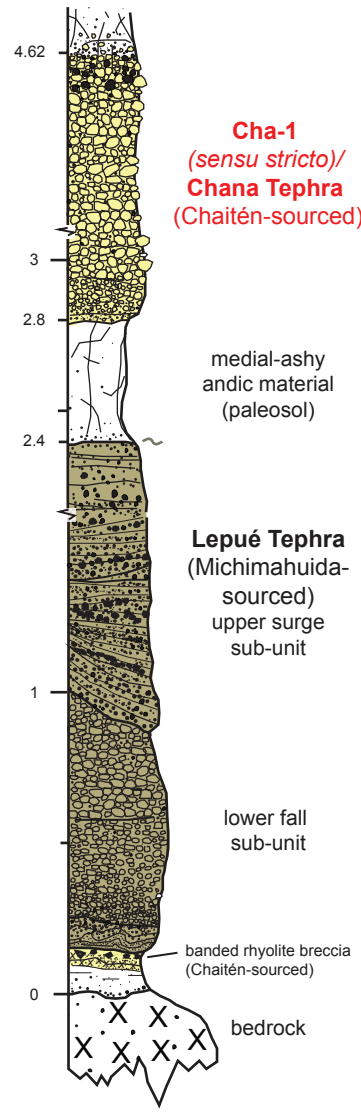


Paso Lago Blanco

(Section 4)

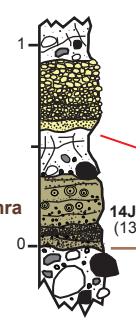
Parque Pumalín,
Chaitén Sector
(S 42° 43' 39.6"
W 72° 35' 56.8")

- 1
- 2
- 3
- 4
- 5
- 6
- 7
- 8
- 9
- 10
- 11
- 12
- 13
- 14
- 15
- 16
- 17
- 18
- 19
- 20
- 21
- 22
- 23
- 24
- 25
- 26
- 27
- 28
- 29
- 30
- 31
- 32
- 33
- 34
- 35
- 36
- 37
- 38
- 39
- 40
- 41
- 42
- 43
- 44
- 45
- 46
- 47

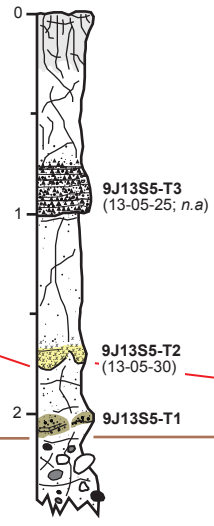


1
2
3
4
5
6
7
8
9
10
11
12
13
14
15
16
17
18
19
20
21
22
23
24
25
26
27
28
29
30
31
32
33
34
35
36
37
38
39
40
41
42
43
44
45
46
47

**Puente Águila
Section 5**
S 42° 37' 29.5"
W 72° 35' 21.6"

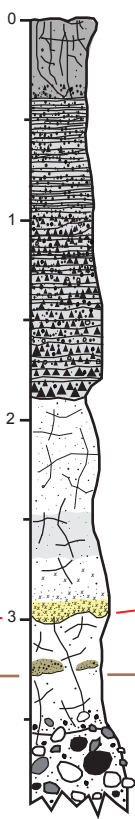


Cholgo
S 42° 04' 31.0"
W 72° 27' 23.5"

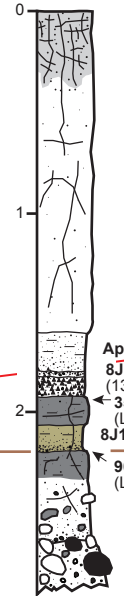


n.a - not analysed

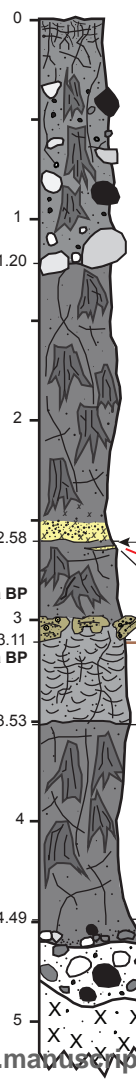
Hornopirén
S 41° 56' 49.0"
W 72° 29' 41.9"



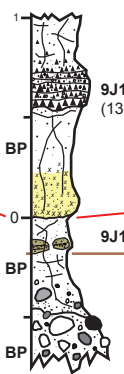
Pte Pichileufú
S 41° 58' 00.4"
W 72° 40' 19.6"



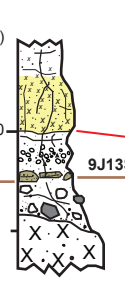
Puelche
S 41° 44' 46.0"
W 72° 39' 28.4"



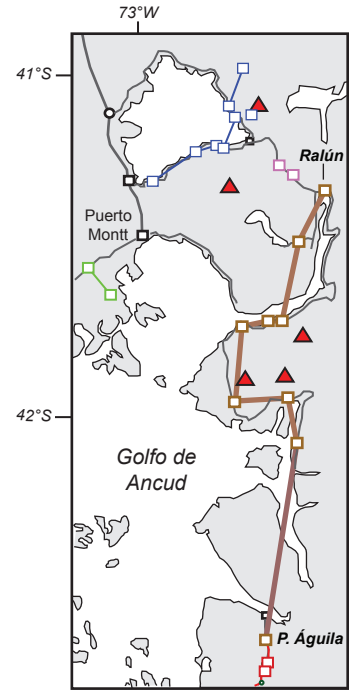
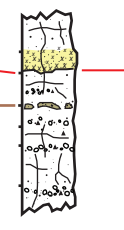
**Seno Reloncaví
13-S7**
S 41° 43' 29.0"
W 72° 30' 26.8"



**Seno Reloncaví
13-S8**
S 41° 43' 27.0"
W 72° 30' 11.2"



Chapo-S1
S 41° 30' 52.2"
W 72° 21' 02.4"



Ralún
S 41° 22' 56.1"
W 72° 18' 18.0"



Cha-1/Chana Tephra
← 8625 ± 25 14C a BP (LLNL-122961; charcoal)
← 8970 ± 30 14C a BP (UCIAMS-145484; charcoal)



1
2
3
4
5
6
7
8
9
10
11
12
13
14
15
16
17
18
19
20
21
22
23
24
25
26
27
28
29
30
31
32
33
34
35
36
37
38
39
40
41
42
43
44
45
46
47

Pumalín-3

10.3 km from Ruta 7-
Termas El Amarillo
road junction
(10.020 road marker)
S 42° 57' 49.6"
W 72° 24' 06.4"

Section 13

S 43° 08' 34.9"
W 72° 26' 26.1"

Section 1
(south-side)

S 43° 09' 49.3"
W 72° 25' 44.8"

Sta. Lucía-1

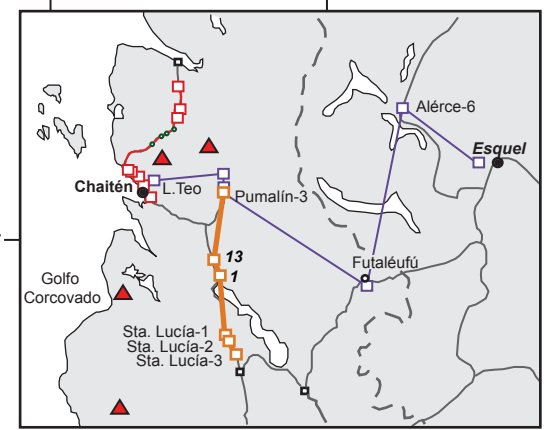
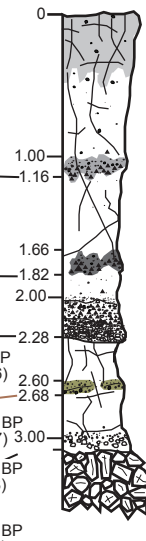
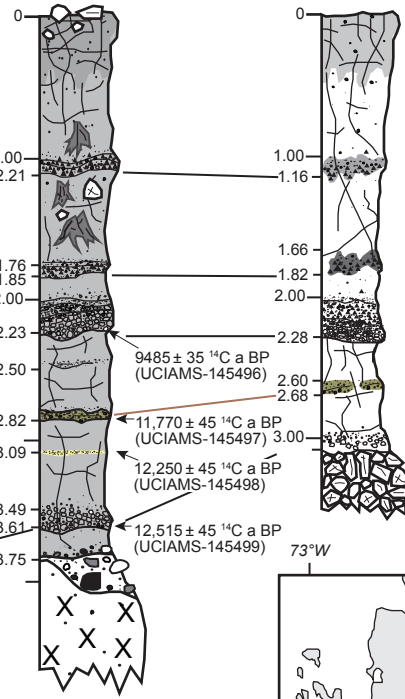
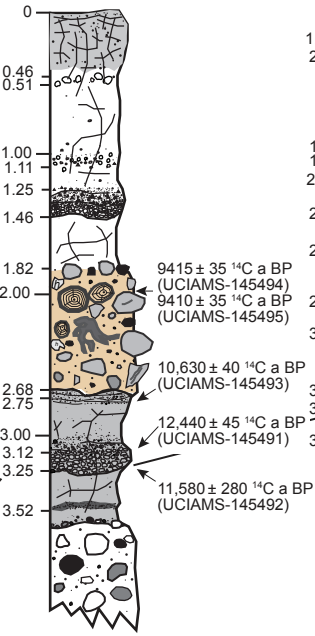
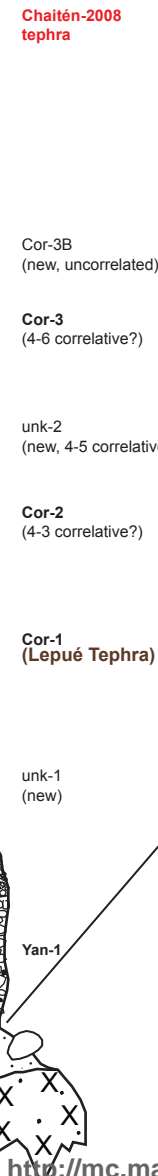
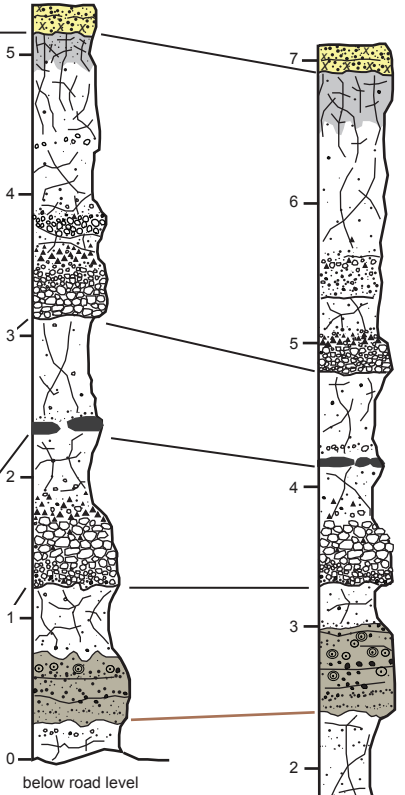
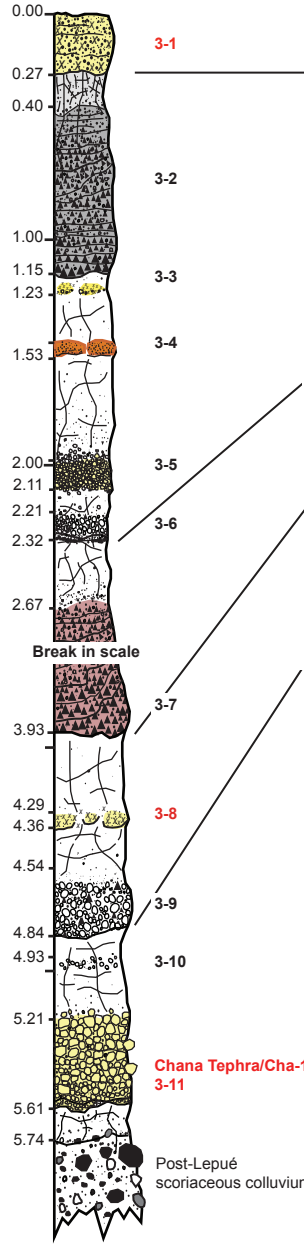
24.3-km south of
Puente Yelcho
(70.060 Road Marker)
S 43° 21' 43.3"
W 72° 23' 28.7"

Sta. Lucía-2

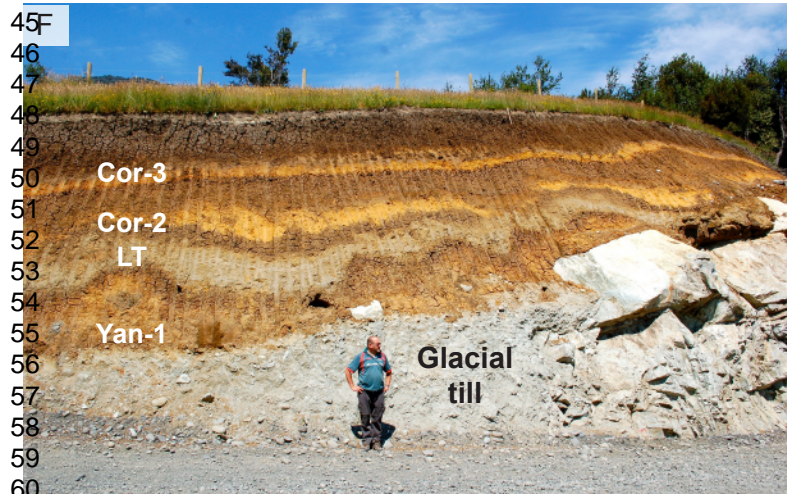
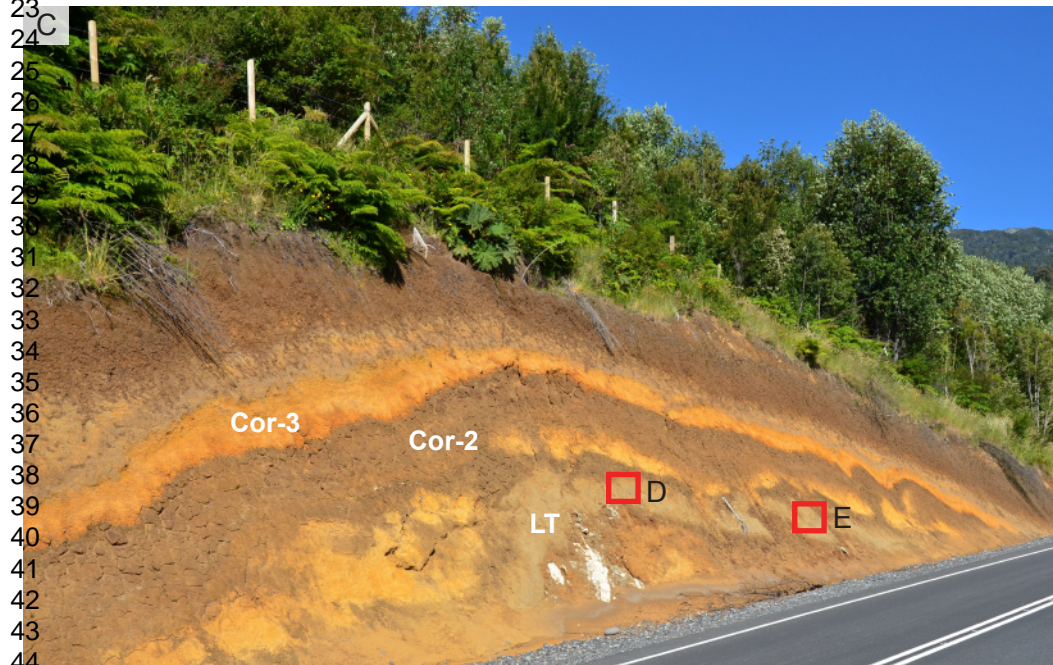
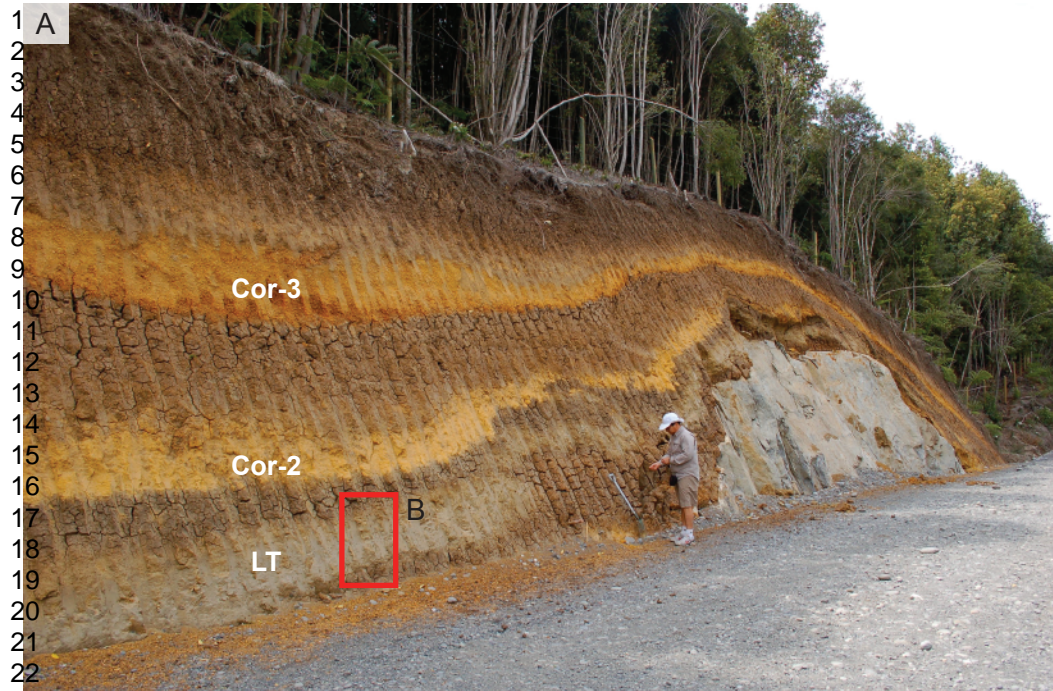
25-km south of
Puente Yelcho
(70.760 Road Marker)
S 43° 22' 01.1"
W 72° 23' 09.9"

Sta. Lucía-3

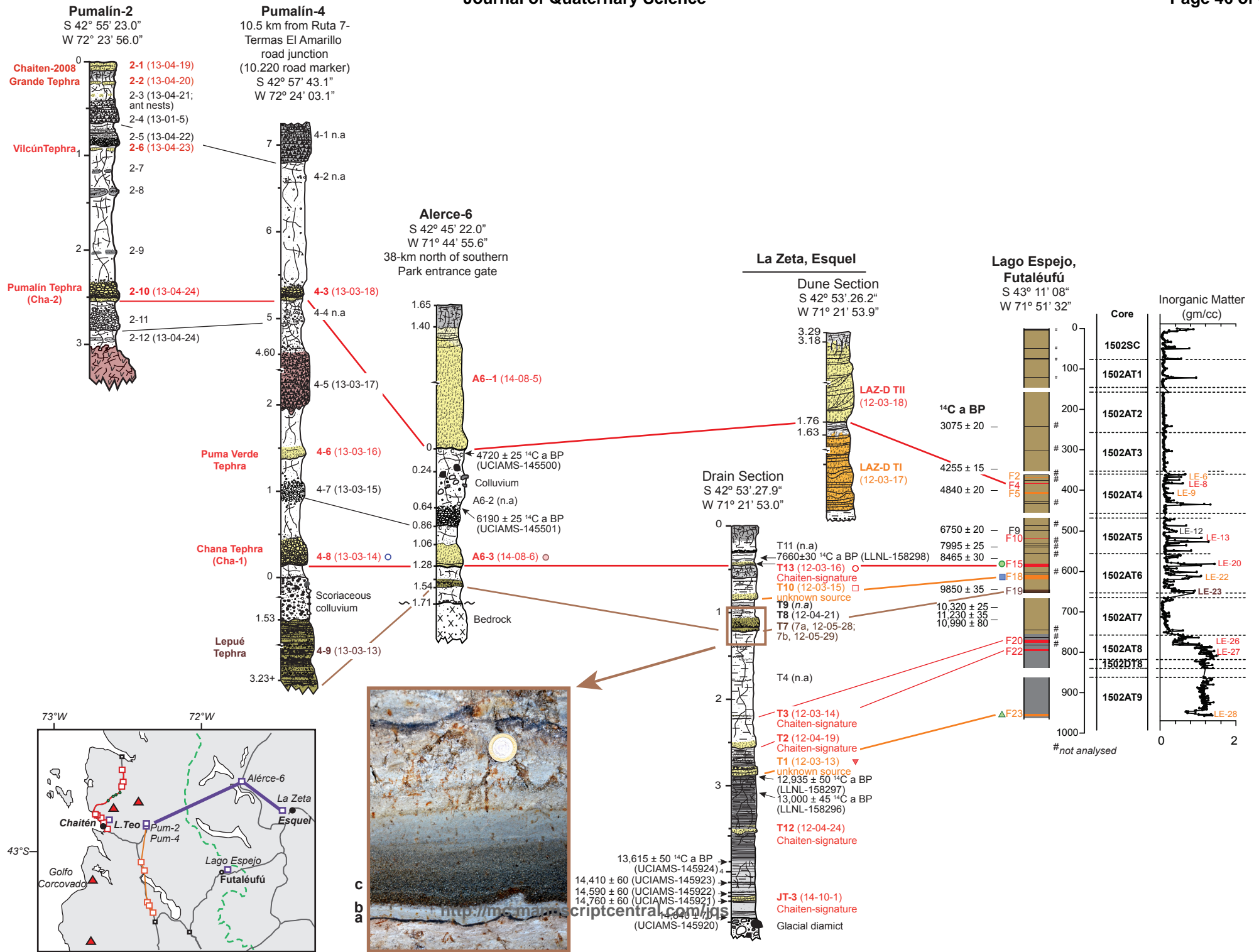
2.4-km north of
Sta. Lucía-Futaléufú
junction
S 43° 23' 25.0"
W 72° 22' 22.3"

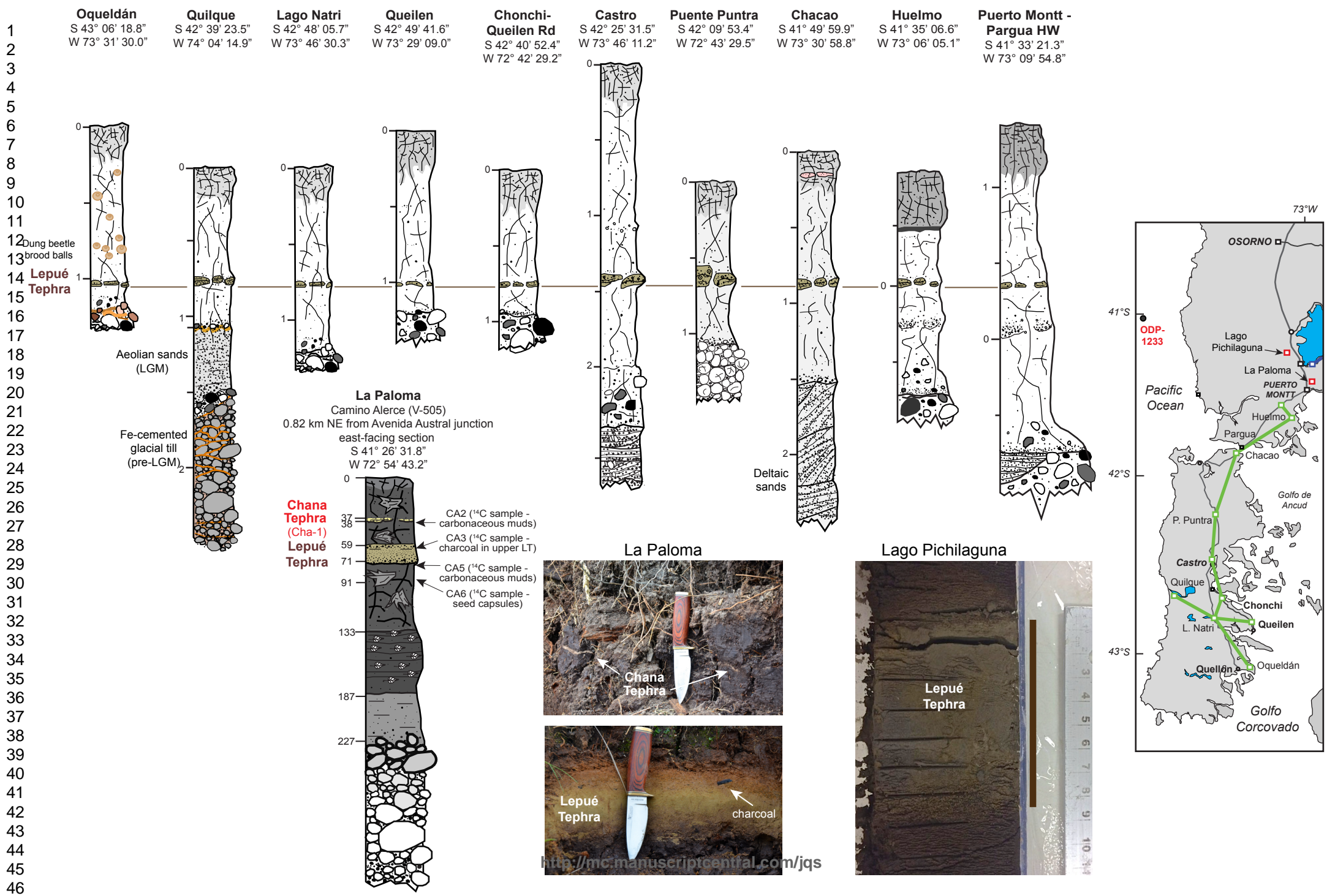


NOTE change in vertical scale

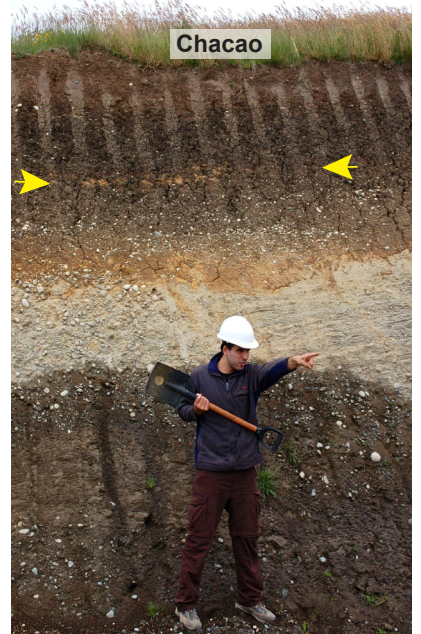


1
2
3
4
5
6
7
8
9
10
11
12
13
14
15
16
17
18
19
20
21
22
23
24
25
26
27
28
29
30
31
32
33
34
35
36
37
38
39
40
41
42
43
44
45
46
47

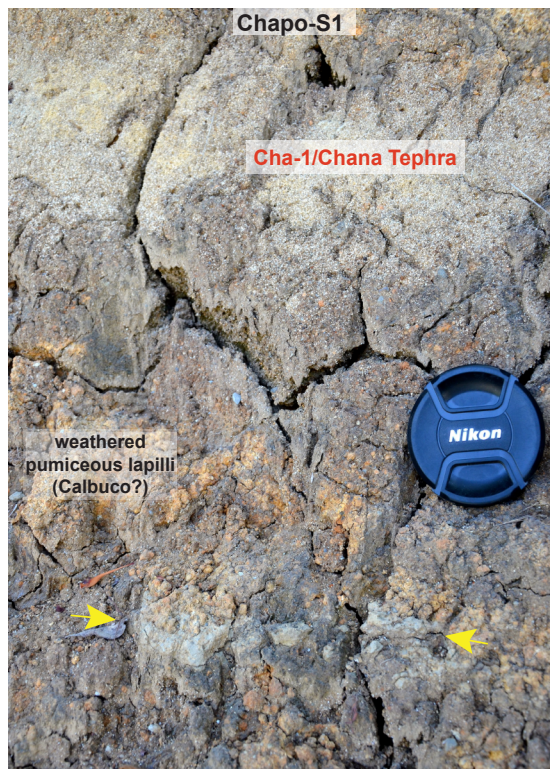
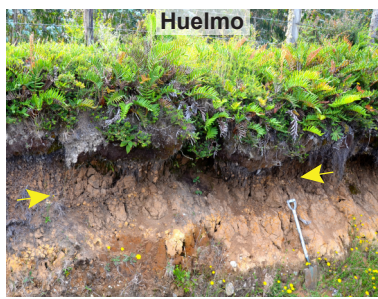
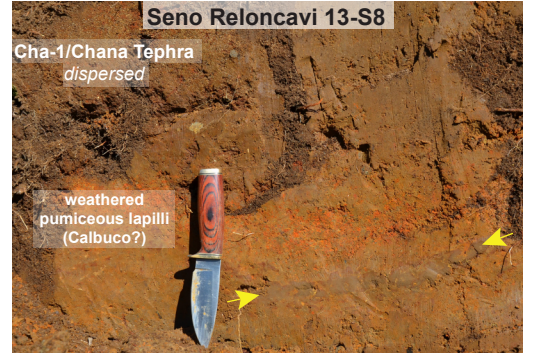
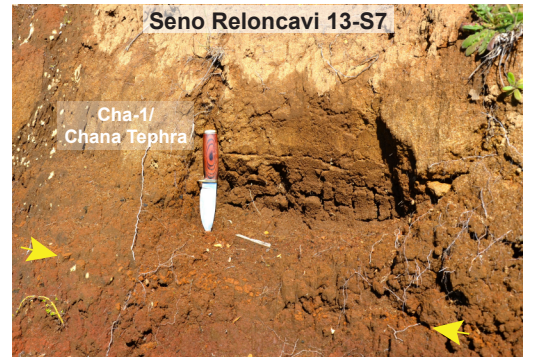




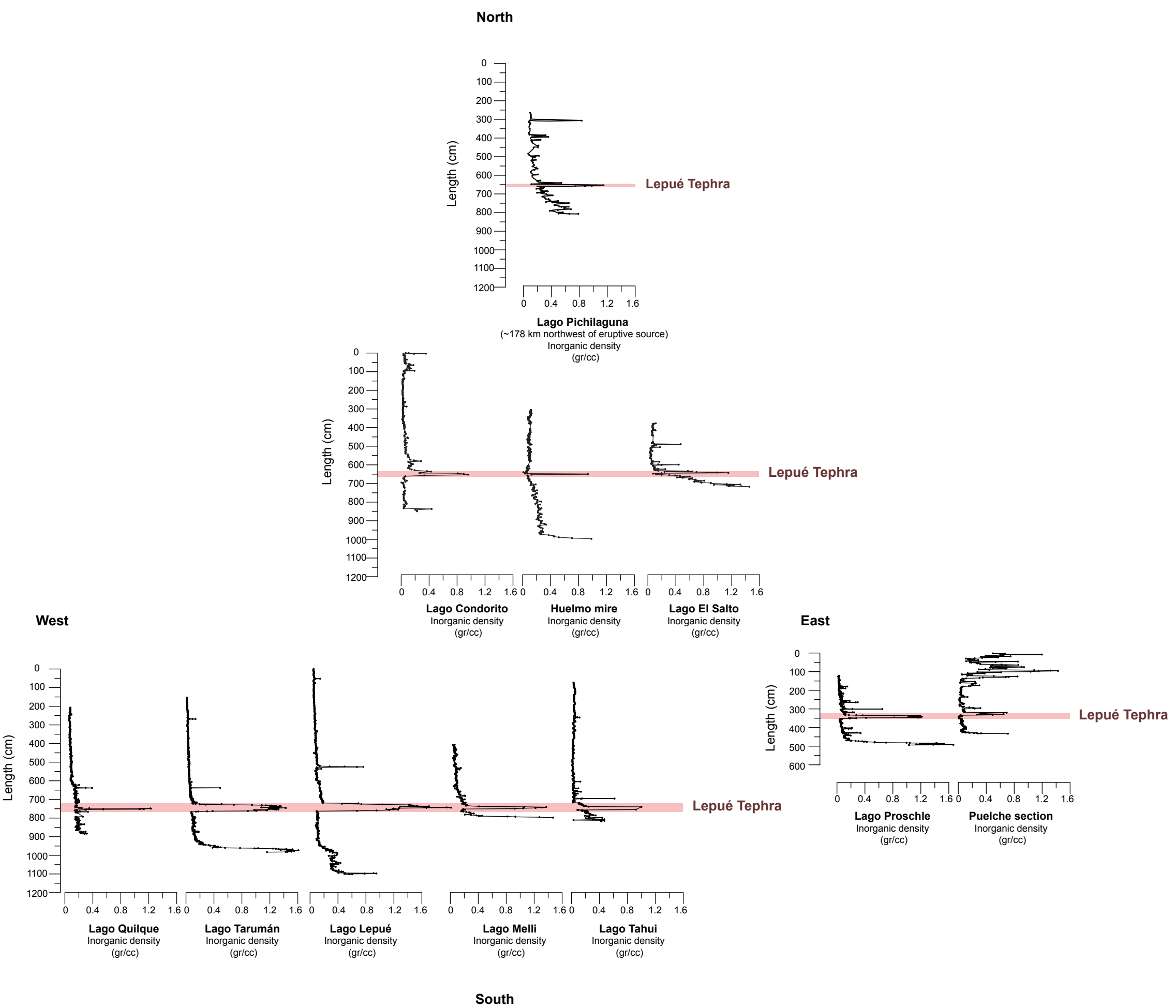
1
2
3
4
5
6
7
8
9
10
11
12
13
14
15
16
17
18
19
20
21
22
23
24
25
26
27
28
29
30
31
32
33
34
35
36
37
38
39
40
41
42
43
44
45
46
47
48
49
50
51
52
53
54
55
56
57
58
59
60



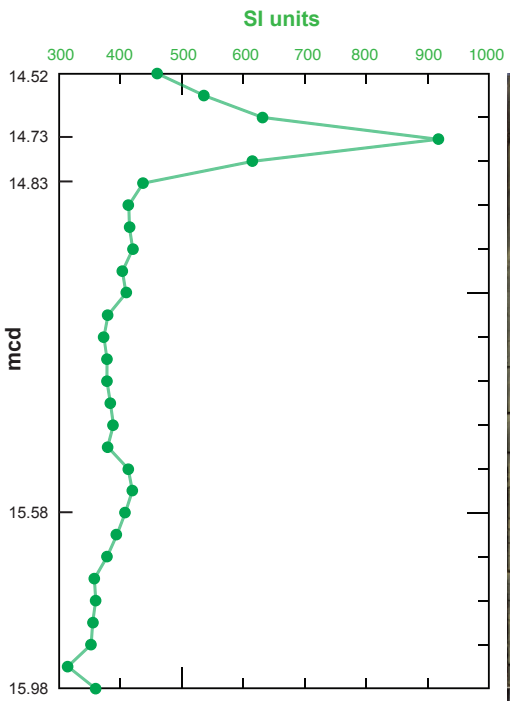
1
2
3
4
5
6
7
8
9
10
11
12
13
14
15
16
17
18
19
20
21
22
23
24
25
26
27
28
29
30
31
32
33
34
35
36
37
38
39
40
41
42
43
44
45
46
47
48
49
50
51
52
53
54
55
56
57
58
59
60



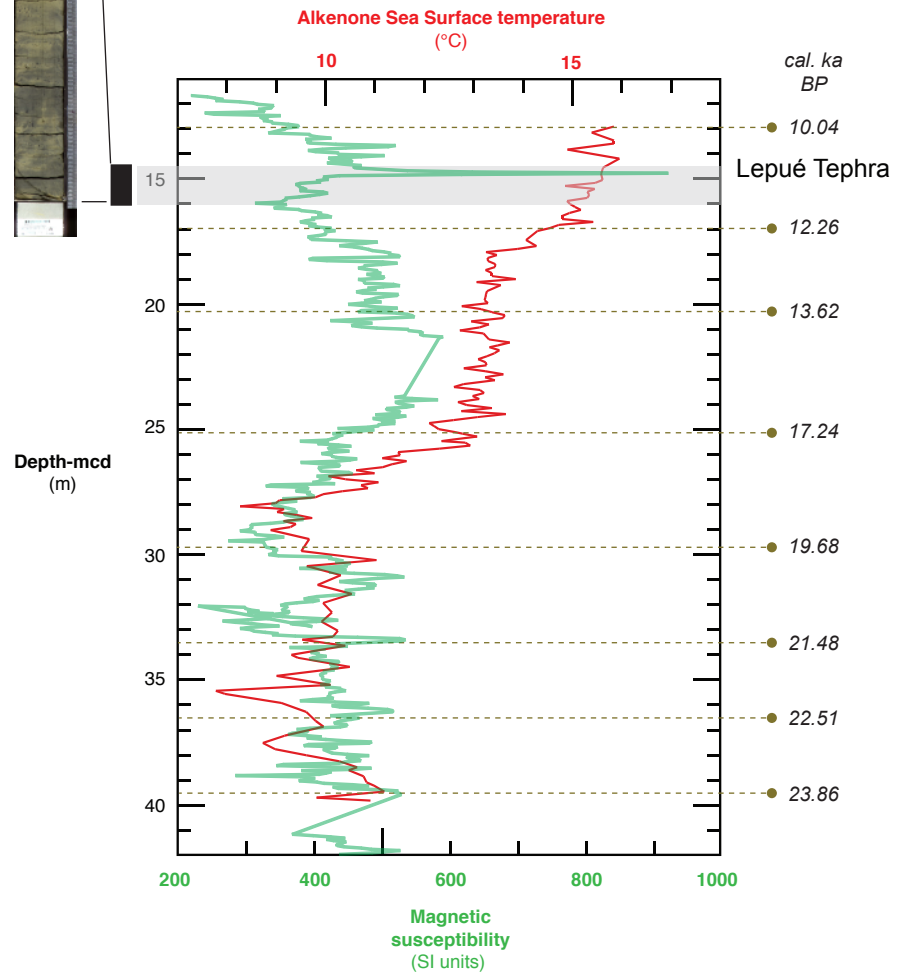
1
2
3
4
5
6
7
8
9
10
11
12
13
14
15
16
17
18
19
20
21
22
23
24
25
26
27
28
29
30
31
32
33
34
35
36
37
38
39
40
41
42
43
44
45
46
47
48
49
50
51
52
53
54
55
56
57
58
59
60

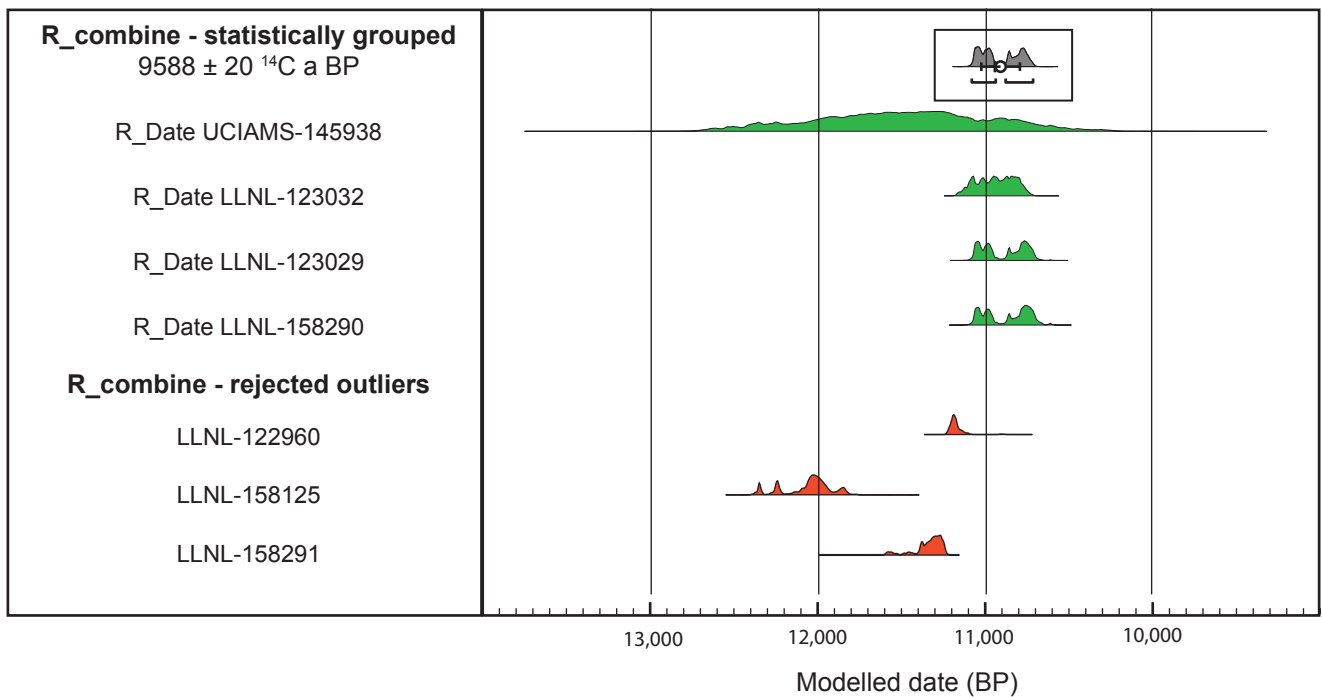
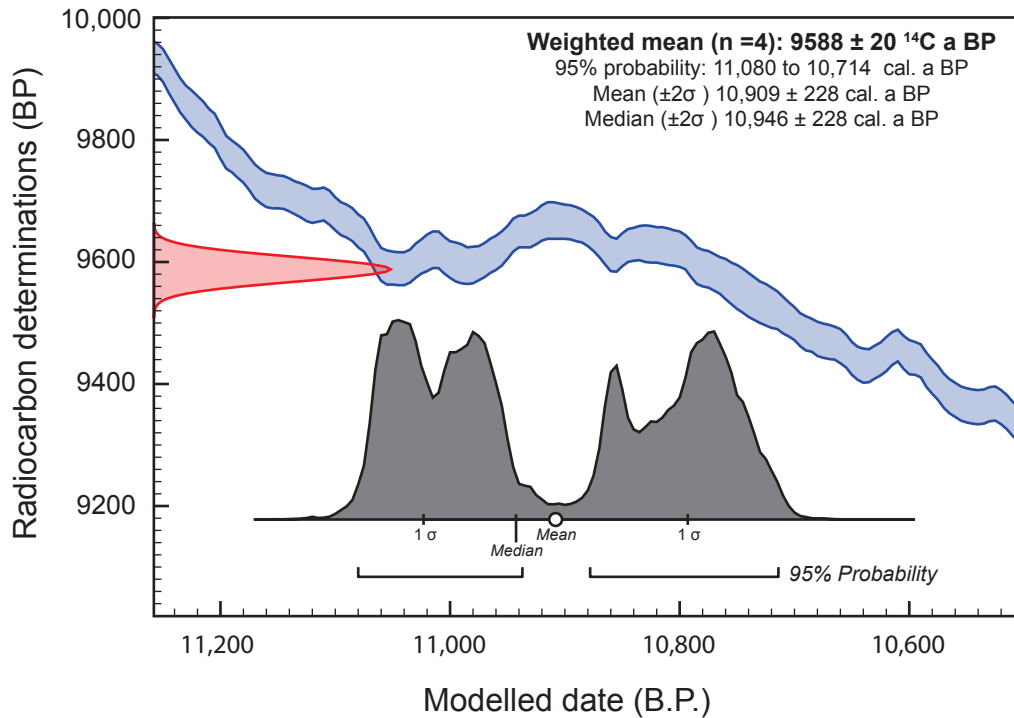


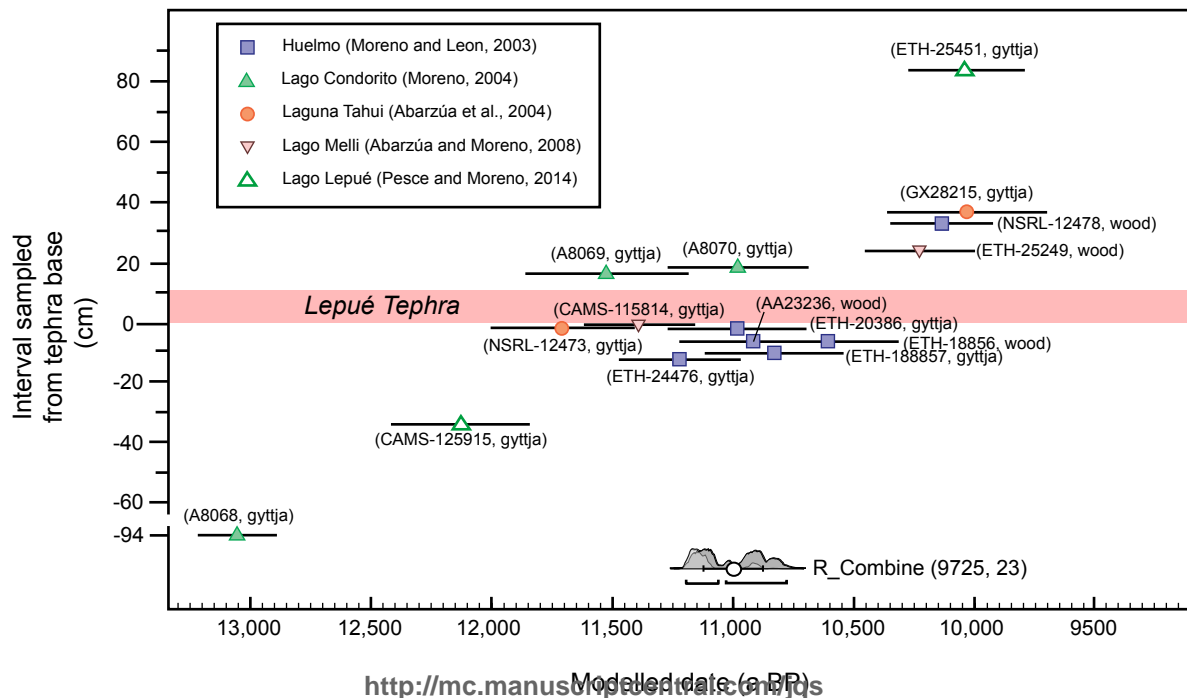
1
2
3
4
5
6
7
8
9
10
11
12
13
14
15
16
17
18
19
20
21
22
23
24
25
26
27
28
29
30
31
32
33
34
35
36
37
38
39
40
41
42
43
44
45
46
47
48
49
50
51
52
53
54
55
56
57
58
59
60

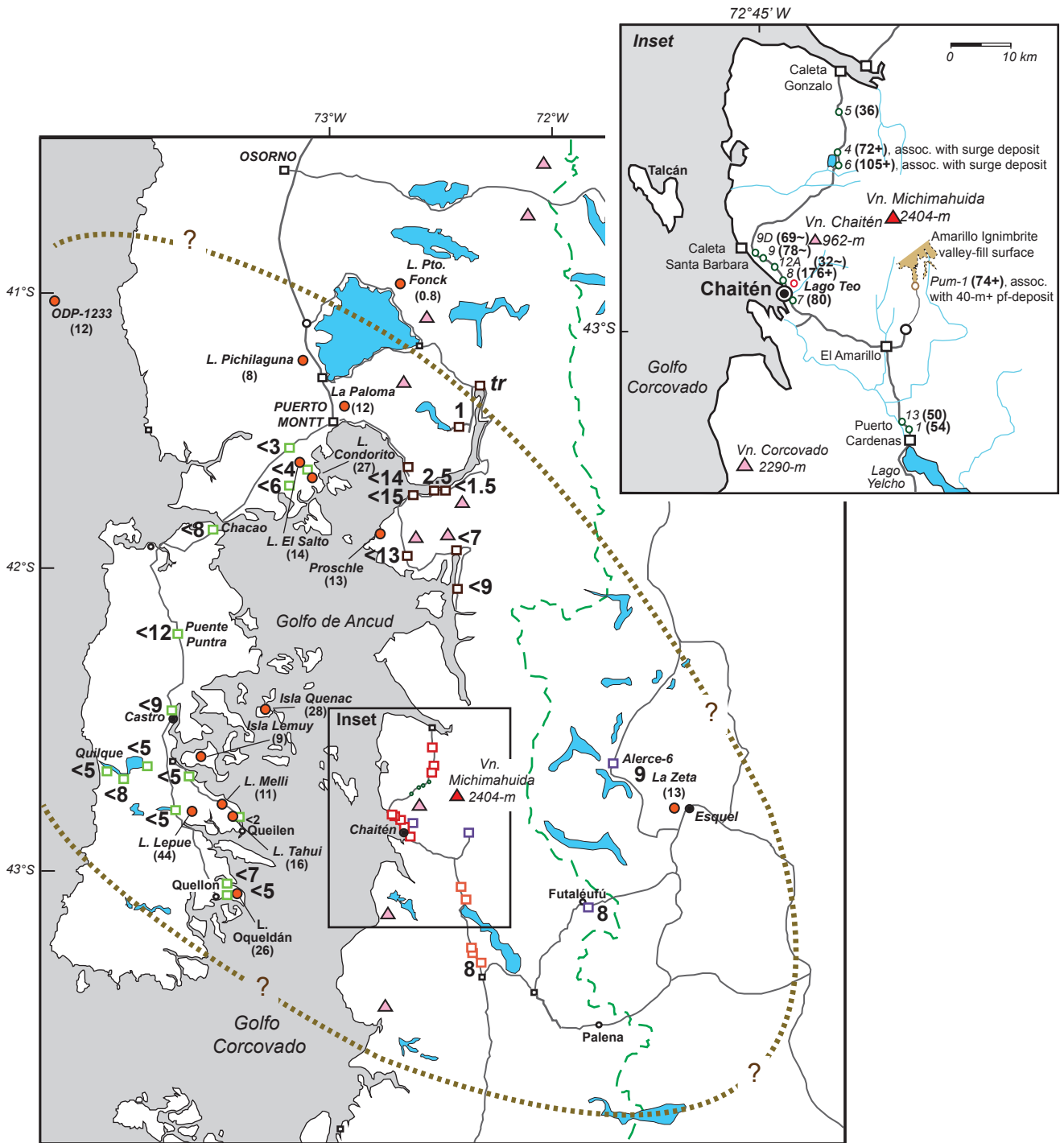


Lepu  Tephra

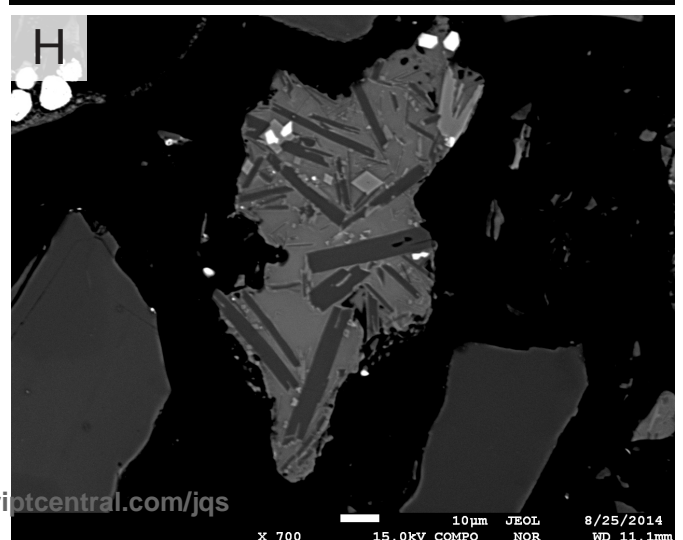
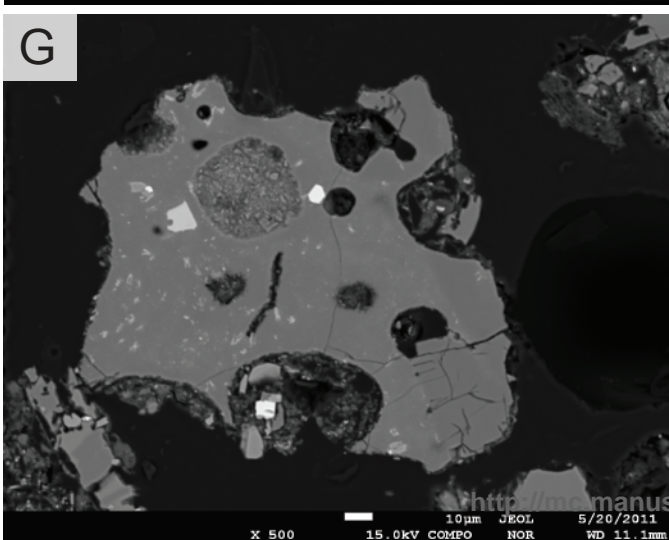
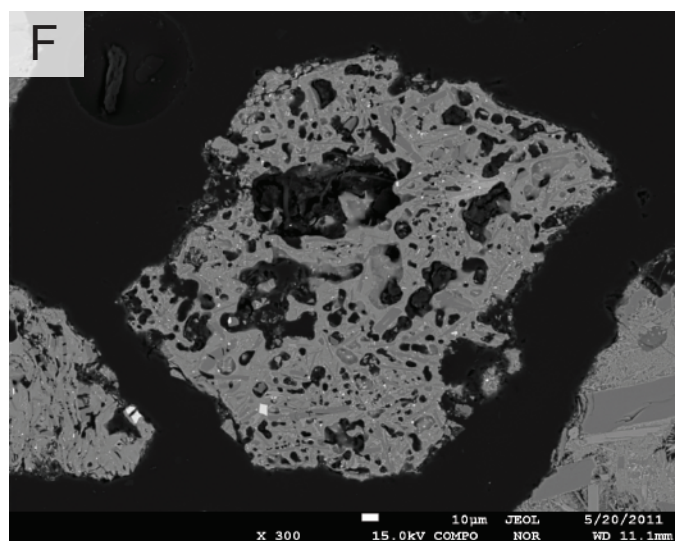
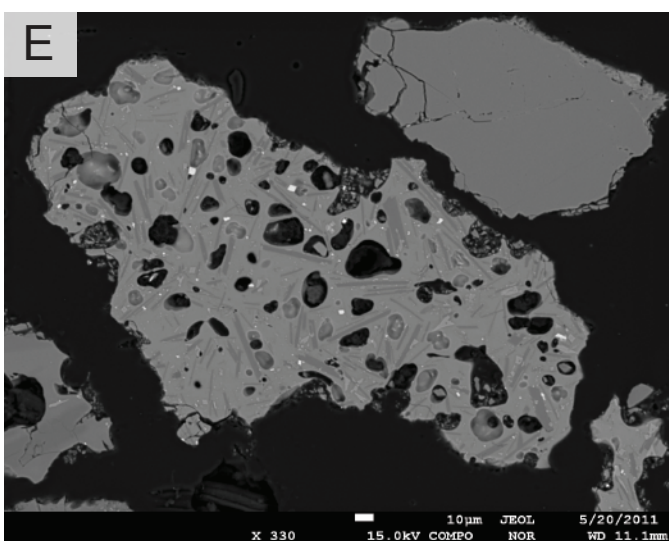
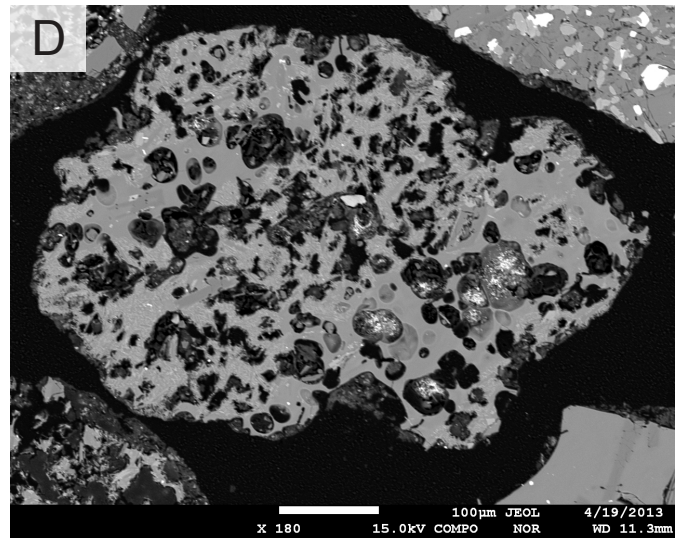
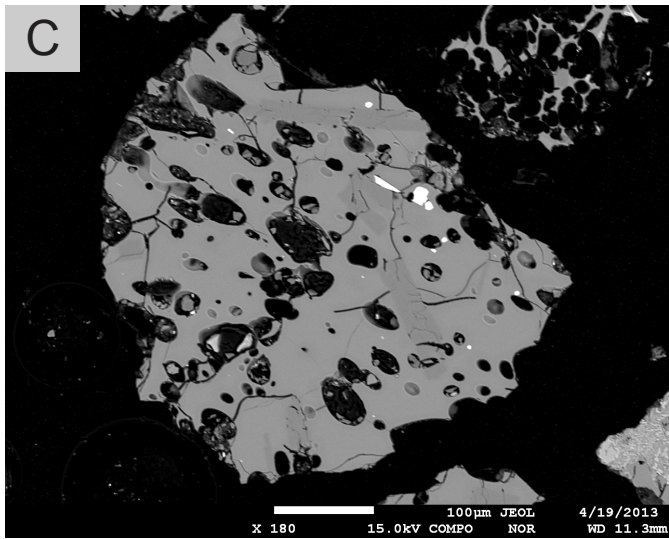
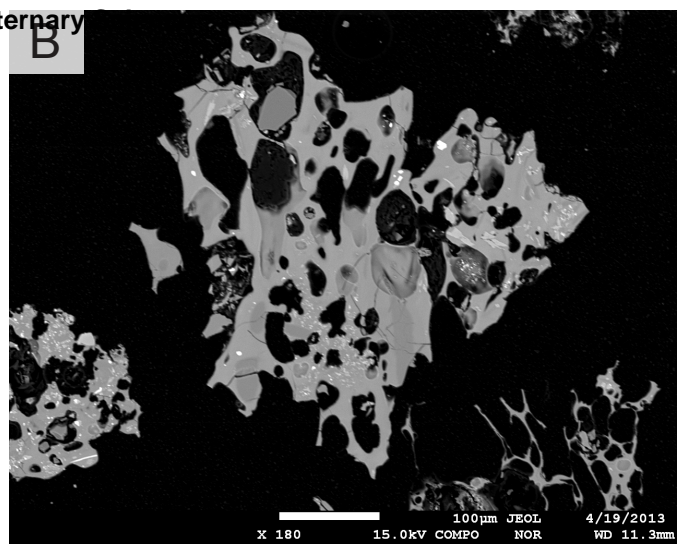
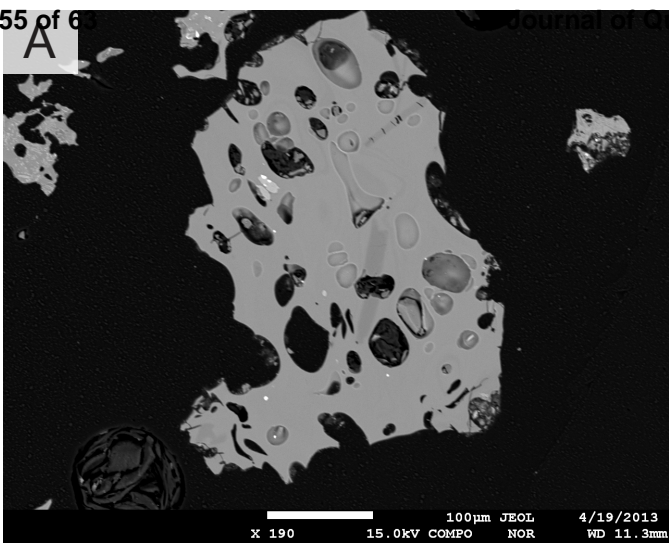


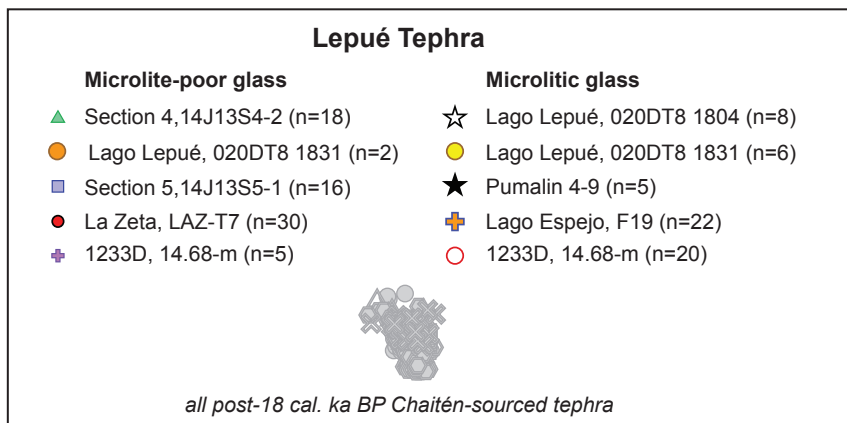
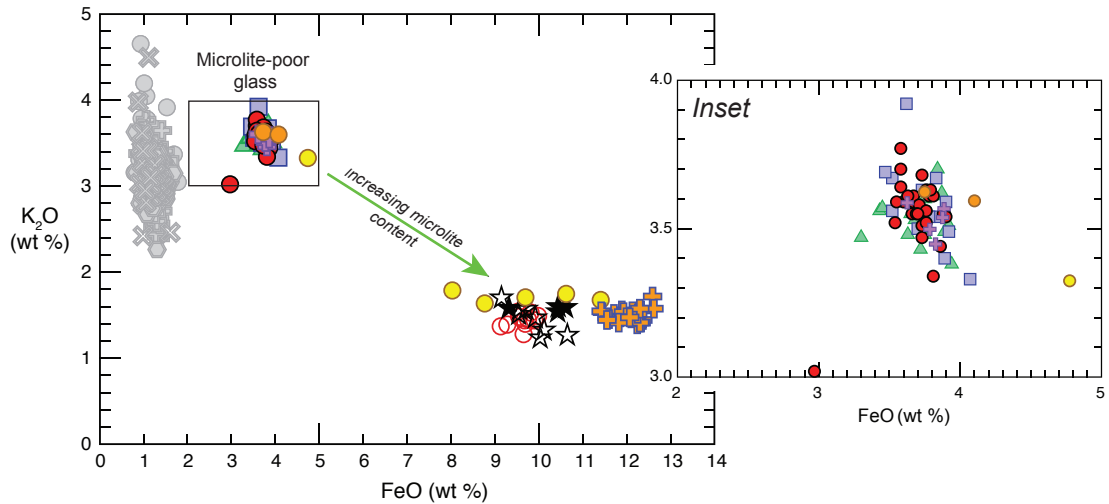
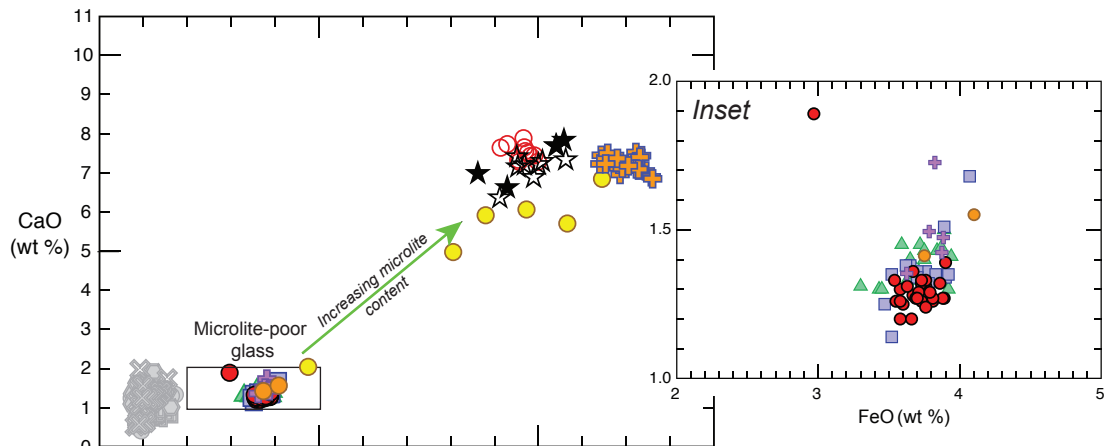
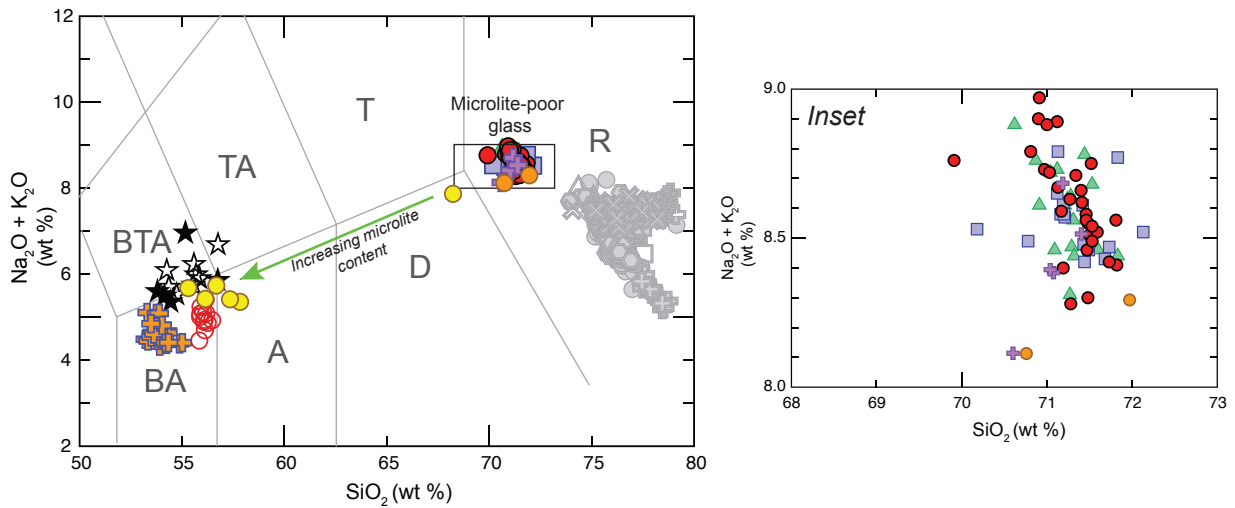






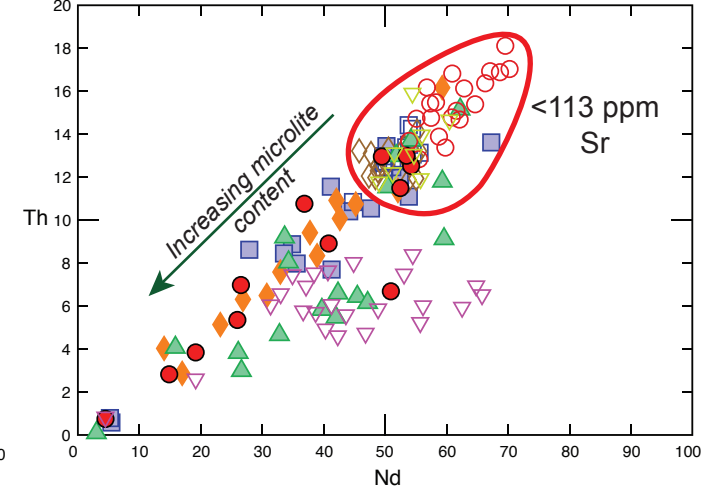
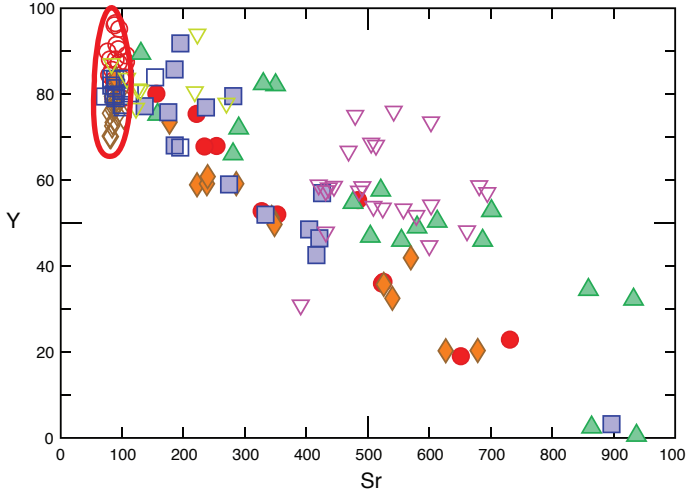
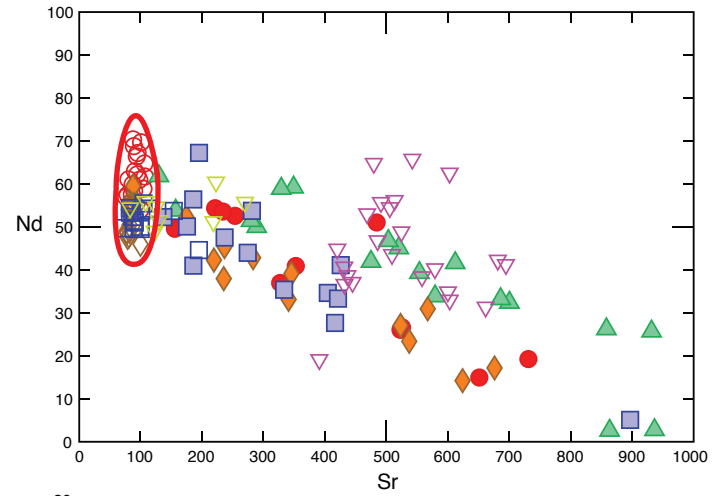
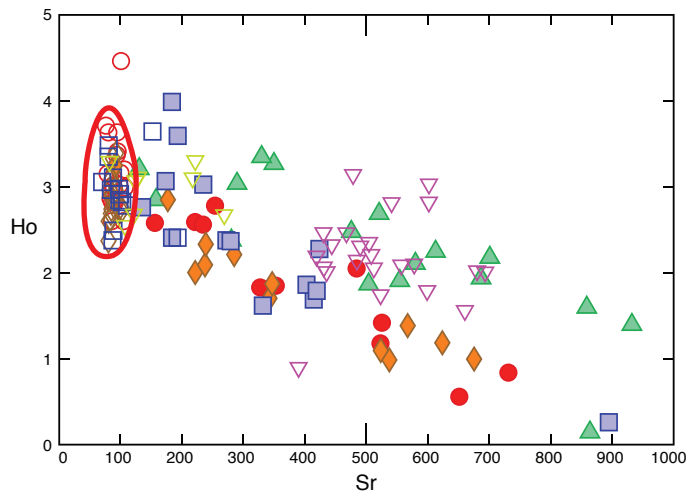
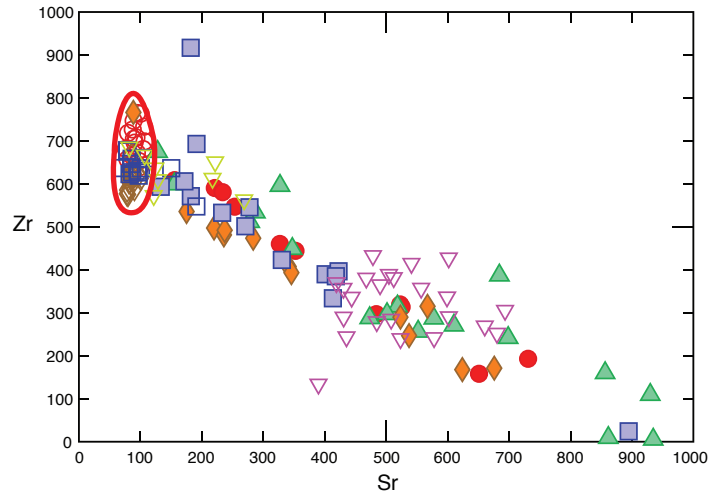
1
2
3
4
5
6
7
8
9
10
11
12
13
14
15
16
17
18
19
20
21
22
23
24
25
26
27
28
29
30
31
32
33
34
35
36
37
38
39
40
41
42
43
44
45
46
47
48
49
50
51
52
53
54
55
56
57
58
59
60



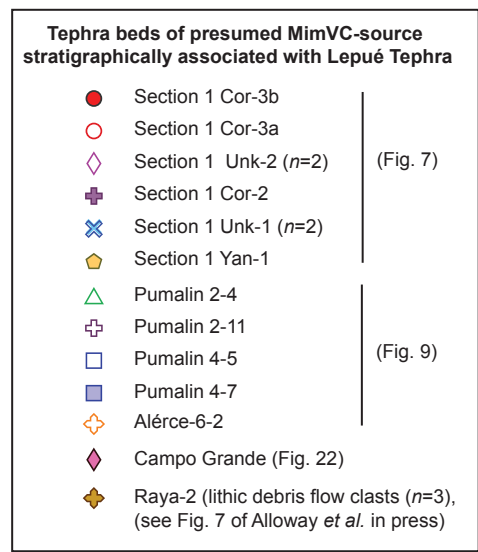
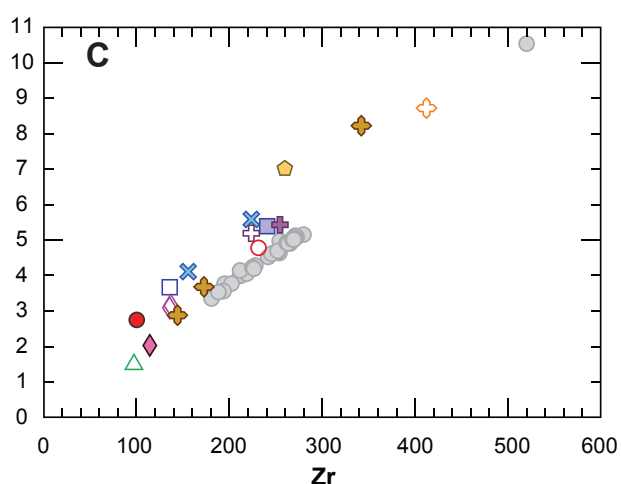
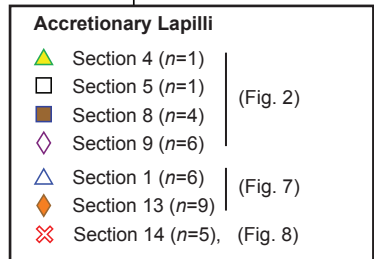
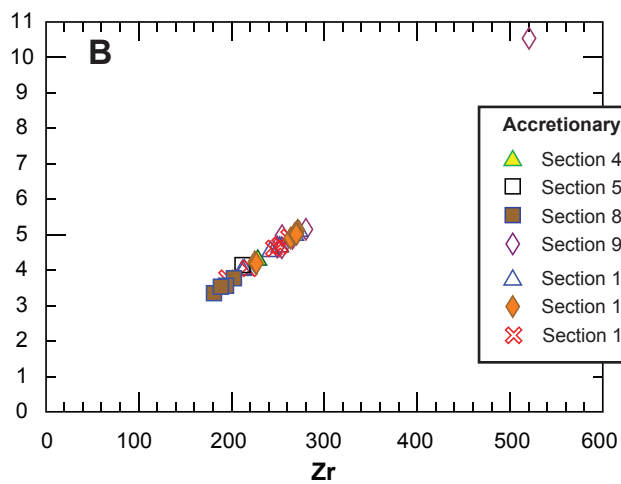
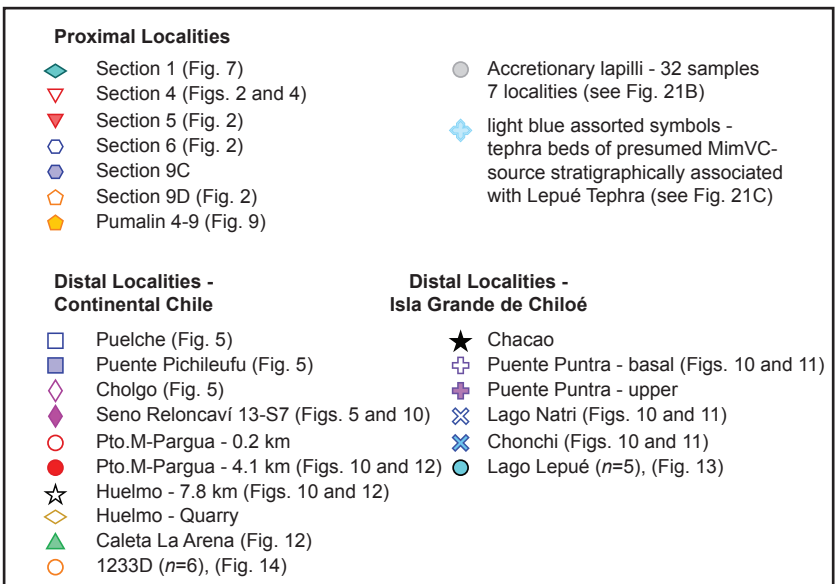
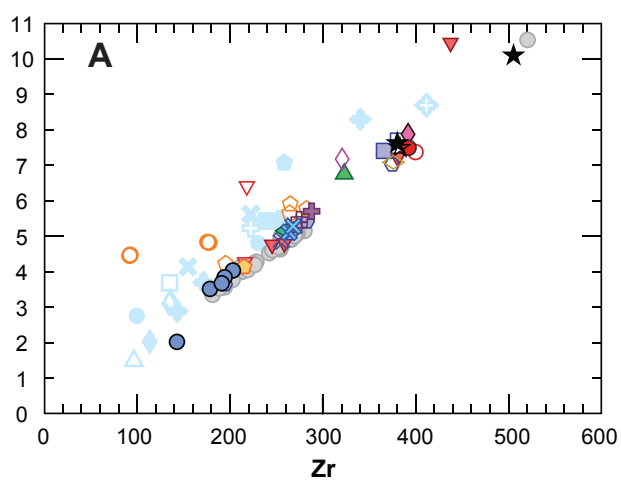


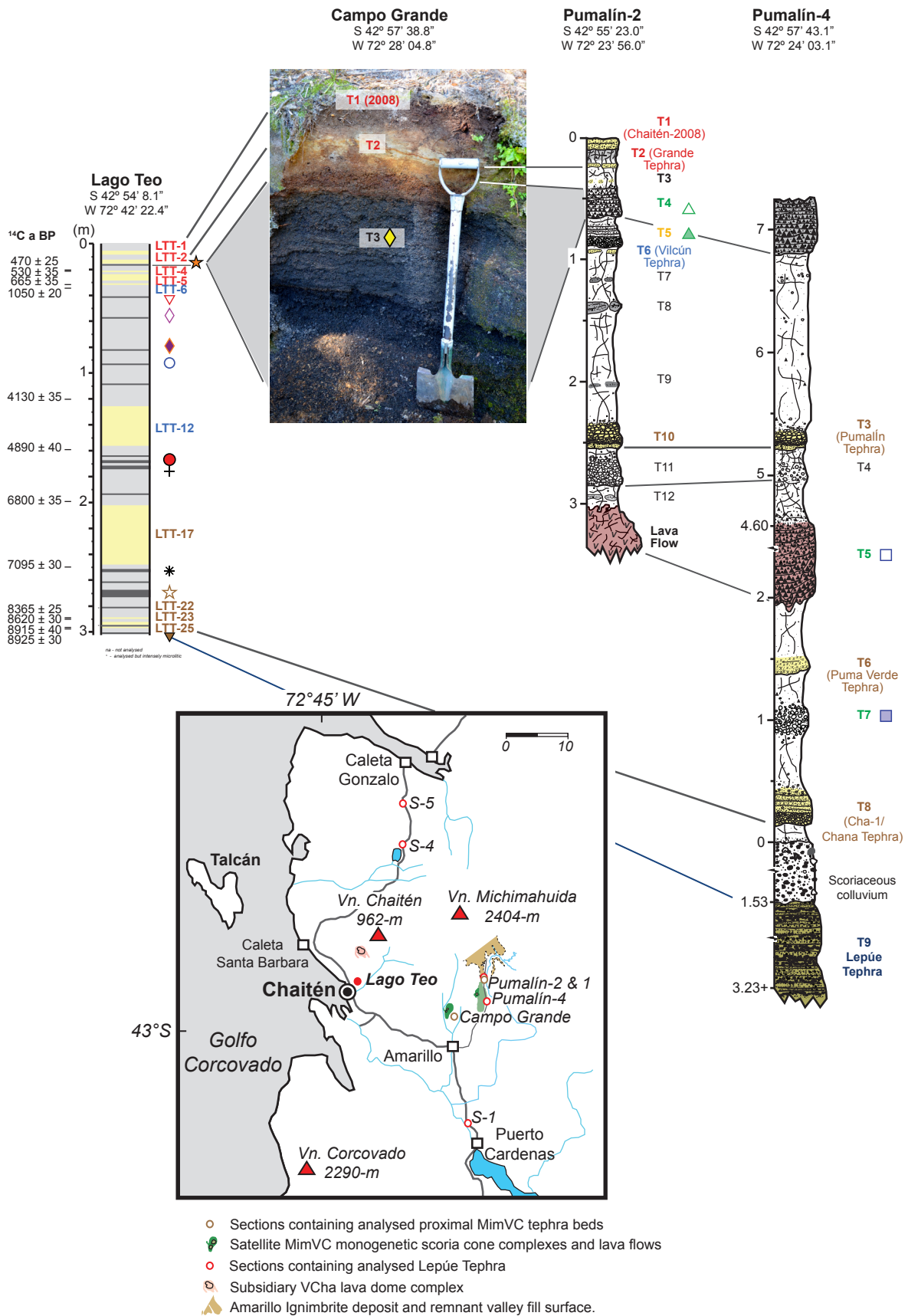
1
2
3
4
5
6
7
8
9
10
11
12
13
14
15
16
17
18
19
20
21
22
23
24
25
26
27
28
29
30
31
32
33
34
35
36
37
38
39
40
41
42
43
44
45
46
47
48
49
50
51
52
53
54
55
56
57
58
59
60

1
2
3
4
5
6
7
8
9
10
11
12
13
14
15
16
17
18
19
20
21
22
23
24
25
26
27
28
29
30
31
32
33
34
35
36
37
38
39
40
41
42
43
44
45
46
47
48
49
50
51
52
53
54
55
56
57
58
59
60



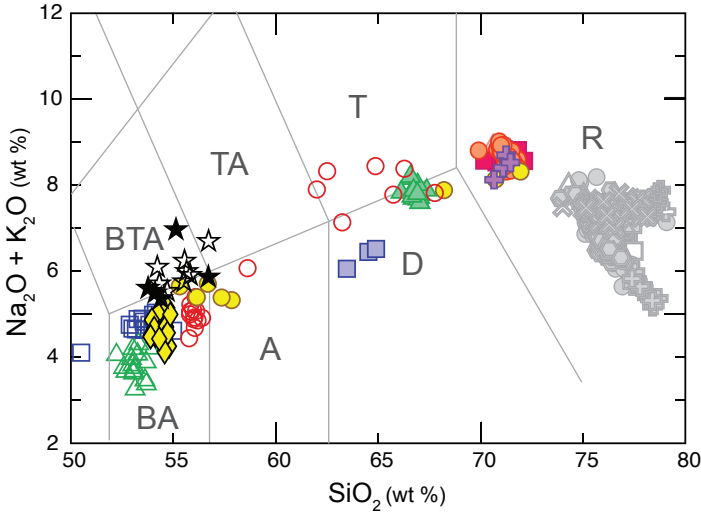
1
2
3
4
5
6
7
8
9
10
11
12
13
14
15
16
17
18
19
20
21
22
23
24
25
26
27
28
29
30
31
32
33
34
35
36
37
38
39
40
41
42
43
44
45
46
47
48
49
50
51
52
53
54
55
56
57
58
59
60





1
2
3
4
5
6
7
8
9
10
11
12
13
14
15
16
17
18
19
20
21
22
23
24
25
26
27
28
29
30
31
32
33
34
35
36
37
38
39
40
41
42
43
44
45
46
47
48
49
50
51
52
53
54
55
56
57
58
59
60

1
2
3
4
5
6
7
8
9
10
11
12
13
14
15
16
17
18
19
20
21
22
23
24
25
26
27
28
29
30
31
32
33
34
35
36
37
38
39
40
41
42
43
44
45
46
47
48
49
50
51
52
53
54
55
56
57
58
59
60

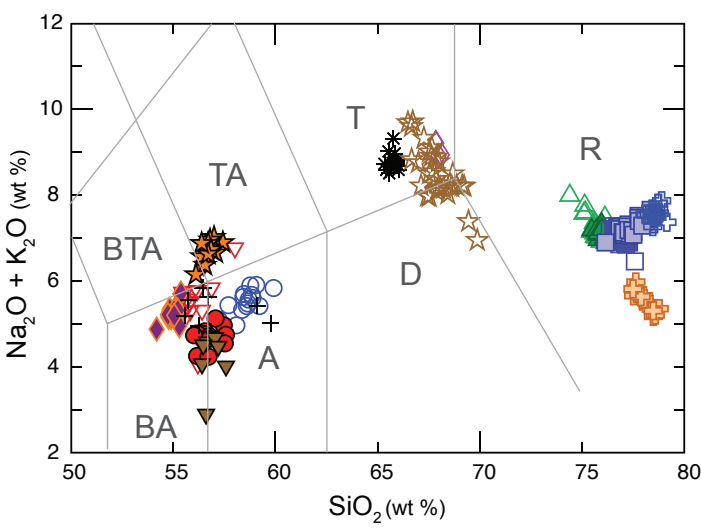


Proximal-distal Lepúe Tephra

- △ Section 4, 14J13S4-2 (aphyric, n=18)
- Section 5, 14J13S5-1 (aphyric, n=16)
- ★ Pumalin 4-9 (microlitic, n=5)
- La Zeta, LAZ-T7 (aphyric, n=30)
- Lago Lepué, 020DT8 1831 (aphyric, n=8)
- ☆ Lago Lepué, 020DT8 1804 (microlitic, n=8)
- ⊕ 1233D, 14.68-m (aphyric, n=5)
- 1233D, 14.68-m (microlitic, n=20)

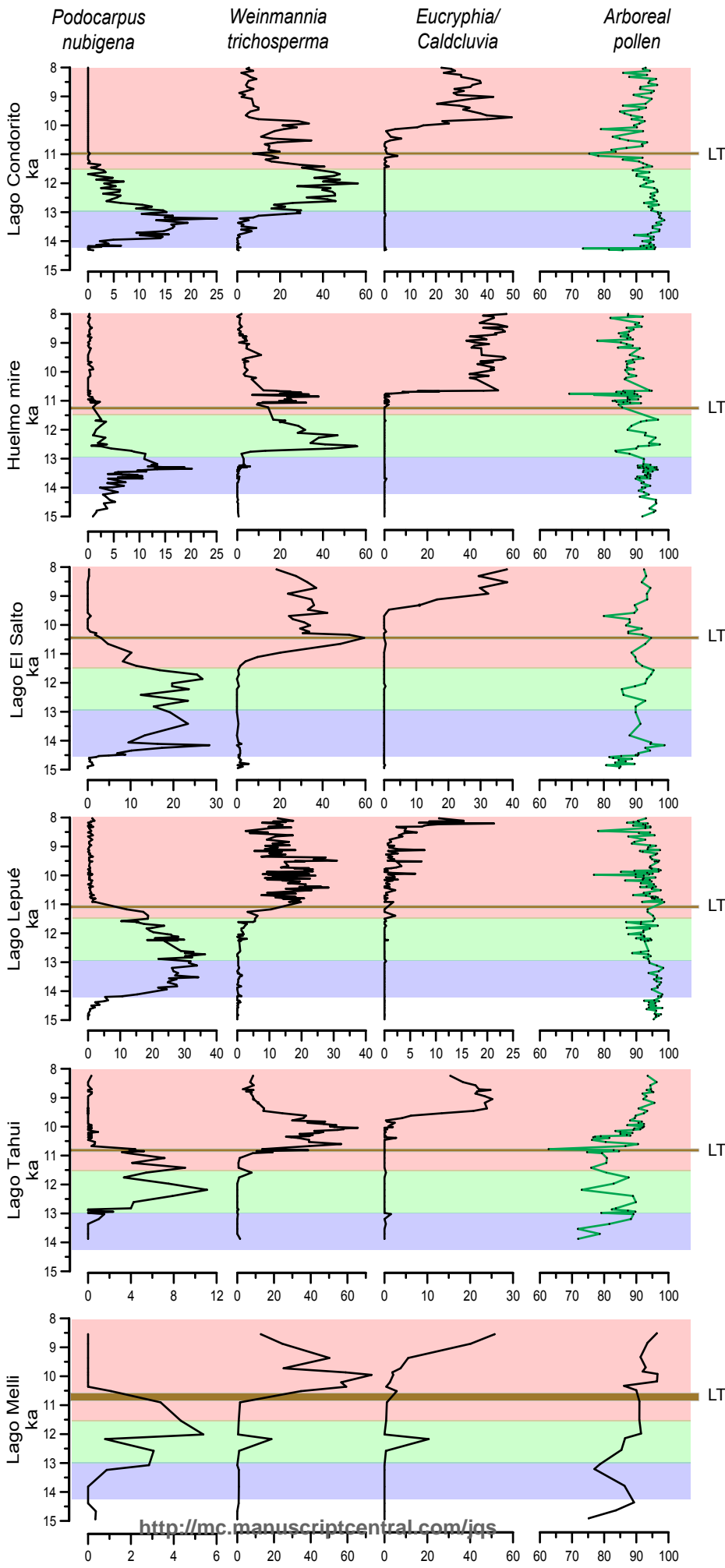
Proximal Michimahuida Volcanic Complex (MimVC) deposits

- △ Pum 2-T4 (n=17)
- ▲ Pum 2-T5 (n=17)
- Pum 4-T5 (n=13)
- Pum 4-T7 (n=3)
- ◇ Campo Grande T3 (n = 17)
- All post-18 cal. ka BP Chaitén (VCha)-sourced tephra



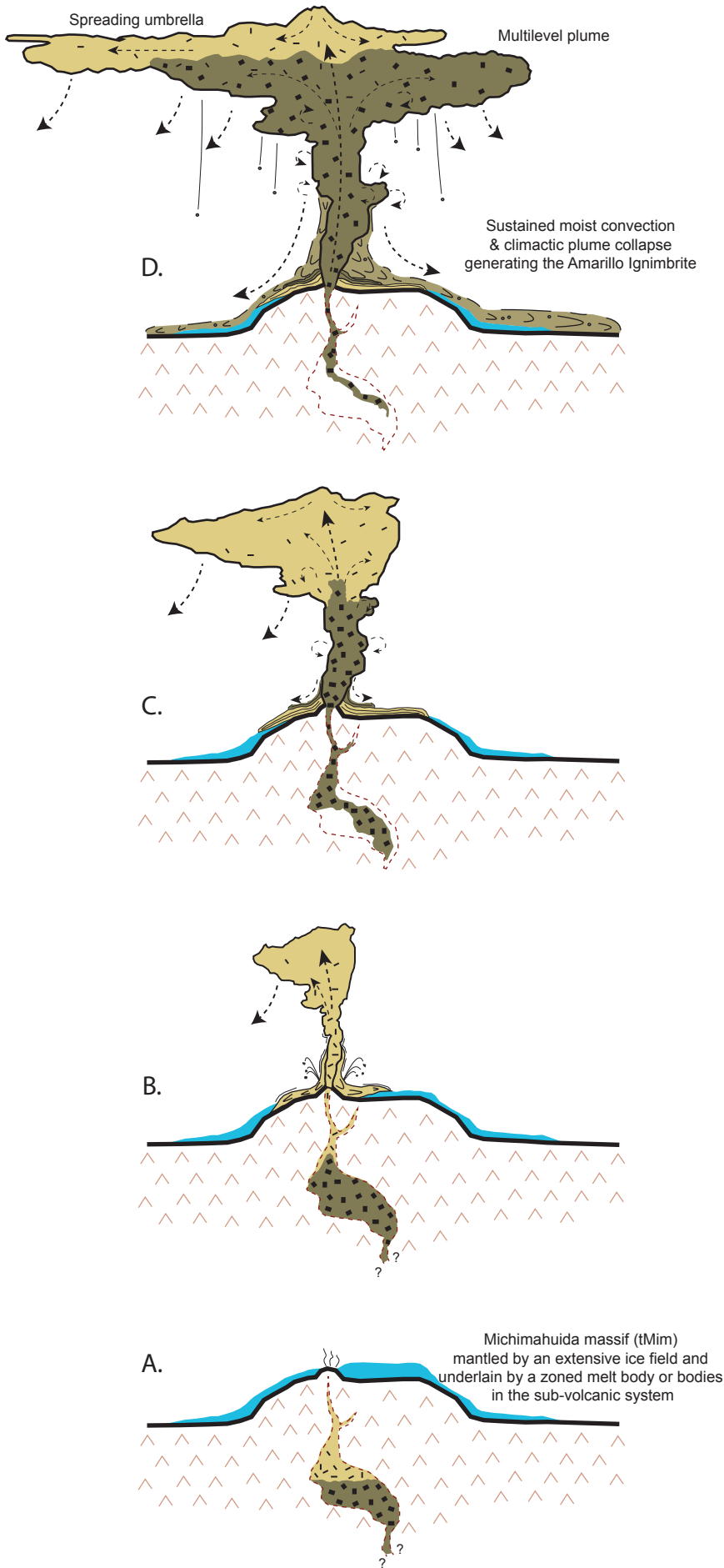
Lago Teo - post 11 cal. ka tephra interbeds

- | GROUP-1
(VCha-sourced) | GROUP-2 | GROUP-3 |
|---------------------------|-----------------|-----------------|
| ○ LTT-1 (n=70) | ◇ LTT-8 (n=33) | ★ LTT-3 (n=30) |
| ● LTT-2 (n=102) | * LTT-18 (n=15) | ▽ LTT-7 (n=33) |
| ⊗ LTT-4 (n=18) | ☆ LTT-20 (n=30) | ◆ LTT-9 (n=16) |
| △ LTT-5 (n=138) | | ○ LTT-10 (n=15) |
| ⊗ LTT-6 (n=37) | | ● LTT-14 (n=13) |
| ▲ LTT-12 (n=48) | | + LTT-15 (n=8) |
| □ LTT-17 (n=62) | | ▼ LTT-26 (n=9) |
| ■ LTT-22 (n=31) | | |
| ⊕ LTT-23 (n=16) | | |
| ⊕ LTT-25 (n=15) | | |



1
2
3
4
5
6
7
8
9
10
11
12
13
14
15
16
17
18
19
20
21
22
23
24
25
26
27
28
29
30
31
32
33
34
35
36
37
38
39
40
41
42
43
44
45
46
47
48
49
50
51
52
53
54
55
56
57
58
59
60

1
2
3
4
5
6
7
8
9
10
11
12
13
14
15
16
17
18
19
20
21
22
23
24
25
26
27
28
29
30
31
32
33
34
35
36
37
38
39
40
41
42
43
44
45
46
47
48
49
50
51
52
53
54
55
56
57
58
59
60



Location	Lab ID	Sample type	Sample position	¹⁴ C AMS age (¹⁴ C a BP)	Calibrated ‡ Age (± 2σ) (cal. a BP)	95% HPDF* (cal. a BP)
Onshore						
<i>(this study)</i>						
S-4, Chaitén *	UCIAMS-145938	Charcoal (twig)	Within surge deposit (co-eruptive correlative)	9,960 ± 330	11,483 ± 1,034	10,561-12,552
Pumalín-1, Chaitén	LLNL-122960	Charcoal (outer small tree)	Within pyroclastic deposit (co-eruptive correlative)	9,785 ± 30	11,190 ± 88	11,108-11,237
Pte Pichileufú *	LLNL-123032	Bulk carbonac. muds	Immediately below lower contact	9,635 ± 35	10,934 ± 118	10,753-11,134
Puelche *	LLNL-123029	Bulk highly carbonac. muds	Immediately below lower contact	9,570 ± 30	10,862 ± 250	10,595-11,080
S-9, Chaitén	LLNL-158125	Bulk carbonac. muds	Immediately below lower contact	10,330 ± 40	12,033 ± 280	11,825-12,383
S-12A, Chaitén *	LLNL-158290	Bulk carbonac. muds	Immediately below lower contact	9,560 ± 35	10,841 ± 262	10,563-11,081
	LLNL-158291	Wood in growth position	Immediately below lower contact	9,970 ± 35	11,321 ± 170	11,234-11,500
				9,588 ± 20	10,909 ± 228	10,714-11,080
R_combine modelled age (n=4 *)						
<i>(Previous studies)</i>						
Huelmo (Moreno & Leon, 2003)	NSRL-12478	Wood	901B-601A, 666.5- cm	9,030± 60	10,139 ± 214	9,914-10,246
		Lepúe tephra correlative (10-cm thick), 700-cm depth (basal contact)				
	ETH-20386	Bulk gyttja	901B-601A, 702-cm	9,695± 90	10,982 ± 290	10,735-11,225
	ETH-18856	Wood	901B-601A, 706-cm	9,415± 80	10,595 ± 286	10,289-11,063
	AA23236	Wood	901B-601A, 706-cm	9,635± 85	10,938 ± 284	10,696-11,196
	ETH-188857	Bulk gyttja	901B-601A, 710-cm	9,545± 70	10,820 ± 308	10,580-11,100
	ETH-24476	Bulk gyttja	901B-601A, 712-cm	9,830± 75	11,208 ± 244	10,800-11,399
Lago Condorito (Moreno, 2004)	A8070	Bulk gyttja	PM10, 685-688-cm	9,680± 85	10,967 ± 282	10,732-11,211
	A8069	Bulk gyttja	PM10, 710-713-cm	10,060± 80	11,527 ± 328	11,245-11,917
		Lepúe tephra correlative (27-cm thick), 726-cm depth (basal contact)				
	A8068	Bulk gyttja	PM10, 821-824-cm	11,265 ± 65	13,090 ± 148	12,928-13,258
Laguna Tahui (Abarzúa et al., 2004)	GX28215		004D, 891-895-cm	8,990 ± 110	10,029 ± 332	9,635-10,367
		Lepúe tephra correlative (16-cm thick), 932-cm depth (basal contact)				
	NSRL-12473	Bulk gyttja	004D, 934-936-cm	10,150± 50	11,703 ± 296	11,403-11,960
Lago Meli (Abarzúa and Moreno, 2008)		Terrestrial macrofossil	818-819-cm	9,105 ± 70	10,227 ± 218	9,930-10,479
		Lepúe tephra correlative (11-cm thick), 843-cm depth (basal contact)				
	CAMS-115814	Bulk gyttja	844-cm	10,000± 40	11,377 ± 218	11,247-11,610
Lago Lepúe (Pesce & Moreno, 2014)	ETH-25451	Bulk gyttja	0201 DT8, 786-cm	8,965 ± 65	10,033 ± 234	9,781-10,227
		Lepúe Tephra (44-cm thick), 870-cm depth (basal contact)				
	CAMS-125915	Bulk gyttja	0201 DT9, 904-cm	10,360 ± 40	12,123 ± 272	11,948-12,401
Offshore						
ODP Site 1233D (Lamy et al. 2004)	KIA 21451	Mixed planktonic foraminifera	12.94 mcd	9,340 ± 80	10,175 ± 288	9,916-10,387
		Lepúe Tephra (12-cm thick), 14.80 mcd (basal contact)				
	KIA21473	Mixed planktonic foraminifera	17.01 mcd	10,800 ± 70	12,276 ± 280	12,019-12,534

‡ The Southern Hemisphere terrestrial calibration curve (SHCal13) and OxCal Program (v. 4.2.4) were used for all samples; * Highest Probability Density Function Radiocarbon laboratories used in this study: UCIAMS - University of California at Irving AMS Facility; LLNL - Lawrence Livermore National Laboratory.